NTNU – Trondheim
Norwegian University of
Science and Technology

The Chiral Phase Transition in QCD

Mean-Field Versus the Functional
Renormalisation Group

Jonas Rylund Glesaaen

Physics
Submission date: May 2013
Supervisor: Jens Oluf Andersen, IFY

Norwegian University of Science and Technology
Department of Physics

Sammendrag

I denne masteroppgaven har vi studert fasediagrammet tilhørende den kirale faseovergangen til kvantekromodynamikk (QCD) i T-μ-planet. Vi bruker den lineære sigmamodellen med kvarker for å modellere QCD ved små energier. For å regne ut fasediagrammet benytter vi oss først av middelfeltteori. Med denne tilnærmingen finner vi en førsteordens faseovergang i hele T-μ-planet i den kirale grensen. Imidlertid finner vi en crossover ved null kjemisk potensial med fysiske kvarkmasser, som endres til en førsteordens faseovergang når μ økes. Dette impliserer eksistensen av det kritiske punktet.

Etter dette flytter vi fokuset til en mer raffinert teknikk, nemlig den funksjonale renormaliseringsgruppen. Vi bruker så lokalpotensialtilnærmingen for å finne en likning for det effektive potensialet. Med denne tilnærmingen finner vi en annenordens faseovergang ved null kjemisk potensial i kiralgrensen, som endres til en førsteordens overgang når vi øker μ. Dette betyr at ved bruk av renormaliseringsgruppen fant vi et kritisk punkt også i den kirale grensen. Når vi sammenligner fasediagrammet vi fikk ved å bruke middelfeltteori med fasediagrammet vi fikk ved å bruke renormaliseringsgruppen observerer vi at det sistnevnte fasediagrammet faller av raskerer for høye kjemiske potensial enn førstnevnte.

Selv om denne oppgaven i hoveddel angår QCD med to kvarker, så har en tre-kvark-modell også blitt introdusert, og vi finner faseovergangen til denne ved bruk av middelfeltteori. Sammenlignet med to-kvark-modellen ser vi at effekten av å inkludere særkvarken på fasediagrammet er svært liten. Forskjellen mellom diagrammene med og uten særkvarken blir større dersom vi velger en høyere verdi for sigmamassen, men selv ved 800 MeV er forskjellen fortsatt liten.

Abstract

In this thesis we map out the phase diagram of the chiral phase transition of quantum chromodynamics (QCD) in the plane of temperature and quark chemical potential. We use the linear sigma model with quarks (LSMq) as a low energy effective theory of QCD. We first employ the mean-field approximation to calculate the phase diagram. With this approximation we find a first-order phase transition in the whole T-μ plane in the chiral limit. However at the physical point we find a crossover at zero chemical potential, which changes into a first-order transition as we increase μ, implying the existence of a critical endpoint.

We then turn our attention to the more sophisticated functional renormalisation group and nonperturbative approximations. Using the local potential approximation (LPA), which is the simplest nonperturbative approximation, we found a second-order phase transition in the chiral limit at zero chemical potential. As we increased μ, the transition changed into a first-order one, which means that in contrast to the results from the mean-field approximation we found a critical endpoint also in the chiral limit. When comparing the phase diagrams obtained in the mean-field approximation with the phase diagrams from the LPA, we see that the latter phase diagram declines faster for high chemical potentials.

While this work is primarily concerned with two-flavour QCD, we also introduce the three-flavour LSMq model and map out the phase diagram in the mean-field approximation. We find that the inclusion of the strange quark only has a minor effect on the phase diagram. The difference becomes more prominent as we increase the mass of the sigma particle to 800 MeV, but the difference is still small.

Acknowledgements

I would like to thank Professor Jens Oluf Andersen for excellent supervision during the past two years, and for giving me a project to work on that has been both challenging and interesting, not only within the domain of physics, but also numerics.

I would also like to thank my fellow students for fruitful discussions throughout my time at NTNU, and for joining me in my thought experiments whenever I needed a sanity check.

Contents

Notation

Natural units $\hbar = c = k_B = 1$ are used throughout the thesis.

The metric is

$$\eta^{\mu\nu} = \mathrm{diag}(1, -1, -1, -1).$$

If coordinates are denoted by a simple x or y, the full space-time vectors x^μ, y^μ are implied, and with multiplication of these, the contraction has already been carried out $xp = x_\mu p^\mu$. Space vectors will be written in boldface $\mathbf{x}$, $\mathbf{y}$.

Greek indices take values starting at 0, while Latin letters take values starting at 1. Einstein's sum convention is always implied, meaning that Greek indices are always contracted up with down, while Latin ones are summed if repeated. Examples:

$$x^\mu x_\mu = x_0^2 - x_1^2 - x_2^2 - x_3^2$$
$$a_i b_i = \sum_i a_i b_i$$

Whenever d is denoted as the dimension, both space and time dimensions are included. In most cases we will work in $4d$ Minkowski space, meaning one time dimension and three spatial dimensions with the metric signature above.

Space-time integrals with no boundary conditions imply that they are taken to infinity

$$\int \mathrm{d}^4 x = \int_{-\infty}^{\infty} \mathrm{d}t \int_{-\infty}^{\infty} \mathrm{d}x \int_{-\infty}^{\infty} \mathrm{d}y \int_{-\infty}^{\infty} \mathrm{d}z$$

If the integration measure is $\mathrm{d}^d x$, this implies integration over all space-time dimensions. The integration measure $\mathrm{d}\mathbf{x}$ is over all spatial dimensions. Sometimes the notation

$$\int_x \quad \text{and} \quad \int_q$$

will be used. This also implies integration over all space-time dimensions, but it is context dependent. In the sections on quantum field theory, they are integration over Minkowski space-time, while in the sections on thermal field theory they include the thermal limit in Euclidean space, or are identical to the sum-integral in Fourier space:

$$\int_x = \int_0^\beta \mathrm{d}\tau \int \mathrm{d}\mathbf{x}, \quad \int_q \equiv T \sum_{n=-\infty}^{\infty} \int \frac{\mathrm{d}\mathbf{p}}{(2\pi)^3}$$

I have chosen to use the standard representation of the γ matrices

$$\gamma^0 = \begin{pmatrix} \mathrm{I} & 0 \\ 0 & -\mathrm{I} \end{pmatrix}, \quad \gamma^i = \begin{pmatrix} 0 & \tau^i \\ -\tau^i & 0 \end{pmatrix}, \quad \gamma^5 = \begin{pmatrix} 0 & I \\ I & 0 \end{pmatrix},$$

where τ^i are the three Pauli matrices, I is the 2×2 identity matrix, and $\gamma^5 = i\gamma^0\gamma^1\gamma^2\gamma^3$.

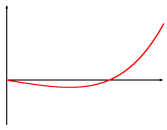

Introduction

The phase diagram in the plane of temperature T and baryon chemical potential μ_B (i.e. baryon density) of quantum chromodynamics (QCD), the theory describing the dynamics and interactions of quarks and gluons, has in recent years received a lot of attention due to its rich structure [1, 2]. At low temperature and density, QCD is in in the so called hadronic phase, where quarks and gluons only appear as bound states such as the baryons and mesons. This owes to the confining nature of the strong force. At high energy scales on the other hand, QCD possesses asymptotic freedom, which allows for interesting and exotic phases at high temperatures and/or high densities. For example heavy-ion collider experiments at RHIC (Relativistic Heavy Ion Collider) and LHC (Large Hadron Collider) has verified the existence of quark-gluon plasma at high temperatures, and the same phase is strongly believed to have existed in the very early universe. At low temperatures but high densities, a quark matter phase as well as multiple colour-superconducting phases are predicted. These phases are believed to exist inside compact stars and be present at the collapse of neutron stars [3].

The aforementioned confining properties of QCD makes it an exceedingly difficult theory to work with, as perturbative techniques break down at energy scales lower than that of deconfinement. One therefore has to resort to other methods of calculation such as lattice QCD, a numerical technique using a discretised version of QCD to calculate various quantities from first principles. Another option, which we will make use of in this thesis, is to model QCD with effective theories, simplifying the picture considerably. One such model is the linear sigma model with quarks, in which gluons have effectively been replaced by mesons, and quark-gluon interactions with quark-meson interactions. On top of being a very successful model, it has an historic background as Yukawa proposed in 1934 [4] that the force particle corresponding to the strong force was in fact the meson, for which he later received the Nobel Prize in 1949.

Even using effective models for QCD we still can not find analytic expressions for the quantities needed to calculate the phase diagrams, and further approximation is needed. We will first use the mean-field approximation, to calculate said quantities, but we will quickly turn to a more sophisticated nonperturbative functional renormalisation group technique. One should notice the small figures in the upper right corner of every odd page. This is the plot of an effective potential at various stages of renormalisation, calculated using the renormalisation group equations we will derive later in this thesis, and is meant to be flipped through like a flip book.

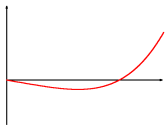

CHAPTER 1

Preliminaries

In this thesis I will assume that the reader is familiar with the basics of quantum field theory (QFT) and I will therefore only give a very brief derivation of it. Afterwards I will continue with a study of some of its properties and applications before proceeding to a formalism in which the temperature is nonzero.

1 Quantum field theory

In the early 20^{th} century, at the discovery of the quantum theory, physicists realised that physics might not be as predictive as they first thought. Quantum theory, which seemingly governed the mechanics at very small scales, could only calculate probabilities for outcomes. Meaning that any quantum process would have a fundamental element of uncertainty tied to it. One manifestation is Heisenberg's uncertainty principle, which states that if the position of a particle is known to a certain precision, there is a limit to how precise one can know the momentum of the same particle. This limit is determined by the Planck constant found almost 30 years earlier by Planck in relation to the energy distribution of black body radiation. Therefore, in any quantum theory, for a given process one would calculate the probability for a certain outcome, and use that to make predictions of what will generally occur. These probabilities are called transition amplitudes, and we will have a look at how they are defined and calculated using quantum field theory.

A transition amplitude is defined as $\langle B, t_f | A, t_i \rangle$, where the square of this is the probability of finding the system in state $|B\rangle$ at time t_f given it was in state $|A\rangle$ at time t_i. This is in the so called Scrödinger representation, in which the state of the particle is time dependent, and can be evolved in time by applying the time-evolution operator $e^{-i\hat{H}(t_f - t_i)}$. In the Heisenberg representation on the other hand, particle states are time independent, however quantum mechanical operators are not. We will not concern ourselves with this representation here, and in the Schrödinger representation, the transition amplitude is

$$\langle B | \, e^{-i\hat{H}(t_f - t_i)} \, | A \rangle \, . \tag{1.1}$$

The time-evolution operator stems from the stationary solution to the Schrödinger equation

$$i\frac{\partial \phi}{\partial t} = \hat{H}\phi \, , \tag{1.2}$$

where $\hat{H}$ is the quantum mechanical operator corresponding to the classical Hamiltonian.

First let us derive a formula for the transition amplitude of a specific system. The algebra and identities needed is listen in appendix A1. To calculate Eq. (1.1) we insert N (taken to infinity)

complete sets of states $|\phi\rangle$ at times t_n separated by an infinitesimal time $\Delta t = (t_f - t_i)/N$. We also insert a complete set of states in momentum space ($|\pi\rangle$). This yields

$$\langle\phi_f| e^{-i\hat{H}(t_f-t_i)} |\phi_i\rangle = \lim_{N\to\infty} \int \left(\prod_{n=1}^{N} \mathrm{d}\phi_n \frac{\mathrm{d}\pi_n}{2\pi} \right) \langle\phi_f|\pi_N\rangle \langle\pi_N| e^{-i\hat{H}\Delta t} |\phi_N\rangle \langle\phi_N|\pi_{N-1}\rangle \\ \times \langle\pi_{N-1}| e^{-i\hat{H}\Delta t} |\phi_{N-1}\rangle \dots \langle\pi_1| e^{-i\hat{H}\Delta t} |\phi_1\rangle \langle\phi_1|\phi_i\rangle . \tag{1.3}$$

Here $|\phi_n\rangle$ is the state at time $t_n = t_i + n\Delta t$, while $|\pi_n\rangle$ is the momentum rep. at time t_n. Expanding the exponents to first order in Δt we should obtain terms on the form $\hat{H}|\phi_n\rangle$. We assume that all $|\phi_n\rangle$'s are eigenstates to the operator $\hat{H}$ with eigenvalues H_n. Identifying this as the series expansion of an exponential, and evaluating the scalar products $\langle\phi_n|\pi_m\rangle$ using (A.9) we finally arrive at

$$\langle\phi_f| e^{-i\hat{H}(t_f-t_i)} |\phi_i\rangle = \lim_{N\to\infty} \int \left(\prod_{i=1}^{N} \mathrm{d}\phi_i \frac{\mathrm{d}\pi_i}{2\pi} \right) \delta(\phi_1 - \phi_i) \\ \times \exp\left\{ -i\Delta t \sum_{i=1}^{N} \int \mathrm{d}^{d-1}x \left[\mathcal{H}(\phi_i, \pi_i) - \pi_i(\phi_{i+1} - \phi_i)/\Delta t \right] \right\} . \tag{1.4}$$

Taking the continuum limit we rewrite the sum in the exponential as an integral over time, and recognise the last term as the formal definition of the partial derivative w.r.t. time, of the field ϕ. A new notation for the outer integration measure is also introduced symbolising functional integration, but is identical to what is defined above:

$$\langle\phi_f| e^{-i\hat{H}(t_f-t_i)} |\phi_i\rangle = \int_{\phi(t_i)=\phi_i}^{\phi(t_f)=\phi_f} \mathcal{D}\phi\mathcal{D}\pi \exp\left\{ i \int_{t_I}^{t_f} \mathrm{d}t \int \mathrm{d}^{d-1}x \left(\pi \frac{\partial\phi}{\partial t} - \mathcal{H}(\phi,\pi) \right) \right\} . \tag{1.5}$$

1.1 Transition amplitudes for bosons

To continue the calculations from Eq. (1.5), we will choose a simple Hamiltonian describing a system of scalar fields with a standard kinetic term and a momentum independent potential,

$$\mathcal{H} = \frac{1}{2}\pi^2 + \frac{1}{2}\big(\nabla\phi\big)^2 + \frac{1}{2}m^2\phi^2 + U(\phi). \tag{1.6}$$

Even though this might seem simple, it can be easily extended to other fields by using the associated kinetic term. Actually, the Hamiltonian describing the famous Standard Model of particle physics is this form, only extended to all the various fields. Inserted into Eq. (1.5), we have

$$\langle\phi_f, t_f|\phi_i, t_i\rangle = \lim_{N\to\infty} \int \mathcal{D}\phi\mathcal{D}\pi \exp\Bigg\{ \sum_{i=1}^{N} \int \mathrm{d}^{d-1}x \Big[i\pi_i(\phi_{i+1} - \phi_i) \\ - i\Delta t \Big(\tfrac{1}{2}\pi_i^2 + \tfrac{1}{2}(\nabla\phi_i)^2 + \tfrac{1}{2}m^2\phi_i^2 + U(\phi_i) \Big) \Big] \Bigg\}. \tag{1.7}$$

The fields are all discretised in time, but also need to be discretised in space for us to be able to evaluate the integrals. This we do by dividing space into M^3 boxes with sides of length a and

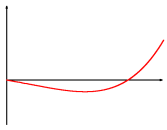

take the limit $a \to 0$. To make sure we keep track of all dimensionfull quantities, we substitute π_i with a dimensionless one $\pi_i(\mathbf{x}) = \rho_i(\mathbf{x})/\sqrt{a^3\Delta t}$. As the π's in Eq. (1.7) is term by term only dependent upon the current space-time coordinate, we end up with NM^3 Gaussian integrals that can be evaluated using Eq. (B.4),

$$\int_{-\infty}^{\infty} \frac{\mathrm{d}\rho_j}{2\pi} \exp\left\{ -i\tfrac{1}{2}\rho_j^2 + i\sqrt{\frac{a^3}{\Delta t}}(\phi_{j+1} - \phi_j)\rho_j \right\} = \frac{1}{\sqrt{2\pi i}} \exp\left\{ \frac{ia^3(\phi_{j+1} - \phi_j)^2}{2\Delta t} \right\}. \tag{1.8}$$

Taking the continuum limit again in both space and time yields the final result

$$\begin{aligned} \langle \phi_f, t_f | \phi_i, t_i \rangle &= \left(\frac{1}{2\pi i a^3 \Delta t} \right)^{(NM^3/2)} \int \mathcal{D}\phi \exp\left\{ i \int \mathrm{d}t \int \mathrm{d}^{d-1}x \left[\tfrac{1}{2}\left(\frac{\partial\phi}{\partial t}\right)^2 - \tfrac{1}{2}(\nabla\phi)^2 - \tfrac{1}{2}m^2\phi^2 - U(\phi) \right] \right\}, \\ &= C \int \mathcal{D}\phi \exp\left\{ i \int \mathrm{d}t \int \mathrm{d}^{d-1}x \, \mathcal{L}(\partial_\mu\phi, \phi) \right\}. \end{aligned} \tag{1.9}$$

The term in the exponential is known as the action, $S = \int \mathrm{d}t\, L = \int_x \mathcal{L}$. To get a physical interpretation of this result, it is easier to turn to the quantum mechanical result. Assume we have a particle at position x_i at time t_i, and want to calculate the probability that it is at position x_f at time t_f. Analogous to the calculation we just did, the transition amplitude is given as

$$\langle x_f | x_i \rangle = \int \left(\prod_{n=1}^{N} \mathrm{d}x_n \right) e^{i\int_{t_i}^{t_f} L(x_n, \dot{x}_n)}. \tag{1.10}$$

The transition amplitude can therefore be interpreted as the interference between all possible paths in space the particle can take to get from position x_i to position x_t. The phase associated with each path is given by the action said path generated. This method for calculating the transition amplitudes is therefore often referred to as the *path-integral formalism*. In an analogous manner, the transition amplitudes in field theory is the sum of all intermediate field configurations the field ϕ can take "moving" from configuration ϕ_i to configuration ϕ_f.

1.2 Generating functional

The transition function calculated in Eq. (1.9) calculates the probability for a state given at time t_i evolving into a specific state at time t_f. Usually what happens both before and after the measured time, as well as everything happening in the background is irrelevant. It is therefore customary to simplify it by choosing both $|\phi_i\rangle$ and $|\phi_f\rangle$ to be the vacuum state $|\Omega\rangle$, and take the limits $t_i \to -\infty$ and $t_f \to \infty$. Now that we have removed the initial and final state from the transition, how can this predict any physics? In the spirit of quantum mechanics, we promote the field ϕ to an operator and expand it in Fourier space,

$$\hat{\phi}(x) = \int \frac{\mathrm{d}^3p}{(2\pi)^3\sqrt{2E_{\mathbf{p}}}} \left(\hat{a}_{\mathbf{p}} e^{-ipx} + \hat{a}^\dagger_{\mathbf{p}} e^{ipx} \right). \tag{1.11}$$

$\hat{a}_{\mathbf{p}}$ and $\hat{a}^\dagger_{\mathbf{p}}$ are the annihilation and creation operators respectively of states with particles having momentum $\mathbf{p}$. Meaning that

$$\hat{a}^\dagger_{\mathbf{p}} |\Omega\rangle = |\mathbf{p}\rangle, \tag{1.12}$$

$$\hat{a}_{\mathbf{p}} |\mathbf{p}\rangle = |\Omega\rangle, \tag{1.13}$$

in which $|\mathbf{p}\rangle$ is a one particle state with momentum $\mathbf{p}$. Transitions from a state with a set of particles to another state with another set of particles can therefore be expressed using the correlation functions:

$$G_n(x_1, x_2, \ldots, x_n) = \langle\Omega|T\big\{\phi(x_1)\phi(x_2)\cdots\phi(x_n)\big\}|\Omega\rangle\,, \tag{1.14}$$

where T is the time ordering operator making sure that for instance destruction of a particle cannot happen before is has been created. The relation between the transition amplitude and the correlation function is summed up in the Lehmann-Symanzik-Zimmermann (LSZ) reduction formula which we will not go into here. A full derivation can be found in introductory books on the subject, e.g. [5, 6]. Using the results from the transition amplitude calculations, the correlation functions (also called n-point functions) can be expressed on integral form:

$$\langle\Omega|T\big\{\phi(x_1)\phi(x_2)\cdots\phi(x_n)\big\}|\Omega\rangle = N^{-1}\int \mathcal{D}\phi\;\phi(x_1)\phi(x_2)\cdots\phi(x_n)\exp\Big\{i\int \mathrm{d}^d x\,\mathcal{L}(\partial_\mu\phi,\phi)\Big\}. \tag{1.15}$$

In the above expression N is a normalisation constant. We want the probability normalised so that $\langle\Omega|\Omega\rangle = 1$, implying that

$$N = \int \mathcal{D}\phi\exp\Big\{i\int \mathrm{d}^d x\,\mathcal{L}\Big\}. \tag{1.16}$$

There exists a simpler method for calculating these correlation functions based on an object called the *generating functional*. Suppose we included a new term in the action in the form of an external source $J(x)$ coupled to the field

$$\int \mathrm{d}^d x\,J(x)\phi(x). \tag{1.17}$$

We call the resulting object the generating functional and denote it $W[J]$ (also often written $Z[J]$),

$$W[J] = \int \mathcal{D}\phi\exp\Big\{i\int \mathrm{d}^d x\,\big[\mathcal{L} + J(x)\phi(x)\big]\Big\}. \tag{1.18}$$

Taking the functional derivative of W with respect to J, then setting $J = 0$, results in

$$\frac{1}{iW[0]}\frac{\delta}{\delta J(x_1)}W[J]\Big|_{J=0} = \frac{1}{W[0]}\int \mathcal{D}\phi\;\phi(x_1)\exp\Big\{i\int \mathrm{d}^d x\,\mathcal{L}\Big\}, \tag{1.19}$$

which is exactly the correlation function of one field at position x_1. This is easily generalised, and the correlation functions can therefore be conveniently expressed as derivatives of the generating functional

$$\langle\Omega|T\big\{\phi(x_1)\phi(x_2)\cdots\phi(x_n)\big\}|\Omega\rangle = \frac{1}{W[0]}\frac{\delta}{i\delta J(x_1)}\frac{\delta}{i\delta J(x_2)}\cdots\frac{\delta}{i\delta J(x_n)}W[J]\Big|_{J=0}. \tag{1.20}$$

If the Lagrangian is a dependent on more than one field, every field can have a separate external source coupled to it. For example Lagrangians with fermionic fields will have one source $\bar\eta$ coupled to the Dirac field ψ, and another source η coupled to the Dirac adjoint of ψ:

$$W[\eta,\bar\eta] = \int \mathcal{D}\bar\psi\psi\exp\Big\{i\int \mathrm{d}^d x\,\big[\mathcal{L}(\psi,\bar\psi) + \bar\eta\psi + \bar\psi\eta\big]\Big\}. \tag{1.21}$$

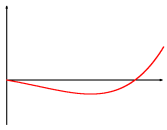

1.3 Symmetries

Now that the basics of QFT has been introduced we turn to a short analysis of the symmetries of the transition amplitudes. Then we state and prove Noether's theorem, which will be important when we later wish to couple the quarks to a quark number chemical potential.

Symmetries of the Lagrangian

Arguably the most important symmetries are those of the Lagrangian itself, as one usually defines a physical system by its Lagrangian density and not e.g. its action. In fact, there are many situations where one requires the Lagrangian to be invariant under certain transformations, and in that way constructs the Lagrangian based on which symmetries it must satisfy. For example the Lagrangian of a relativistic model must be invariant under a Lorentz boost, implying that only terms where all Lorentz indices have been contracted are allowed.

Symmetries of the action

While all symmetries of the Lagrangian also are symmetries of the action, there exists transformations that are symmetries of the action, but not the Lagrangian. To see this, assume we have a transformation which adds a total derivative to the Lagrangian density

$$\mathcal{L} \to \mathcal{L} + \partial_\mu \mathcal{J}^\mu. \tag{1.22}$$

The corresponding action is

$$S' = \int_V \mathrm{d}x\, \mathcal{L} + \partial_\mu \mathcal{J}^\mu = S + \int_\Omega \mathrm{dS}\, \hat{n} \cdot \vec{\mathcal{J}}, \tag{1.23}$$

where we used the divergence theorem to convert the integral over $\partial_\mu \mathcal{J}^\mu$ to a surface integral. If the flux running out of the surface Ω is zero (which is often the case for physical current densities), the action is invariant under the transformation of Ref. (1.22).

Euler-Lagrange equation

The equations of motion in classical mechanics can actually be expressed as a symmetry of the action. In classical mechanics, the physical field configuration is that which minimises the action. At the minimum, the derivative of the action with respect to ϕ and $\partial\phi$ is zero, and therefore the action should be invariant under an infinitesimal transformation of these two quantities

$$S(\phi + \delta\phi, \partial\phi + \delta\partial\phi)\big|_{\phi_0} = S(\phi, \partial\phi)\big|_{\phi_0}. \tag{1.24}$$

Rewriting this using the definition of the action, we get

$$\begin{aligned} S\big(\phi + \delta\phi, \partial\phi + \partial\delta\phi\big) &= \int \mathrm{d}x\, \mathcal{L}\big(\phi + \delta\phi, \partial\phi + \partial\delta\phi\big), \\ &= \int \mathrm{d}x \left\{ \mathcal{L}\big(\phi, \partial\phi\big) + \frac{\partial\mathcal{L}}{\partial\phi}\delta\phi + \frac{\partial\mathcal{L}}{\partial\partial_\mu\phi}\partial_\mu\delta\phi \right\}, \\ &= \int \mathrm{d}x \left\{ \mathcal{L}\big(\phi, \partial\phi\big) + \Big[\frac{\partial\mathcal{L}}{\partial\phi} - \partial_\mu \frac{\partial\mathcal{L}}{\partial\partial_\mu\phi}\Big]\delta\phi \right\} + \underbrace{\int_\Omega \mathrm{dS}\, \hat{n}_\mu \frac{\partial\mathcal{L}}{\partial\partial_\mu\phi}\delta\phi}_{=0}, \\ &= S(\phi, \partial\phi) + \int \mathrm{d}x \Big[\frac{\partial\mathcal{L}}{\partial\phi} - \partial_\mu \frac{\partial\mathcal{L}}{\partial\partial_\mu\phi}\Big]\delta\phi. \end{aligned} \tag{1.25}$$

The surface integral in the third line is zero because the variation of the field must be zero at the boundary ($\delta\phi(\Omega) = 0$). Comparing Eqs. (1.24) and (1.25), we see that the last term must be zero for the action to be invariant. The deviation from the minimum, $\delta\phi$, is arbitrary, and therefore the expression in the parenthesis must vanish, giving the equations

$$\partial_\mu \frac{\partial \mathcal{L}}{\partial \partial_\mu \phi} = \frac{\partial \mathcal{L}}{\partial \phi}. \tag{1.26}$$

These are the equations of motion for the classical field ϕ, also known as the Euler-Lagrange equations.

Noether's theorem

Noether's theorem is an important result in field theory which summarises the connection between continuous symmetries and conservation laws. The theorem is as follows:

> For every continuous symmetry there exists a conserved current (j^μ) corresponding to that symmetry

Proof:

A continuous transformation is one where the field can be transformed by an infinitesimal amount ($\phi \longrightarrow \phi + \delta\phi$). Inserted into the Lagrangian:

$$\begin{aligned} \mathcal{L}\big(\phi + \delta\phi, \partial\phi + \partial\delta\phi\big) &= \mathcal{L} + \frac{\partial \mathcal{L}}{\partial \phi}\delta\phi + \frac{\partial \mathcal{L}}{\partial \partial_\mu \phi}\partial_\mu \delta\phi, \\ &= \mathcal{L} + \partial_\mu\Big(\frac{\partial \mathcal{L}}{\partial \partial_\mu \phi}\delta\phi\Big) + \Big[\frac{\partial \mathcal{L}}{\partial \phi} - \partial_\mu \frac{\partial \mathcal{L}}{\partial \partial_\mu \phi}\Big]\delta\phi, \end{aligned} \tag{1.27}$$

where we have written one of the terms as a total derivative plus a partial derivative, similar to the partial integration done in Eq. (1.25). The expression in the [ ]-bracket is the Euler-Lagrange equation, and is therefore zero. As noted previously, a symmetry transformation of the action is one which at most adds a total derivative to the Lagrangian. Therefore we can equate the right hand sides of Eqs. (1.22) and (1.27), and we are left with a conservation law,

$$\partial_\mu\Big(\frac{\partial \mathcal{L}}{\partial \partial_\mu \phi}\delta\phi - \mathcal{J}_\mu\Big) = 0 \equiv \partial_\mu j^\mu. \tag{1.28}$$

The conserved current, j^μ is often called the Noether current, emphasising that it is a conserved current corresponding to a continuous symmetry. There is an analogue to Noether's theorem in QFT, where every continuous symmetry has a Schwinger-Dyson equation associated with its Noether current conservation law. We will not derive this here, but a derivation can be found in [6], pp. 308.

Example: $U(1)$ symmetry

Probably the simplest demonstration of Noether's theorem is by constructing a $U(1)$ symmetric Lagrangian and applying Noether's theorem to an infinitesimal $U(1)$ symmetry transformation. The Lagrangian of a massive, noninteractive complex field ϕ is

$$\mathcal{L} = \tfrac{1}{2}\partial_\mu \phi^* \partial^\mu \phi - \tfrac{1}{2}m^2 \phi^* \phi. \tag{1.29}$$

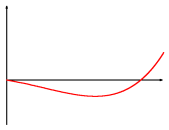

A complex field has two independent components, and we will therefore treat ϕ and ϕ^* as independent fields. One can easily see that the above Lagrangian is symmetric under a $U(1)$ transformation, $\phi \longrightarrow e^{i\alpha}\phi$ and $\phi^* \longrightarrow e^{-i\alpha}\phi$, where α is a constant. On infinitesimal form, these transformations are

$$\phi \longrightarrow \phi + i\alpha\phi \ , \tag{1.30}$$
$$\phi^* \longrightarrow \phi^* - i\alpha\phi^*, \tag{1.31}$$

from which we can see that $\delta\phi = i\alpha\phi$ and $\delta\phi^* = -i\alpha\phi^*$. As the Lagrangian was constructed to be invariant under a $U(1)$ symmetry, this is not only a symmetry of the action, but also the Lagrangian, meaning that the current $\mathcal{J}^\mu$ in Eq. (1.28) is zero. The Noether current is therefore

$$j_\mu = \tfrac{1}{2}i\phi\partial_\mu\phi^* - \tfrac{1}{2}i\phi^*\partial_\mu\phi = \mathfrak{Im}\big[\phi^*\partial_\mu\phi\big], \tag{1.32}$$

which can be shown to be the number density four-current of the complex field ϕ.

1.4 Abelian gauge theories

In the previous example we described a theory which was invariant under a global continuous transformation, meaning that the phase of the $U(1)$ transformation is the same for all space-time coordinates. It is interesting to see how we can promote this symmetry to be local ($\alpha \longrightarrow \alpha(x)$). A theory invariant under such a local continuous symmetry is referred to as a *gauge theory*. To illustrate, let us return to the $U(1)$ symmetric Lagrangian.

Example: $U(1)$

Transforming the Lagrangian in Eq. (1.29) using a space-time dependent phase $\alpha(x)$ we end up with the following:

$$\begin{aligned}\mathcal{L}' &= \partial_\mu\big(e^{-i\alpha(x))}\phi^*\big)\partial^\mu\big(e^{i\alpha(x)}\phi\big) - m^2\phi^*\phi, \\ &= \mathcal{L} + i\phi\partial_\mu\alpha\partial^\mu\phi^* - i\phi^*\partial_\mu\alpha\partial^\mu\phi + \phi^*\phi\partial_\mu\alpha\partial^\mu\alpha.\end{aligned} \tag{1.33}$$

This Lagrangian is clearly not invariant under a local $U(1)$ transformation, and we see that the problem resides in the derivative terms. When α was a constant, the two operations of transforming the field ϕ and taking the derivative of ϕ commuted, and we could therefore pull the factor $e^{i\alpha}$ outside the derivative and cancel it with the factor coming from ϕ^*, just as we do for the mass term. Therefore, to ensure gauge invariance of the Lagrangian in Eq. (1.29) we introduce a new derivative D_μ, called the covariant derivative, which also transforms under the gauge transformation in such a way as to cancel the term caused by the commutator of ∂ and $e^{i\alpha(x)}$:

$$\partial^\mu \longrightarrow D^\mu = \partial^\mu + iA^\mu, \tag{1.34}$$

where the gauge transform of the gauge field A_μ is

$$A^\mu \longrightarrow A^\mu - \partial^\mu\alpha, \tag{1.35}$$

The definition of the covariant derivative ensures that

$$D_\mu(A)\phi \longrightarrow D_\mu(A')e^{i\alpha(x)}\phi = e^{i\alpha(x)}D_\mu(A)\phi, \tag{1.36}$$

which implies that the new Lagrangian where we have replaced derivatives with covariant derivatives

$$\mathcal{L} = \tfrac{1}{2}\big(D_\mu\phi\big)^*\big(D^\mu\phi\big) - \tfrac{1}{2}m^2\phi^*\phi, \tag{1.37}$$

is invariant under a local $U(1)$ symmetry transformation, but what is the meaning of these gauge fields? In its current state we see that the gauge fields are coupled to ϕ, but they are not propagating as there are no kinetic terms associated with them. We are allowed to include such a term in the Lagrangian but it must also be gauge invariant. An example of such a kinetic term can be found in electrodynamics, namely the electrodynamic field-strength tensor

$$F^{\mu\nu} = \partial^\mu A^\nu - \partial^\nu A^\mu. \tag{1.38}$$

Which when contracted with itself gives the Lagrangian of the electromagnetic fields

$$\mathcal{L} = -\frac{1}{4}F^{\mu\nu}F_{\mu\nu} = -\frac{1}{2}\big(\mathbf{E}^2 - \mathbf{B}^2\big). \tag{1.39}$$

With the gauge field A_μ behaving suspiciously like the electrodynamic four-potential, one would suspect that A_μ can be used to describe photons. In fact, gauging with the $U(1)$ symmetry group is one of the easiest ways to couple a theory to electrodynamics. The substitution of the derivative with the covariant derivative can be seen as field theory's answer to the minimal substitution often used in particle mechanics, and the gauge transformation of of the gauge field A_μ is the same as the gauge transformation of electrodynamic four-potential. In a similar manner the weak force is described by an $SU(2)$ gauge symmetry and the strong force by an $SU(3)$ gauge symmetry, but as neither of these symmetry groups are Abelian, there are some complications which we will tackle in Sec. 5.

1.5 Symmetry breaking

Now that we have analysed symmetries and their usefulness in QFT we will turn our attention to the dynamics behind breaking these symmetries. Spontaneous symmetry breaking (SSB) and the appearance of Goldstone bosons is of particular interest.

Breaking of a discrete symmetry

First of all, let us look at breaking of a discrete symmetry. The simplest discrete symmetry is the Z_1 symmetry, an example of a Z_1 symmetric Lagrangian is

$$\mathcal{L} = \tfrac{1}{2}\partial_\mu\phi\partial^\mu\phi - \tfrac{1}{2}m^2\phi^2 - \tfrac{1}{4}\lambda\phi^4 \equiv \tfrac{1}{2}\partial_\mu\phi\partial^\mu\phi - U(\phi). \tag{1.40}$$

Knowing that classical dynamics is governed by configurations which minimises the energy, the minimum of the potential $U(\phi)$ is of some interest as the quantum ground state of the system should be close to this values. The minimum is given by

$$\phi_0 = \begin{cases} 0 & m^2 > 0, \\ \pm\sqrt{-\frac{m^2}{\lambda}} & m^2 < 0. \end{cases} \tag{1.41}$$

If we have a mass parameter less than zero, we have two possible minima to choose from. While they are themselves related by a Z_1 transformation, choosing a minimum breaks Z_1 symmetry as

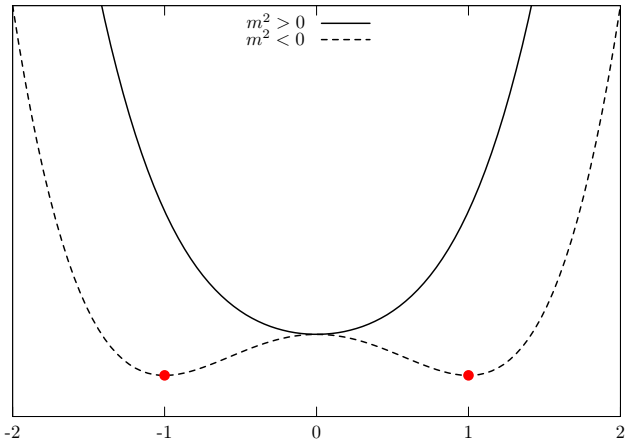

Figure 1.1: Discrete spontaneous symmetry breaking.

the ground state is not Z_1 symmetric. This is what is known as spontaneous symmetry breaking, its name owing to the fact that we "spontaneously" break the symmetry at the point of choosing a minimum. An illustration is given in Fig. 1.1.

A little side note. One can argue that the choice $m^2 < 0$ is not physical, as no particle can have imaginary mass. But by analysing the fluctuations around the minimum, which is why were interested in the minimum in the first place, we see that the fluctuating fields ($\phi = \phi_0 + \tilde{\phi}$) has acquired a positive mass $\sqrt{2}m$

$$U(\tilde{\phi}) \approx U(\phi_0) + \frac{1}{2}U''(\phi_0)\tilde{\phi}^2 = U_0 + |m^2|\tilde{\phi}^2. \tag{1.42}$$

Breaking of a continuous symmetry

The simplest example of a continuous symmetry being spontaneously broken can be studied by simply expanding the previous example to be $O(2)$ symmetric by including an additional independent field ($\phi \longrightarrow \phi = [\phi_1, \phi_2]$):

$$\mathcal{L} = \tfrac{1}{2}\partial_\mu\phi_1\partial^\mu\phi_1 + \tfrac{1}{2}\partial_\mu\phi_2\partial^\mu\phi_2 - \tfrac{1}{2}m^2\big(\phi_1^2 + \phi_2^2\big) - \tfrac{1}{4}\lambda\big(\phi_1^2 + \phi_2^2\big)^2. \tag{1.43}$$

If $m^2 < 0$, the minima satisfies $m^2 + \lambda(\phi_1^2 + \phi_2^2) = 0$. This time the minima are located on the circle $(\phi_1^2 + \phi_2^2) = -m^2/\lambda$, and once again we have to choose. Choosing $\phi_{1_0} = \sqrt{-m^2/\lambda}$, $\phi_{2_0} = 0$, and expanding the fields around this solution, we obtain

$$\mathcal{L} = \tfrac{1}{2}\big(\partial_\mu\tilde{\phi}_1\big)^2 + \tfrac{1}{2}\big(\partial_\mu\tilde{\phi}_2\big)^2 - |m^2|\tilde{\phi_1}^2 - U_0 + \mathcal{O}(\tilde{\phi}^3). \tag{1.44}$$

Again, even though we chose $m^2 < 0$, a physical particle with positive mass appears, but also a particle with no mass at all (here $\tilde{\phi}_2$). Looking at a plot of the potential in Fig. 1.2, we can identify the massive particle as fluctuations perpendicular to the minimum curve (the red curve), and the massless mode as fluctuations parallel to it. The massless mode is normally named the Goldstone boson, as it is predicted by Goldstone's theorem.

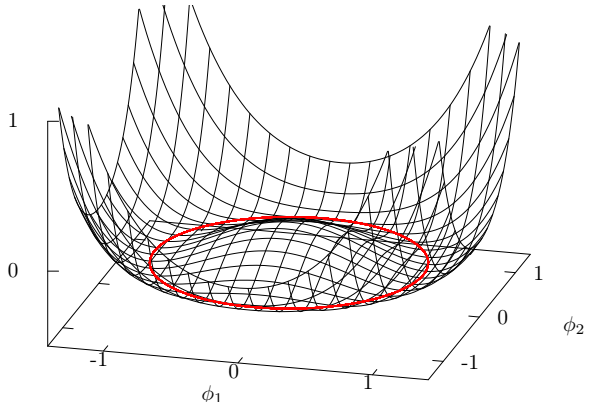

Figure 1.2: Breaking of a continuous symmetry.

Goldstone's theorem

> For every spontaneously broken continuous symmetry, there appears at least one massless particle. The number of massless particles is equal to the number of generators of the broken group [7].

Proof:

Assume we have a Lagrangian on the form:

$$\mathcal{L} = (\text{kinetic terms}) - U(\phi_i), \tag{1.45}$$

with N fields, ϕ_i. Expanding the potential around its minimum, we get

$$U(\phi_i) = U(\phi_{i0}) + \tfrac{1}{2}(\phi_i - \phi_{i0})(\phi_j - \phi_{j0}) \frac{\partial^2 U}{\partial\phi_i \partial\phi_j}\bigg|_{\phi_{i0},\phi_{j0}} + \ldots, \tag{1.46}$$

where the double derivatives are positive as ϕ_0 is the minimum of U. A continuous transformation of the field ϕ can be written on its infinitesimal form:

$$\phi_i \longrightarrow \phi_i + \delta\phi_i. \tag{1.47}$$

The system is symmetric under this transformation, and therefore $U(\phi + \delta\phi) = U(\phi)$. Expanding the left hand side around $\delta\phi = 0$, we get

$$U(\phi_i) = U(\phi_i + \delta\phi_i) \implies \delta\phi_i \frac{\partial U}{\partial \phi_i} = 0. \tag{1.48}$$

Differentiating this expression with respect to ϕ_j and evaluating it at the minimum, we get

$$\left(\frac{\partial \delta\phi_i}{\partial \phi_j}\right)_{\phi_0} \left(\frac{\partial U}{\partial \phi_i}\right)_{\phi_0} + \delta\phi_i \left(\frac{\partial^2 U}{\partial\phi_i \partial\phi_j}\right)_{\phi_0} = 0, \tag{1.49}$$

where the first term is zero, being the definition of the minimum. This implies that in any direction ϕ_j in which $\delta\phi_j \neq 0$, the double derivative is zero, and looking at the series expansion in Eq. (1.46) this corresponds to a massless particle. These directions are exactly those in which the symmetry has been spontaneously broken, proving Goldstone's theorem. Additional proofs of Goldstone's theorem can be found in a paper by Goldstone, Salam and Weinberg form 1962 [8].

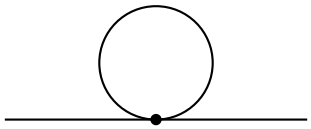

Figure 1.3: The tadpole diagram.

1.6 Renormalisation

We will in this section look at some examples of perturbative renormalisation before we move on to more advanced methods in Sec. 3. A simple $\lambda\phi^4$ theory will be used to illustrate. The Lagrangian for this system has already been written down multiple times, and is

$$\mathcal{L}_{\lambda\phi^4} = \tfrac{1}{2}\partial_\mu\phi\partial^\mu\phi - \tfrac{1}{2}m^2\phi^2 - \tfrac{1}{4!}\lambda\phi^4. \tag{1.50}$$

It is common to make use of the Feynman diagrams for keeping track of calculations in QFT. We will not go into the formalism behind these diagrams, as a more complete overview can be found in any introductory QFT text, e.g. [5, 6]. The Feynman rules for $\lambda\phi^4$ are

$= \dfrac{i}{p^2 - m^2},$
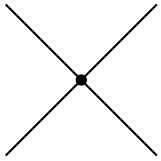
$= -i\lambda.$ (1.51)

First let us calculate the "tadpole diagram" shown in figure 1.3. Using the Feynman rules given in Eq. (1.51), the diagram is given by the expression

$$\mathcal{M}_{1\to1} \propto \lambda \int_q \frac{1}{q^2 - m^2}. \tag{1.52}$$

The momentum q is a variable in Minkowski space, but we can rotate the time-component to the imaginary axis (known as a Wick-rotation) and we get the expression below in d-dimensional Euclidean space

$$\mathcal{M}_{1\to1} \propto \lambda \int \frac{\mathrm{d}^d q}{q^2 + m^2}. \tag{1.53}$$

If d is larger than, or equal to, 2, this expression diverges for large q. We therefore have to find a way to rid ourselves of such divergences, but first a quick note. One might wonder what the quantity $\mathcal{M}$ in the calculations above is. It is related to the transition amplitudes in the following way,

$$\langle \phi_{f1}, \phi_{f2}, \ldots, \phi_{fn} | \phi_{i1}, \phi_{i2}, \ldots, \phi_{im} \rangle = (2\pi)^4 \delta\big(\text{en-mom. cons.}\big) i\mathcal{M}_{if} \tag{1.54}$$

Also, unless otherwise stated, all calculations involving diagrams are "amputated", meaning that external lines have the Feynman rules,

$= 1,$

$= 1.$ (1.55)

Regularisation

To be able to cure such divergences, some measure of their divergence is needed, one cannot simply cancel infinity with infinity unless it is known that they cancel. The process of getting an analytic expression for divergent terms in QFT is referred to as regularisation. There are multiple schemes to follow when regularising a theory, and each of them have different virtues. We will use cut-off regularisation for this example as it is easy to implement and easy to grasp. Other options include dimensional regularisation[9], Pauli-Villars regularisation [10], lattice regularisation and Schwinger's proper time regularisation [11].

With cut-off regularisation one only takes momentum integrals up to some cut-off scale Λ by either cutting the integration sharply at that scale ($\int^{\infty} \to \int^{\Lambda}$), or by introducing a smooth cut-off function, an example of which we will see in Sec. 3.4. Applying a sharp cut-off to Eq. (1.53), we get:

$$\mathcal{M}_{1\to 1} = i\lambda \frac{2\pi^2}{2(2\pi)^4} \int_0^{\infty} \frac{q^3 \mathrm{d}q}{q^2+m^2} \xrightarrow[Reg]{} \frac{-\lambda}{16\pi^2} \int_0^{\Lambda} \frac{q^3 \mathrm{d}q}{q^2+m^2} = \frac{-\lambda}{32\pi^2}\left[\Lambda^2 - m^2 \log\Big(\frac{m^2+\Lambda^2}{m^2}\Big)\right]. \quad (1.56)$$

Even though we have gained an analytic result for the contribution of the tadpole diagram, it is still clearly ambiguous. The scale Λ is somewhat arbitrary and in the end we would like to take the limit $\Lambda \to \infty$.

Renormalisation

It is time to cure the divergences accumulated so far. To motivate the method of renormalisation, we will first look at how the propagator is altered by the inclusion of loop diagrams in general, but first, some notation is needed.

Diagrams can be conveniently grouped depending on how many sub diagrams they contain. Those which cannot be divided into sub diagrams, are called one particle irreducible (1PI). Diagrams that can be cut into two 1PI diagrams are called 2PI and so on. For example the diagram

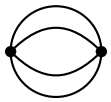

is 1PI, while the diagram

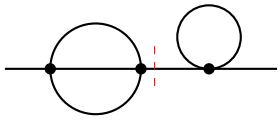

is 2PI as it can be cut into two 1PI diagrams (illustrated by the dashed line). All definitions aside, let iM^2 denote all propagator like 1PI diagrams (one incoming and one outgoing line):

$iM^2 =$ 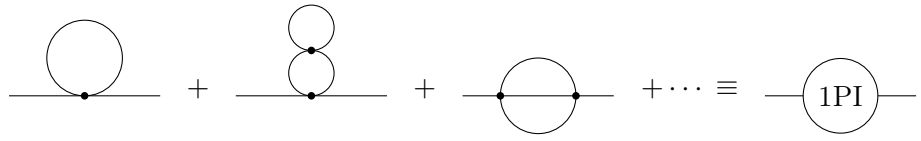 (1.57)

The exact propagator is the two-point function ($\langle\Omega|\,\phi_f\phi_i\,|\Omega\rangle$), which includes all propagator like diagrams. In terms of iM^2 defined above, it reads:

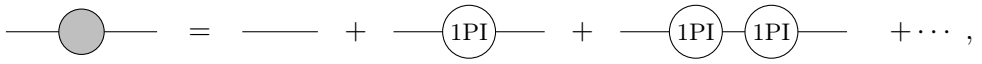

$$
\begin{aligned}
&= \frac{i}{p^2-m^2} + \frac{i}{p^2-m^2} iM^2 \frac{i}{p^2-m^2} + \frac{i}{p^2-m^2} iM^2 \frac{i}{p^2-m^2} iM^2 \frac{i}{p^2-m^2} + \cdots, \\
&= \frac{i}{p^2-m^2} \sum_{n=0}^{\infty} \left(iM^2 \frac{i}{p^2-m^2} \right)^n = \frac{i}{p^2-m^2} \frac{1}{1 - iM^2 \frac{i}{p^2-m^2}} = \frac{i}{p^2-m^2+M^2}.
\end{aligned} \tag{1.58}
$$

The exact propagator therefore describes the propagation of a particle with mass $m^2 - M^2$. Since the exact propagator is the proper one, one would argue that the parameter m^2 is somewhat misleading as it does not give the physical mass at all. Using $m_0^2 = m^2 - M^2$, we should rewrite the Lagrangian to be dependent upon the proper mass parameter

$$
\mathcal{L}_{\lambda\phi^4} = \tfrac{1}{2}\partial_\mu\phi\partial^\mu\phi - \tfrac{1}{2}m_0^2\phi^2 - \tfrac{1}{2}M^2\phi^2 - \tfrac{1}{4}\lambda\phi^4. \tag{1.59}
$$

The theory is said to have been renormalised, and M^2 is commonly called the mass counter term (often written δm^2 to signify this). Similar to this, both λ and Z (the field strength, unrenormalised it is one, $Z\phi = 1\phi$) need to be renormalised when other loop diagrams are included. In perturbation theory, just as the loop diagrams are calculated order by order in λ, the parameters are renormalised order by order. Therefore the parameters are written down order by order:

$$
m^2 = \sum_{i=0}^{\infty} m_i^2 \lambda^i, \tag{1.60}
$$

$$
\lambda = \sum_{i=0}^{\infty} g_i \lambda^i, \tag{1.61}
$$

where m_0 and g_0 are the fully renormalised parameters. Renormalised parameters are often called "dressed" parameters, while nonrenormalised ones are called "bare". In the previous example we calculated iM^2 to first order in λ, which translates to

$$
m_1^2 = -\frac{1}{32\pi^2}\left[\Lambda^2 - m_0^2 \log\left(\frac{m_0^2+\Lambda^2}{m_0^2}\right)\right]. \tag{1.62}
$$

2 Thermal field theory

QFT is a formalism mostly used to predict the physics of quantum systems in a vacuum. Thermal field theory (TFT) on the other hand, even though mathematically very similar to QFT, aims at calculating ensemble properties of a given model. For example thermodynamic pressure, particle density, free energy and other quantities often related to the domain of thermodynamics and statistical mechanics. Despite the apparent difference between the two, they are closely related, and many of the methods and phenomena encountered in QFT are also present in TFT. They are after all the same theory only applied to different systems. While a brief overview of TFT will be given in this section, a more thorough approach can be found in introductory text books on the subject [12, 13].

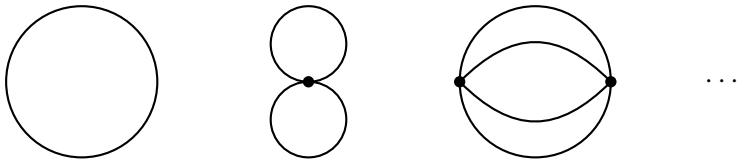

Figure 1.4: Vacuum diagrams.

Before we can introduce TFT, we need to define the grand canonical partition function, arguably the most fundamental object in statistical mechanics. For a system with possible energy states $E_{i,N}$ with N particles, at temperature T and chemical potential μ, we can associate a Boltzmann factor $\exp(-(E_{i,N} - \mu N)/T)$ to estimate how likely it is that the system occupies this configuration. As this is not a normalised probability, we need to multiply all such Boltzmann factors with a global normalisation constant $1/Z$, where

$$Z = \sum_{N,i} e^{-(E_{i,N}-\mu N)/T}. \tag{1.63}$$

and this normalisation constant is known as the grand canonical partition function. From it, a surprising amount of information can be extracted, more than one would think from a single object. A detailed description can be found in e.g. [14]. Converted to the language of quantum mechanics E should be promoted to the Hamilton operator and N to a particle density operator. All in all, the partition function is

$$\mathcal{Z} = \left\langle e^{-(\hat{H}-\mu\hat{N})/T} \right\rangle = \sum_n \langle \phi_n | \, e^{-(\hat{H}-\mu\hat{N})/T} \, |\phi_n\rangle \, . \tag{1.64}$$

Following the same steps as we did deriving an integral representation for the transition amplitude, we can find an integral representation of the partition function in QFT:

$$\mathcal{Z} = \int_{\phi(0)=\phi_0}^{\phi(\beta)=\phi_0} \mathcal{D}\phi\mathcal{D}\pi \, \exp\left\{ \int_0^\beta \mathrm{d}\tau \int \mathrm{d}^d x \left(i\pi \frac{\partial\phi}{\partial\tau} - \mathcal{H}(\phi,\pi) + \mu\mathcal{N}(\phi,\pi) \right) \right\}. \tag{1.65}$$

There are two major differences between this expression and the transition amplitudes in QFT. First, the time variable has been replaced by a new variable $t \longrightarrow -i\tau = -i\frac{1}{T} \equiv -i\beta$. Integrals over the new "space-time" is therefore in Euclidean space instead of Minkowski space, which is why TFT is often referred to as the Euclidean formalism, or the imaginary time formalism. Given a Lagrangian in QFT, it is converted to a Lagrangian of TFT by the simple substitution and redefinition

$$\mathcal{L}(t,\mathbf{x}) \longrightarrow \mathcal{L}(-i\tau,\mathbf{x}) \equiv -\mathcal{L}_E(\tau,\mathbf{x}). \tag{1.66}$$

The second major difference is the boundary condition. Where QFT had boundary conditions decided by the transition one wished to calculate, the boundary conditions for the partition function are periodic. In terms of Feynman diagrams this implies that only closed loop diagrams are allowed, also called vacuum diagrams. Some examples are illustrated in Fig. 1.4.

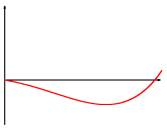

2.1 Thermodynamic quantities

With the simple replacements mentioned in the previous section, we can write down the TFT's equivalent to the generating functional

$$W[J] = \int \mathcal{D}\phi \exp\Big\{ - \int_0^\beta \mathrm{d}\tau \int \mathrm{d}^{d-1}x \left(\mathcal{L}_E(\phi) - J\phi\right)\Big\}. \tag{1.67}$$

This still has periodic boundary conditions, and therefore the relation to the partition function is trivial, $W[0] = \mathcal{Z}$. Using the partition function we can calculate both Helmholtz' and Gibbs' free energy. They are classically defined to be

$$F = -\frac{1}{\beta}\log(Z), \tag{1.68}$$

$$G = F + pV. \tag{1.69}$$

We can construct a functional form of Helmholtz' free energy analogous to the generating functional. It is given by:

$$\mathcal{F}[J] = -\frac{1}{\beta}\log(\mathcal{Z}[J]). \tag{1.70}$$

The functional form of Gibbs' free energy is a bit trickier. It can actually be defined as a Legendre transformation of Helmholtz' free energy (which is why we needed it on its functional form). We define ϕ_{cl} to be

$$\phi_{cl}(x) = \frac{\delta}{\delta J(x)}\mathcal{F}[J] = -\frac{1}{\beta}\frac{\int \mathcal{D}\phi\, \phi(x) e^{-\int(\mathcal{L}-J\phi)}}{\int \mathcal{D}\phi\, e^{-\int(\mathcal{L}-J\phi)}}. \tag{1.71}$$

Gibbs' free energy is then given by the Legendre transform:

$$\Gamma[\phi_{cl}] = -\mathcal{F}[J] + \int \mathrm{d}^d x\, J(x)\phi_{cl}(x). \tag{1.72}$$

As expected from a Legendre transformation, the field J can be recovered by taking the ϕ_{cl} derivative of $\Gamma[\phi_{cl}]$,

$$\frac{\delta}{\delta\phi_{cl}(x)}\Gamma[\phi_{cl}] = J(x). \tag{1.73}$$

From Helmholtz' free energy, the thermodynamic potential is defined as

$$\Omega = \frac{1}{V}F[0], \tag{1.74}$$

which can be used to obtain the pressure (P), the entropy (S), the particle number density (N) and the energy density ($\mathcal{E}$), which are given by [14]

$$P = -\Omega, \tag{1.75}$$

$$S = \frac{\partial P}{\partial T}, \tag{1.76}$$

$$N = \frac{\partial P}{\partial \mu}, \tag{1.77}$$

$$\mathcal{E} = \Omega + TS + \mu N. \tag{1.78}$$

2.2 Partition function for bosons

We want to calculate the partition function for a Lagrangian with a single scalar field ϕ, similar to what we did in Sec. 1.1. The TFT Lagrangian is

$$\mathcal{L}_E = \frac{1}{2}\Big(\frac{\partial\phi}{\partial\tau}\Big)^2 + \frac{1}{2}\big(\nabla\phi\Big)^2 + \frac{1}{2}m^2\phi^2 + U(\phi). \tag{1.79}$$

This Lagrangian does not have any continuous global symmetries, and looking to Noether's theorem, does not have any natural conserved charge to be associated with a chemical potential. $\mu\mathcal{N}$ is therefore set to zero. With a system in place, the integral over π in Eq. (1.65) is done analogous to the calculation in Sec. 1.1, and we end up with:

$$\mathcal{Z} = N\int \mathcal{D}\phi\,\exp\Big\{-\int_0^\beta \mathrm{d}\tau\int \mathrm{d}^d x\,\mathcal{L}_E(\partial_\mu\phi,\phi)\Big\}. \tag{1.80}$$

Letting $U(\phi)=0$ we can carry this calculation a bit further, but first we must Fourier transform the fields:

$$\phi(\tau,\mathbf{x}) = \sum_n\sum_{\mathbf{p}}\phi_{n,\mathbf{p}}e^{i(\omega_n\tau+\mathbf{x}\cdot\mathbf{p})}. \tag{1.81}$$

Because of the periodicity constraint on the field, $\phi(0,\mathbf{x})=\phi(\beta,\mathbf{x})$, $\omega_n = 2n\pi T$. Conversely, fermionic fields have an anti periodicity constraint, $\psi(0,\mathbf{p})=-\psi(\beta,\mathbf{p})$, implying $\nu_n=(2n+1)\pi T$, where ν_n is used instead of ω_n to signify this difference. Inserted into the action, we can carry out the integrals over τ and $\mathbf{x}$ to obtain

$$\begin{aligned} S &= \frac{1}{2}\sum_{n,m}\sum_{\mathbf{p},\mathbf{q}}\big(-\omega_n\omega_m - \mathbf{p}\cdot\mathbf{q}+m^2\big)\phi_{m,\mathbf{q}}\phi_{n,\mathbf{p}}\,\beta\delta_{n,-m}\,V\delta_{\mathbf{p},-\mathbf{q}},\\ &= \frac{1}{2}\beta V\sum_{n,\mathbf{p}}\big(\omega_n^2+\mathbf{p}^2+m^2\big)\phi_{-n,-\mathbf{p}}\phi_{n,\mathbf{p}}. \end{aligned} \tag{1.82}$$

The field ϕ is real, therefore $\phi_{-n,-\mathbf{p}}=\phi^*_{n,\mathbf{p}}=\phi_{n,\mathbf{p}}$ and the partition function is simply

$$\mathcal{Z} = N\int\Big(\prod_{n,\mathbf{p}}d\phi_{n,\mathbf{p}}\Big)\exp\Big\{-\beta V\frac{1}{2}\sum_{n,\mathbf{p}}\big(\omega_n^2+\mathbf{p}^2+m^2\big)\phi^2_{n,\mathbf{p}}\Big\}. \tag{1.83}$$

The field $\phi_{n,\mathrm{p}}$ has mass dimension 2, so we should change variables $\phi\longrightarrow\rho\sqrt{\beta/V}$. The integral is a simple Gaussian, and is evaluated using Eq. (B.3) with $A_{ij}=\frac{1}{2}\beta^2(\omega_i^2+\mathbf{p}_i^2+m^2)\delta_{i,j}$ resulting in:

$$\mathcal{Z} = N'\frac{1}{\sqrt{\det(A_{ij})}} = N'\prod_{n,\mathbf{p}}\frac{1}{\sqrt{\beta^2(\omega_n^2+\mathbf{p}^2+m^2)}}. \tag{1.84}$$

Our ultimate goal is to calculate either of the free energies, so we take the logarithm on both sides and obtain:

$$\log(\mathcal{Z}) = -\frac{1}{2}\mathrm{tr}\big[\log(A_{ij})\big]+K = -\frac{1}{2}\sum_{n,\mathbf{p}}\log\big[\beta^2(\omega_n^2+\mathbf{p}^2+m^2)\big]+K, \tag{1.85}$$

where the trace-log identity, $\log\big[\det(A_{ij})\big]=\mathrm{tr}\big[\log(A_{ij})\big]$, has been used. K is independent of β and V, and will therefore be discarded. The right hand side can either be calculated using the contour

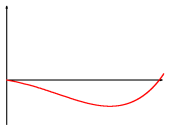

trick described in Appendix B.5, or by using a set of sum identities and mathematical tricks. As the contour sum is frequently used to calculate several other such sums, we will use it here as well to become familiar with it. The other approach is described in [12].

The logarithm has branch cuts instead of poles in the complex plane, and must be rewritten in a more convenient form before proceeding. Rewriting it as an integral

$$\log(\mathcal{Z}) = -\frac{1}{2}\sum_{\mathbf{p}}\sum_{n=-\infty}^{\infty}\int_{1}^{\beta^2(\mathbf{p}^2+m^2)} \mathrm{d}a^2\,\frac{1}{\beta^2\omega_n^2+a^2} + \log(\beta^2\omega_n^2+1), \tag{1.86}$$

we can pull the sum over n inside the integral over a^2, and obtain an expression similar to the formula derived in the appendix. Once again the last term is independent of both temperature and volume, and is discarded. Using the result from Eq. (B.17) we get

$$\log(\mathcal{Z}) = -\frac{1}{2}\sum_{\mathbf{p}}\int\frac{\mathrm{d}a^2}{2a}\big[1-2n_B(Ta)\big]. \tag{1.87}$$

Utilising

$$\int \mathrm{d}a\,\frac{1}{e^a-1} = \log(1-e^{-a}), \tag{1.88}$$

and throwing away constant terms, we end up with the final result

$$\log(\mathcal{Z}) = -\frac{1}{2}V\int \mathrm{d}\mathbf{p}\,\big[\beta\omega + 2\log(1-e^{-\beta\omega})\big], \tag{1.89}$$

where $\omega = \sqrt{\mathbf{p}^2+m^2}$. Using Eq. (1.70), we get the free energy to be

$$\mathcal{F} = \frac{1}{2}V\int \mathrm{d}\mathbf{p}\,\big[\omega + 2T\log(1-e^{-\beta\omega})\big]. \tag{1.90}$$

The first term is badly divergent as we carry out the integral over $\mathbf{p}$, but as this term is temperature independent, it is seen as a background energy. We can only measure differences in energy, and therefore it will never show up in any physical results. Based on this, the divergent term is commonly dropped.

3 Renormalisation group

In Sec. 1.6 we saw that calculations in QFT sometimes result in ultraviolet divergent terms, and that these need to be regularised and then renormalised for the theory to give physically sensible results. This should not come as a surprise as ultraviolet divergences are related to arbitrary high energy scales, at which we cannot even be certain that QFT is the correct theory, not to mention the Lagrangian density.

A good example of a similar ultraviolet catastrophe occurring in classical physics, is the energy radiation of a black body. Classically, the energy radiated from a black body at energy T in a small frequency interval $(\nu,\nu+\mathrm{d}\nu)$ is given by

$$I(\nu,T) = 2\pi\nu^2 T. \tag{1.91}$$

Calculating the total energy flow we integrate over all possible frequencies

$$J(T) = \int_0^\infty I(\nu, T)\,\mathrm{d}\nu = 2\pi T \int_0^\infty \nu^2\,\mathrm{d}\nu. \tag{1.92}$$

Analogous to the UV divergences of QFT, the integrand goes to infinity as $\nu \to \infty$. Large ν, or small wavelengths, is exactly what we struggle with calculating amplitudes of loop diagrams. When quantum mechanics was introduced in the early 20^{th} century, a recalculation of the energy flow resulted in Planck's distribution function

$$I(\nu, T) = \frac{4\pi^2\nu^3}{e^{2\pi\nu/T} - 1}. \tag{1.93}$$

For small ν, Eq. (1.93) can be series expanded in ν, and we recover Eq. (1.91). As an example, with $T = 1500K$, the classical expression is a good approximation for values up to $10^{13}s^{-1} = 6.58 \cdot 10^{-9}\text{MeV}$.

Therefore, in a very similar fashion, we expect there to be a different theory explaining physics at very high energies. The high energy particle accelerators are hard at work looking for results which deviate from the standard model of particle physics. For example CERN is quickly approaching proton-proton collisions with energies up to 14 TeV, but above this scale we do not know the validity of our theories.

3.1 Coupling renormalisation

In section 1.6 the notion of "bare" and "dressed" parameters was introduced. The "bare" parameters are the parameters of the Lagrangian, and they had to be renormalised to cure them of their energy scale dependence. This scale dependence is of some interest, and as we will see, it is normally described by differential equations called the renormalisation group equations (RGEs).

The physical interpretation of renormalisation is a bit different in the different fields of physics, but in high energy particle physics it is seen as a screening effect. The most easily grasped example comes from the screening of the electric charge due to vacuum polarisation. Heisenberg's uncertainty principle states that $\Delta x \Delta p \geq \frac{1}{2}$, which in some circumstances can be interpreted as $\Delta E \Delta t \geq \frac{1}{2}$. Therefore massive particles can come into existence for short periods of time, telling us that the vacuum is not strictly empty. Various conservation laws still play their roles, so for every electron coming into existence from these vacuum fluctuations, a positron must also appear. If there is a real electron present in the vacuum, the virtual positrons are attracted towards this by electromagnetic interactions, while the virtual electrons are repelled. Effectively this creates a dielectric cloud of virtual electron-positron pairs surrounding the electron as illustrated in Fig. 1.5.

Measurements of the electric charge can be carried out by looking at the cross section of an electron bombarded by photons. If a low energy photon is used, less energy is needed to deflect it from its path, and interaction with the virtual electron-positron cloud will be significant. On the other hand, if a high energy photon is used, more energy is needed, and the photon will penetrate deeper into the electron-positron cloud, making the screening less dominant. Therefore, a low energy measurement of the electron charge should result in a lower value than a high energy measurement, implying an energy dependence of the electric charge.

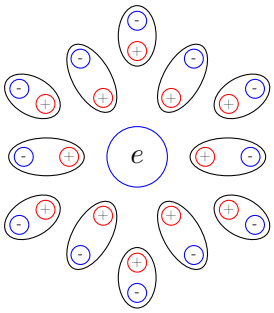

Figure 1.5: Vacuum polarisation of the electric charge.

For a short while it was believed that all interactive terms were screened in a similar matter, and that all such parameters had to increase with scale, but it was later shown that a non-Abelian Yang-Mills Lagrangian (such as in QCD) can have the opposite behaviour. More on this later.

3.2 The Callan-Symanzik equation

When renormalising the mass parameter of $\lambda\phi^4$, we calculated the dressed mass based on the assumption that the sum of all propagator terms should have a simple pole at the renormalised mass. This is known as a renormalisation condition, and for massive particles, choosing the renormalisation scale is straight forward. If, on the other hand the particles are massless, what should the scale be? This question does not only affect massless theories, but all theories in the high energy limit where the mass is much less than the momentum. In those cases a different scale must be chosen.

Setting the renormalisation scale to be Θ, the renormalisation conditions for the propagator of $\lambda\phi^4$ theory reads:

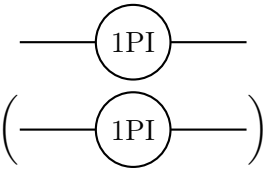

As mentioned, in a massive theory, the physical mass m_R is a natural choice for Θ, but for a massless theory this is a bit arbitrary, and one choice for Θ might be equally good as another. An equation describing how the parameters change based on this choice is therefore desired. For that we look at how the n-point function is renormalised.

With a massless theory, there are only the field strength Z, and the coupling constant(s) g left to renormalise. For simplicity, we choose a theory with only one coupling, which has bosonic degrees of freedom. The renormalised n-point function should only depend upon the renormalised coupling, and the renormalisation scale. The unrenormalised n-point function on the other hand should only depend on the cut-off scale Λ and the unrenormalised coupling. The n-point function can be renormalised through n field strength renormalisation factors, which means we have a simple relation between the two:

$$\mathcal{G}_{Rn}(\lambda_R, \Theta) = Z^{-n/2}\left(g_0(\Lambda), \tfrac{\Lambda}{\Theta}\right)\mathcal{G}_{0n}(g_0(\Lambda), \Lambda). \tag{1.96}$$

Since $\mathcal{G}_0$ is independent of Θ, taking the derivative wrt. it gives the equation

$$\left[\Theta\frac{\partial}{\partial\Theta} + \underbrace{\Theta\frac{\mathrm{d}g_R}{\mathrm{d}\Theta}}_{\beta(g_R)}\frac{\partial}{\partial g_R} + n\underbrace{\frac{1}{2}\Theta\frac{\mathrm{d}}{\mathrm{d}\Theta}\log Z}_{\gamma(g_R)} \right]\mathcal{G}_{Rn} = 0, \tag{1.97}$$

which is known as the Callan-Symanzik equation [15, 16], but it does not end there. What would happen if we chose a different renormalisation scale Θ/b? Following the same arguments as earlier we should get new renormalised parameters (subscript *eff*)

$$\mathcal{G}_{Rn}(g_R, \Theta/b) = Z_{eff}^{-n/2}(b)\mathcal{G}_{Rn}(g_{eff}(b), \Theta). \tag{1.98}$$

The new coupling constant should satisfy the differential equation:

$$b\frac{\mathrm{d}g_{eff}}{\mathrm{d}b} = \beta(g_{eff}(b)), \qquad\qquad g_{eff}(1) = g_R. \tag{1.99}$$

g_{eff} is an effective coupling constant at the new energy scale Θ/b and is called the *running coupling constant*. The β- and γ functions can be calculated by renormalising various n-point functions. With $\lambda\phi^4$, ones has to renormalise both the 2- and 4-point functions to extract the β function. One-loop results for both $\lambda\phi^4$ and QED are given below

$$\beta_{\lambda\phi^4}(\lambda) = \frac{3}{16\pi^2}\lambda^2 + \mathcal{O}(\lambda^3), \tag{1.100}$$

$$\beta_{\mathrm{QED}}(e) = \frac{e^3}{12\pi^2} + \mathcal{O}(e^4). \tag{1.101}$$

In both cases, $\beta > 0$, meaning that the running coupling increases with energy scale, just as we argued in Sec. 3.1.

3.3 Wilson's renormalisation group

A different, but very elegant way to look at renormalisation was introduced by Wilson in [17]. Suppose we have a theory defined up to some cut-off scale Λ. For simplicity let us look at a theory with a single scalar field ϕ, such as the one in Sec. 2.2, with the partition function

$$\mathcal{Z}_\Lambda = \int(\mathcal{D}\phi)_\Lambda \exp\Big\{ -\int \mathrm{d}\tau \int \mathrm{d}\mathbf{x}\, \mathcal{L}(\phi)\Big\}. \tag{1.102}$$

Cutting off the high energy contributions to $\mathcal{Z}$ can be expressed as only integrating over fields with energy less than this scale:

$$(\mathcal{D}\phi)_\Lambda = \prod_{|p|<\Lambda} \mathrm{d}\phi(p). \tag{1.103}$$

Defining a second cut-off scale $\Theta < \Lambda$, we can split the fields ϕ into two sets. One for energies below the new scale, and another for energies in between the new and the old energy scale:

$$\phi_<(p) = \begin{cases} \phi(p) & \text{when } |p| < \Theta \\ 0 & \text{else} \end{cases} \tag{1.104}$$

$$\phi_>(p) = \begin{cases} \phi(p) & \text{when } \Theta \le |p| \le \Lambda \\ 0 & \text{else} \end{cases} \tag{1.105}$$

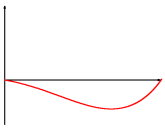

With these new variables, the partition function becomes

$$\mathcal{Z}_\Lambda = \int \mathcal{D}\phi_< \int \mathcal{D}\phi_> \exp\Big\{ - \int \mathrm{d}\tau \int \mathrm{d}\mathbf{x}\, \mathcal{L}(\phi_< + \phi_>) \Big\}. \tag{1.106}$$

The integral over $\phi_>$ can in general not be calculated analytically, and one must resort to either perturbative methods or other nonperturbative approximations, but assuming we could, we would be left with a effective Lagrangian describing the system at the new renormalisation scale:

$$\mathcal{Z}_\Lambda = \int (\mathcal{D}\phi)_\Theta \exp\Big\{ - \int \mathrm{d}\tau \int \mathrm{d}\mathbf{x}\, \mathcal{L}_{eff}(\phi) \Big\}. \tag{1.107}$$

This formalism is a member of a larger group of formalisms known as the *functional renormalisation group* (FRG), a good introduction to which can be found in e.g. Ref. [18]. In contrast to the Callan-Symanzik equations, which are renormalisation group equations for the individual parameters of $\mathcal{L}$, the FRG equations are in general RG equations for $\mathcal{L}$ itself. As a result, a Lagrangian renormalised using an FRG formalism can take on any functional form accepted by its symmetries. E.g. an $\lambda\phi^4$ Lagrangian can after at a lower renormalisation scale include a six and eight point coupling even though it only had a four point coupling at its initial renormalisation scale. We would therefore write the $\lambda\phi^4$ Lagrangian at an arbitrary renormalisation scale to be

$$\mathcal{L} = \frac{1}{2}K_1(\partial_\mu\phi)^2 - \frac{1}{2}K_2\phi^2 + \frac{1}{4!}K_3(\partial_\mu\phi)^4 - \frac{1}{4!}K_4\phi^4 + \frac{1}{6!}K_5(\partial\phi)^6 - \frac{1}{6!}K_6\phi^6 - \dots. \tag{1.108}$$

It is convenient to define a vector $\vec{K} = [K_1, K_2, K_3, K_4, K_5, K_6, \dots]$, whose initial value for a $\lambda\phi^4$ theory is $\vec{K} = [1, m^2, 0, \lambda, 0, 0, \dots]$, as we integrate out momentum shells $\vec{K}$ traces a line in K-space. If we have experimental values our theory should explain, the idea is to choose the correct initial conditions for $\vec{K}$ so that it ends up at a point in K-space that describes a Lagrangian with the correct properties.

3.4 The effective average action

The effective average action (EAA), also an FRG method, is an alternative to Wilson's. With Wilson's method we integrated out high energy modes of the partition function and saw how this could be seen as a change in the Lagrangian. As we saw, the new Lagrangian could include new couplings, and therefore be a very complex object. Instead of looking at how renormalisation evolves the Lagrangian, EAA analyses how Gibbs' free energy is changed[1]. Let us introduce a parameter k to keep track of the modes integrated out in such a way that

$$\Gamma_{k=\Lambda}[\phi_{cl}] = S[\phi = \phi_{cl}], \tag{1.109}$$

$$\Gamma_{k=0}[\phi_{cl}] = \Gamma[\phi_{cl}]. \tag{1.110}$$

At $k = \Lambda$ no modes have been integrated out, and we recover the original Gibbs' free energy, while at $k = 0$ all fluctuations have been integrated out and we should be left with the true free energy, quantum and thermal fluctuations included. A common way to include this k dependence is by adding a momentum dependent mass like term which can work as a regulator similar to the mass term added in Pauli-Villars regularisation. If the effective mass term is taken to infinity for certain

[1] QFT's equivalent to Gibbs' free energy is called the average action, hence the name effective average action

energy modes, they will decouple from the system, and not contribute to the free energy, while if it is set to zero the energy mode will be left unchanged. In terms of the action, we write

$$S[\phi] \longrightarrow S[\phi] + \Delta_k[\phi], \tag{1.111}$$

where

$$\Delta_k[\phi] = \frac{1}{2}\int_{x,y} \phi(x) R_k(x-y)\phi(y) = \frac{1}{2}\int \mathrm{d}^d p\, R_k(p)\phi_p\phi_{-p}. \tag{1.112}$$

Δ_k has the form off a mass term and the conditions (1.109, 1.110) can be translated to R_k

$$R_{k=0}(p) = 0, \tag{1.113}$$
$$R_{k=\Lambda}(p) = \infty, \tag{1.114}$$
$$R_k(|p| > k) \approx 0. \tag{1.115}$$

As long as the function $R_k(p)$ follows these criteria and does not explicitly break any of the symmetries of the Lagrangian, the possible choices for $R_k(p)$ are limitless. Depending on the system some choices are easier to work with than others, but there has also been studies by e.g. Daniel Litim [19, 20], where he tries to optimise this choice.

Exact RG equation for scalar fields

Our goal is, using the k dependent Gibbs' free energy introduced in the last Section, we want to find an differential equation on the form $\partial_k\Gamma_k = f_k(\Gamma_k)$. Recalling Sec. 2.1, Gibbs' free energy is defined using Helmholtz' free energy, which in turn is defined by the generating functional. Including the the cut-off term Δ_k, the generating functional is

$$W_k[J] = \int \mathcal{D}\phi \exp\Big[- S[\phi] - \Delta_k[\phi] + \int J\phi \Big]. \tag{1.116}$$

The definition of the k-dependent object Γ_k has to be slightly different from the definition of Gibbs' free we have in Eq. (1.72) for it to satisfy the condition in Eq. (1.109),

$$\Gamma_k[\phi_{cl}] + \mathcal{F}_k[J] = \int J\,\phi_{cl} - \Delta_k[\phi_{cl}], \tag{1.117}$$

where one should notice the addition of Δ_k. To obtain an expression for $\partial_k\Gamma_k$ we can take the derivative of Eq. (1.117) with respect to k, but there is a difference between taking the derivative keeping the field J constant, or the field ϕ_{cl}. They are related by

$$\partial_{k|J} = \partial_{k|\phi_{cl}} + \int_x \phi_{cl}(x)\frac{\delta}{\delta\phi_{cl}(x)}, \tag{1.118}$$

where $\partial_{k|J}$ is the derivative when J is kept constant and $\partial_{k|\phi_{cl}}$ with ϕ_{cl} constant. To differentiate $\mathcal{F}[J]$, it is easiest to start with $W[J]$.

$$\begin{aligned}\partial_{k|J}W_k[J] &= -\frac{1}{2}\int \mathcal{D}\phi \left(\int_{x,y}\phi(x)\partial_k R_k(x-y)\phi(y)\right) e^{-S_k[\phi]+\int J\phi}, \\ &= -\frac{1}{2}\int_{x,y}\partial_k R_k(x-y)\frac{\delta}{\delta J(x)}\frac{\delta}{\delta J(y)}W_k[J].\end{aligned} \tag{1.119}$$

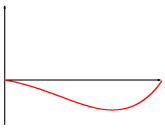

In the last line we used the trick introduced in Sec. 1.2 to rewrite the fields as functional derivatives. Writing $W_k[J]$ in terms of $\mathcal{F}_k[J]$ results in

$$\partial_{k|_J}\mathcal{F}_k[J] = -\frac{1}{2}\int_{x,y}\partial_k R_k(x-y)\left(\frac{\delta^2\mathcal{F}_k}{\delta J(x)\delta J(y)} + \frac{\delta\mathcal{F}_k}{\delta J(x)}\frac{\delta\mathcal{F}_k}{\delta J(y)}\right). \tag{1.120}$$

From here on we will drop the subscript cl from ϕ_{cl} and only include it if there is any doubt. Taking the $k|J$ derivative of Eq. (1.117),

$$\begin{aligned}\partial_{k|_J}\Gamma_k[\phi] = &-\int_{x,y}\partial_k R_k(x-y)\left(\frac{\delta^2\mathcal{F}_k}{\delta J(x)\delta J(y)} + \frac{\delta\mathcal{F}_k}{\delta J(x)}\frac{\delta\mathcal{F}_k}{\delta J(y)}\right) + \int_x J(x)\partial_k\phi(x)\\ &-\frac{1}{2}\int_{x,y}(\partial_k R_k(x-y))\phi(x)\phi(y) - \frac{1}{2}\int_{x,y}R_k(x-y)(\partial_k\phi(x))\phi(y)\\ &-\frac{1}{2}\int_{x,y}R_k(x-y)\phi(x)(\partial_k\phi(y)),\end{aligned} \tag{1.121}$$

and using Eq. (1.118) to convert the derivative, we end up with

$$\partial_{k|_\phi}\Gamma_k[\phi] = \frac{1}{2}\int_{x,y}\partial_k R_k(x-y)\Big[\frac{\delta^2\mathcal{F}_k}{\delta J(x)\delta J(y)}\Big]. \tag{1.122}$$

To convert this into a proper differential equation of Γ_k, we will have to analyse the expression further. First we note that the modified Legendre transformation in Eq. (1.117) results in slightly modified Legendre identities

$$\frac{\delta\mathcal{F}_k[J]}{\delta J(x)} = \phi(x), \tag{1.123}$$

$$\frac{\delta\Gamma_k[\phi]}{\delta\phi(x)} = J(x) - \int_y R_k(x-y)\phi(y). \tag{1.124}$$

Making use of these, we can write

$$\begin{aligned}\delta(x-y) = \frac{\delta^2 W_k}{\delta\phi(x)\delta J(y)} &= \int_z \frac{\delta^2 W_k}{\delta J(z)\delta J(y)}\frac{\delta J(z)}{\delta\phi(x)},\\ &= \int_z \frac{\delta^2 W_k}{\delta J(z)\delta J(y)}\,\frac{\delta}{\delta\phi(y)}\Big(\frac{\delta\Gamma_k}{\delta\phi(z)} + \int_w R_k(z-w)\phi(w)\Big),\\ &= \int_z \frac{\delta^2 W_k}{\delta J(z)\delta J(y)}\,\Big(\frac{\delta^2\Gamma_k}{\delta\phi(y)\delta\phi(z)} + R_k(z-y)\Big).\end{aligned} \tag{1.125}$$

The last line implies that the two factors are the functional inverse of each other, therefore we can symbolically write

$$\partial_k\Gamma_k = \frac{1}{2}\int_{x,y}\partial_k R_k(x-y)\Big(\Gamma_k^{(2)}(x,y) + R(x-y)\Big)^{-1}, \tag{1.126}$$

or, more conveniently in Fourier space,

$$\partial_k\Gamma_k = \frac{1}{2}\int_q \partial_k R_k(q)\Big(\frac{\delta^2\Gamma_k}{\delta\phi(p)\delta\phi(p')} + \delta(p+p')R_k(p)\Big)^{-1}_{q,-q}, \tag{1.127}$$

The subscript indicates that we later have to evaluate the momenta (p, p') at $(q, -q)$. A diagram representation is sometimes also used, with the notation

$$\text{———} \;=\; \frac{1}{\Gamma_k^{(2)}(p) + R_k(p)}, \qquad \otimes \;=\; \partial_k R_k(p), \tag{1.128}$$

the exact RGE can be expressed as

$$\partial_k \Gamma_k = \frac{1}{2}$$ 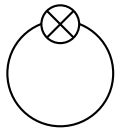 . (1.129)

The RG equation can be easily generalised to theories with more than one field ϕ,

$$\partial_k \Gamma_k = \frac{1}{2}\mathrm{tr} \int_q \partial_k R_{k,i,j}(q) \Big(\frac{\delta^2 \Gamma_k}{\delta\phi_i(p)\delta\phi_j(p')} + \delta(p+p') R_{k,i,j}(p) \Big)^{-1}_{q,-q}, \tag{1.130}$$

where $()^{-1}$ has been promoted to the matrix inverse of $[\Gamma_k^{(2)}(p) + R_k(p)]_{ij}$

Exact RG equation for fermionic fields

For fermionic fields, the calculation is almost identical. The generating functional is dependent on two fermionic sources η and $\bar{\eta}$, $W_k[\eta, \bar{\eta}]$. We define the two new fermionic fields ψ_{cl} and $\bar{\psi}_{cl}$ to be

$$\psi_{cl}(x) = \frac{\delta \mathcal{F}}{\delta \bar{\eta}(x)}, \tag{1.131}$$

$$\bar{\psi}_{cl}(x) = \frac{\delta \mathcal{F}}{\delta \eta(x)}. \tag{1.132}$$

The cut-off function $P_k(x-y)$ is, analogous to the scalar case, included as a mass term,

$$\Delta_k[\psi, \bar{\psi}] = \int_{x,y} \bar{\psi}(y) P_k(x-y) \psi(x). \tag{1.133}$$

Dropping the subscript cl on ψ_{cl} and $\bar{\psi}_{cl}$, the parameter dependent Gibbs' free energy is thus

$$\Gamma_k[\psi, \bar{\psi}] = -\mathcal{F}[\eta, \bar{\eta}] + \int_x \bar{\eta}(x)\psi(x) + \int_x \bar{\psi}(x)\eta(x) - \Delta_k[\psi, \bar{\psi}], \tag{1.134}$$

with the RG equation

$$\partial_k \Gamma_k = -\mathrm{tr} \int_q \partial_k P_k(q) \Big(\frac{\delta^2 \Gamma_k}{\delta\psi(q)\bar{\psi}(q)} + P_k(q) \Big)^{-1}. \tag{1.135}$$

where the trace is over the spinor indices of ψ. Using dashed lines to symbolise the true fermion propagator, the diagram representation is

$$\partial_k \Gamma_k = -$$ 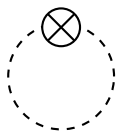 . (1.136)

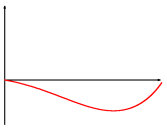

Approximations of the RGE

The two Eqs. (1.127) and (1.135) are exact RGEs, and solving them is just as hard as finding an analytic expression for the partition function. We will therefore approximate Γ_k by expanding it in derivatives of ϕ, and truncate the series after a few terms, see e.g. Ref [21]. At order $\mathcal{O}(\partial^2)$, the free energy is

$$\Gamma_k[\phi] = \int \mathrm{d}^d x \left(\frac{1}{2} Z_k(\phi)(\nabla_4 \phi)^2 + U_k(\phi)\right). \tag{1.137}$$

where ∇_4 is the Euclidean derivative operator ($\nabla_4 = [\partial_\tau, \vec{\partial}]$). The factor Z_k is a field normalisation term, whose components are in general different for the space and time derivatives of ϕ. The lowest order derivative expansion, $\mathcal{O}(\partial^0)$, is named the local potential approximation (LPA), in which the field strength renormalisation Z_k is set to one:

$$\Gamma_k[\phi] = \int \mathrm{d}^d x \left(\frac{1}{2} (\nabla_4 \phi)^2 + U_k(\phi)\right). \tag{1.138}$$

As one can see, the only k-dependent term remaining is U_k, and we would therefore like to find a differential equation for $\partial_k U_k$ instead of the one we have. This can be acomplished by evaluating the free energy in uniform fields $\phi(x) = \phi_{\mathrm{uni}}$, in which case it is

$$\Gamma_k[\phi_{\mathrm{uni}}] = \mathcal{V} U(\phi_{\mathrm{uni}}), \tag{1.139}$$

where $\mathcal{V}$ (in contrast to V) is the full space-time volume. The rest of the calculation will be carried out in Fourier space. The Fourier transform of Γ_k is

$$\Gamma_k = \int \mathrm{d}^d p \left(\frac{1}{2} p^2 \phi(p)\phi(-p) + U(\phi(p))\right). \tag{1.140}$$

Using this expression, we can calculate $\Gamma^{(2)}_{k,q,q'}$

$$\frac{\delta^2 \Gamma_k}{\delta\phi(q)\delta\phi(q')} = \int \mathrm{d}^d p \left(p^2 \delta(p-q)\delta(p+q') + \frac{\partial^2 U}{\partial\phi(q)\phi(q')}\right). \tag{1.141}$$

The second term can be identified by

$$\begin{aligned}
\int_z \frac{\partial U(\phi_z)}{\partial\phi_x \partial\phi_y} &= \int_z \frac{\partial^2 U}{\partial\phi^2_{\mathrm{uni}}} \delta(x-z)\delta(y-z), \\
&= \int_{q,q'} \int_z \frac{\partial^2 U}{\partial\phi^2_{\mathrm{uni}}} e^{iq(x-z)} e^{iq'(y-z}, \\
&= F^2_{q,q'} \left[\delta(q+q') \frac{\partial^2 U}{\partial\phi^2_{\mathrm{uni}}}\right],
\end{aligned} \tag{1.142}$$

where F^2 is the double Fourier transform. Collecting all the terms, we can write

$$\mathcal{V}\partial_k U_k = \frac{1}{2} \int_q \partial_k R_k(q) \Big(\delta(q+q')\Big[q^2 + \frac{\partial^2 U}{\partial\phi^2}\Big] + \delta(q+q') R_k(q)\Big)^{-1}_{q,-q}. \tag{1.143}$$

We can make use of the functional inverse introduced in Eq. (1.125) to identify:

$$\Big(\delta(q+q')\Big[q^2 + \frac{\partial^2 U}{\partial\phi^2}\Big] + \delta(q+q') R_k(q)\Big)^{-1} = \frac{\delta(q+q')}{q^2 + \frac{\partial^2 U}{\partial\phi^2} + R_k(q)}. \tag{1.144}$$

Finally, with $\delta(0) = \mathcal{V}$, we arrive at

$$\partial_k U_k = \frac{1}{2} \int_q \frac{\partial_k R_k(q)}{q^2 + \frac{\partial^2 U_k}{\partial \phi^2} + R_k(q)}. \tag{1.145}$$

CHAPTER 2

Quantum chromodynamics

This thesis, as mentioned earlier, is about the phase transition taking place at high temperature, or high particle density, where the bound quarks in the hadrons and mesons becomes deconfined. If the temperature is high enough, the resulting phase can be a plasma like state of quarks and gluons known in the literature as *quark-gluon plasma* (QGP). The full phase diagram is discussed later in Sec. 9. Before we get to the result, we will study the standard theory of the quarks and gluons known as quantum chromodynamics (QCD), as well as some effective models used to approximate this theory.

4 General overview

The interactions between the quarks and gluons, known as the *strong force*, is described by a theory called quantum chromodynamics. The theory consists of six quarks each carrying one of three colour charges [1]. The six quarks are named up (u), down (d), strange (s), charm (c), bottom (b) and top (t), and the type of quark is referred to as *flavour*. Each of the quarks has a corresponding anti quark which can carry negative colour charge. It might seem a bit confusing, but it is equivalent to electric charge in QED, the electron carries negative electric charge, and the positron carries positive electric charge. One could argue that there are actually 18 quarks and not six, as up-blue, up-green and up-red are all different particles, but this is not common practise. The quarks and their properties can be conveniently arranged into three families by their masses, and is given as:

Generation			Electric charge
1.	2.	3.	
up	charm	top	$2/3\,e$
down	strange	bottom	$-1/3\,e$

Quarks have spin $1/2$, and are therefore fermions. The mediators of the strong force are gluons. They are massless vector bosons with spin 1. In contrast to photons, gluons also carry colour charge, and do therefore interact with each other. Gluons actually carry one positive and one negative colour charge. This would add up to nine possible gluons, but only eight of these exist. The ninth possible gluon would be a colourless free state, and nothing like that has been observed experimentally.

[1] The strong charge is named colour charge, of which there are three, red, blue and green, hence the name *chromo*dynamics

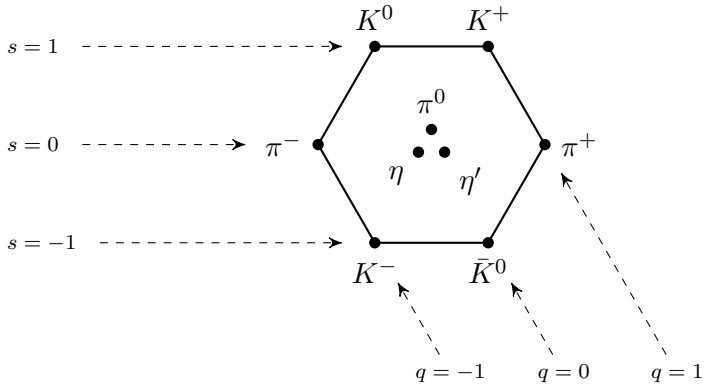

Figure 2.1: The spin zero meson nonet.

The self interactiveness of the gluons is one of the reasons why QCD possesses many interesting properties, and why it is a notoriously difficult theory to work with. QCD is confining, meaning that at low energies (or conversely large distance) the potential energy between a quark-anti quark pair becomes very high [22]. This is why we never see free quarks, because as one tries to pull the pair apart, the potential energy between them rises to a level where there is enough energy to create a new quark anti-quark pair which in turn form new bound states of quarks. On the other hand, QCD is also *asymptotically free*[23, 24], meaning that the strength of the coupling decreases for high energies (short distance). In terms of the theory we introduced in Sec. 3.2, the β-function for the QCD coupling is negative. At low energies, this coupling [2] is $\mathcal{O}(1)$, which has bothered theorists for a long time as perturbation theory breaks down. While at high energies, the coupling decreases, making perturbation theory viable again. At scale m_Z (= 91 GeV), it is measured to be $\alpha_s(m_Z) \approx 0.118$ [25].

4.1 Bound states

As already mentioned, only bound states of quarks appear in nature. There is actually a simple rule of thumb for this, all physical states must be colour singlets. This can only be achieved by having either one anti-colour for every colour, or an equal number of the three colours. With this in mind, only a limited number of possible configurations of bound states are possible. So far only two such configurations have been found experimentally, bound states of a quark-anti quark pair ($q\bar{q}$), called mesons, and bound states of three quarks (qqq), called baryons. Combinations of these two configurations are also theoretically possible, such as the four-quark mesons ($q\bar{q}q\bar{q}$) or the pentaquark ($qqqq\bar{q}$), but decisive evidence of their existence has yet to come from experiments.

On top of this classification, the mesons and baryons can be grouped based on their intrinsic spins. As they are bound states of particles with spin, they can themselves have spin values resulting from the addition of the constituents' spins as well as any possible angular momentum excitation. We will not go into details on this, but it can be found in any introductory text to quantum mechanics, e.g. [26, 27]. The mesons, being a bound state of two spin 1/2 particles, have integer spin, while the baryons have half integer spin. Based on these two groupings, the mesons and baryons can

[2] By the coupling we mean a generalised fine-structure constant, $\alpha_s = g^2/4\pi$, where g is the QCD analogy to the electric charge e.

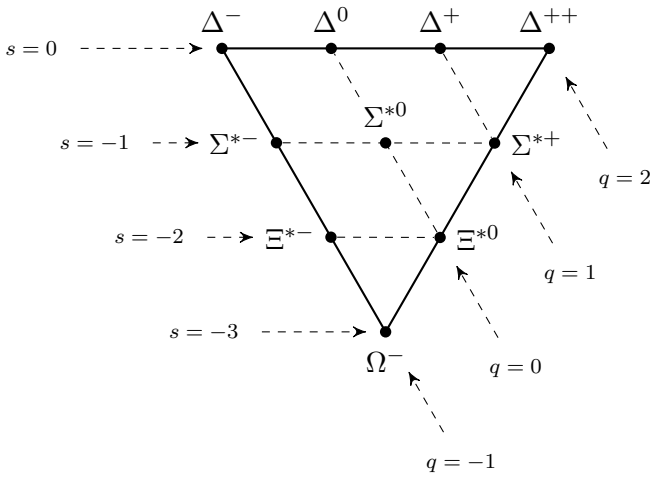

Figure 2.2: The spin 3/2 baryon decuplet.

be quite elegantly displayed in diagrams where they have been sorted according to their electric charge and flavour charge. The first of these diagrams were found by Gell-Mann [28, 29], before the introduction of the quark model, displaying the eight baryons with spin 1/2. The diagrams for the spin zero meson nonet and the spin 3/2 baryon octet is shown in Figs. 2.1 and 2.2. The quark model was in fact originally motivated by how neatly all the newly discovered particles could fit into such diagrams, hinting at an underlying structure.

Hypothetically there should also exist bound states of gluons, dubbed *glueballs*. These have not yet been found experimentally, but they have been simulated using lattice QCD.

5 Yang-Mills theory

In Sec. 1.4 we saw how the $U(1)$ symmetry group could be gauged by introducing a gauge field A^μ. Any Lie group can in fact be gauged. However, the procedure for doing so is not as straightforward for non-Abelian Lie groups. We will take a closer look at how to define the Lagrangian of a gauged non-Abelian symmetry group, known as Yang-Mills theory [30], but first let us have a short recap of Lie groups and their properties.

5.1 Lie groups

A Lie group G is a group whose members depend continuously and smoothly on a set of parameters α_i, $i = 1, 2, \ldots, N$. If a group element is denoted by $u(\alpha)$, the parameters can be chosen in such a way that $u(0) = e$, where e is the identity element. A linear representation R of a group element u is a linear mapping

$$u \longrightarrow D_R(u), \tag{2.1}$$

where D_R has to satisfy $D_R(e) = 1$, and $D_R(u_1 u_2) = D_R(u_1) D_R(u_2)$. In physics, a matrix representation is the most convenient one, as it lets us make use of the Lie group through standard matrix multiplication.

Because any group element can be mapped to different regions of parameter-space through continuous translations, a study in the region around the identity suffices to describe the whole group structure. An element infinitesimally close to the identity can be described as

$$u(\delta\alpha^i) = e + \delta\alpha_i \, L_i, \tag{2.2}$$

where the L_i's are the tangent vectors at e. In a linear representation, this would read

$$D_R(u) = 1 + i\delta\alpha_i T_{Ri}. \tag{2.3}$$

T_{Ri} are called the generators of the symmetry group G in representation R. It can be shown that using the tangent vectors, or the generators, every element u can be expressed in exponential form as:

$$D_R(u) = e^{i\alpha_i T_{Ri}}, \tag{2.4}$$

which reduces to Eq. (2.3) for infinitesimal α. One can inspect the group algebra by testing the second constraint in representation D (we dropped the subscript R) on exponential form. Using elements $u_a = e^{i\alpha_i T_i}$, $u_b = e^{i\beta_i T_i}$ and $u_a u_b \equiv u_c = e^{i\gamma_i T_i}$,

$$\gamma_i = \alpha_i + \beta_i - \tfrac{1}{2}\eta_i, \quad \text{with } \eta_i \text{ so that} \quad \alpha_i\beta_j\big[T_i, T_j\big] = i\eta_k T_k. \tag{2.5}$$

Therefore,

$$\big[T_i, T_j\big] = f_{ijk} T_k, \tag{2.6}$$

is called the Lie algebra of the group. One nice property of the algebra is that even though the generators T_i depend upon the representation, the *structure constants* f_{ijk} are representation invariant. It is possible to use the structure constants themselves as a linear representation of the group, this is referred to as the *adjoint representation*. If the members of the group G commute, G is said to be an Abelian group, if not it is said to be non-Abelian.

5.2 Yang-Mills Lagrangian

Assume we have a Lagrangian on the form

$$\mathcal{L}_G = \mathcal{L}_{\text{kin.}}(\partial\phi) - U_G(\phi), \tag{2.7}$$

where the full Lagrangian is symmetric under global transformations of the group G ($\phi \longrightarrow u\phi$, $u \in G$). Upon promoting this symmetry to a local one, we want to introduce the covariant derivative D so the combined transformations

$$\left.\begin{array}{l} \phi \longrightarrow u\phi \\ D \longrightarrow \tilde{D} \end{array}\right\} \quad \Longrightarrow \quad D\phi \longrightarrow \tilde{D}u\phi = uD\phi, \tag{2.8}$$

make sure the kinetic term is invariant. Including new fields A^i_μ, the covariant derivative can be written as

$$D_\mu = \partial_\mu - iA_\mu. \tag{2.9}$$

Here, A_μ is a matrix, depending on the representation of the group. This dependence can be extracted by setting $A_\mu = A^i_\mu T^i$, where T^i are the generators of G. To fulfil the criterion in Eq. (2.8), A^i_μ must transform according to

$$A_\mu \longrightarrow uA_\mu u^\dagger - i(\partial_\mu u)u^\dagger. \tag{2.10}$$

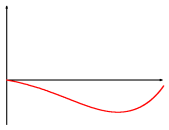

Using the exponential form of the group G ($u(x) = e^{ig\alpha^i(x)T^i}$), where a number g is introduced as a coupling constant, the transformations are written on their infinitesimal forms

$$\phi \longrightarrow \big(1 + ig\alpha^i(x)T^i\big)\phi, \tag{2.11}$$

$$A^i_\mu \longrightarrow A^i_\mu + \partial_\mu\alpha^i - gf^{ijk}\alpha^j A^k_\mu. \tag{2.12}$$

Having introduced the new gauge fields A^i_μ, the only thing missing in a proper Lagrangian is a kinetic term for A_μ. In addition to being a kinetic term for A_μ, it has to be invariant under the gauge transformation in Eq. (2.12). The commutator of the covariant derivative $\big[D_\mu, D_\nu\big]$ does exactly that, and in writing it out we see that it is not a differential operator at all:

$$\frac{i}{g}\big[D_\mu, D_\nu\big] \equiv F_{\mu\nu} = \partial_\mu A_\nu - \partial_\nu A_\mu - ig\big[A_\mu, A_\nu\big], \tag{2.13}$$

and it transforms as expected

$$F_{\mu\nu} \longrightarrow uF_{\mu\nu}u^\dagger. \tag{2.14}$$

On component form, $F_{\mu\nu} = F^i_{\mu\nu}T^i$, it is

$$F^i_{\mu\nu} = \partial_\mu A^i_\nu - \partial_\nu A^i_\mu + gf^{ijk}A^j_\mu A^k_\nu. \tag{2.15}$$

From this, a gauge invariant kinetic term for the A^i's can be constructed. It is given by

$$\mathcal{L}_{YM} = -\frac{1}{2}\mathrm{tr}\big(F_{\mu\nu}F^{\mu\nu}\big). \tag{2.16}$$

It is conventional to choose a representation in which T^i is normalised so that $\mathrm{tr}(T^iT^j) = \frac{1}{2}\delta_{ij}$. Inserted into Eq. (2.16) is reduces to

$$\mathcal{L}_{YM} = -\frac{1}{4}F^i_{\mu\nu}F^{i,\mu\nu}. \tag{2.17}$$

Notice that any reference to the representation has disappeared as one would expect from a physical theory.

6 QCD Lagrangian

Quantum chromodynamics is a Yang-Mills theory based on the local $SU(3)$ symmetry group coupled to six quarks described by massive fermionic fields $\psi^{f,c}_s$. All indices included (flavour $f = 1, 2, \ldots, 6$, colour $c, d = 1, 2, 3$, spin $s = 1, 2$ and gauge-index $i = 1, 2, \ldots, 8$), the complete Lagrangian is

$$\mathcal{L}_{QCD} = i\bar\psi^{f,c}_s\big(\gamma^\mu\partial_\mu - m_f\big)\psi^{f,c}_s + gA^i_\mu\bar\psi^{f,d}_s\gamma^\mu T^i_{c,d}\psi^{f,c}_s - \frac{1}{4}F^i_{\mu\nu}F^{i,\mu\nu}. \tag{2.18}$$

The algebra governing the generators T^i are summarised in appendix. A2.

The Lagrangian above only describes the chromodynamics of the quarks, not the other interactions they also take part in as they possess both electric- and flavour charge. Electrodynamics can be easily included by gauging the $U(1)$ symmetry group as we did in Sec. 1.4, while flavourdynamics is a bit trickier, but as neither of these forces play any role in the forming of QGP, they are left out.

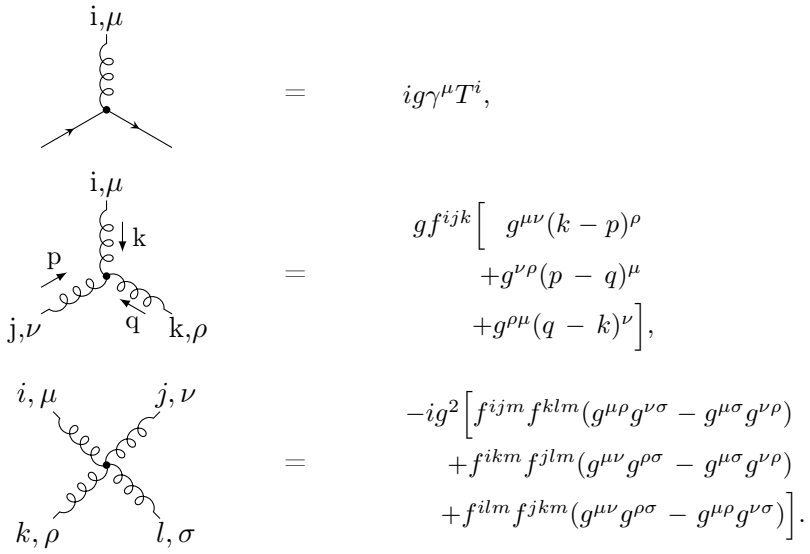

Figure 2.3: Feynman rules for the QCD interactions

Using the Feynman rules displayed in Fig. 2.3, one can perturbatively calculate the β-function for a Yang-Mills theory. This can be shown for an $SU(N)$ Yang-Mills theory to be

$$\beta(g) = -\frac{g^3}{(4\pi)^2}\Big(\frac{11}{3}N - \frac{2}{3}n_f\Big), \tag{2.19}$$

where n_f is the number of massless fermions coupled to the Yang-Mills field. Massless is taken to be approximately massless compared to the energy scale at which the process is measured. With a measurement done at 1 GeV, the u, d and s quarks are considered massless, while c, b and t decouple as their appearance in virtual processes are negligible at this scale. One notices that although the fermions have a positive contribution according to the screening argument of Sec. 3.1, the gauge fields have the opposite effect. Therefore, as long as the total number of quark flavours is less than 17, the β-function will always be negative, and the QCD coupling decreases as the energy increase. In terms of the strong force's fine-structure analogue $\alpha_s = g^2/4\pi$, the solution to Eq. (2.19) is

$$\alpha_s(k) = \frac{\alpha_{s_0}}{1 + b_0\frac{\alpha_{s_0}}{4\pi}\log(k^2/M^2)}, \tag{2.20}$$

in which $b_0 = 11 - \frac{2}{3}n_f$. Having both the arbitrary renormalisation scale M as well as the renormalisation condition α_{s_0} at this scale is somewhat impractical, therefore a second scale Λ is introduced so that

$$1 = b_0\frac{\alpha_{s_0}}{4\pi}\log(M^2/\Lambda^2), \tag{2.21}$$

which gives the equation:

$$\alpha_s(k) = \frac{2\pi}{b_0\log(k/\Lambda)}. \tag{2.22}$$

The parameter Λ can be measured experimentally, and at $n_f = 3$, it is $\Lambda \approx 250$MeV [25]. Fig. 2.4 shows the behaviour of α_s above 1 GeV where perturbation theory holds. At lower energy scales,

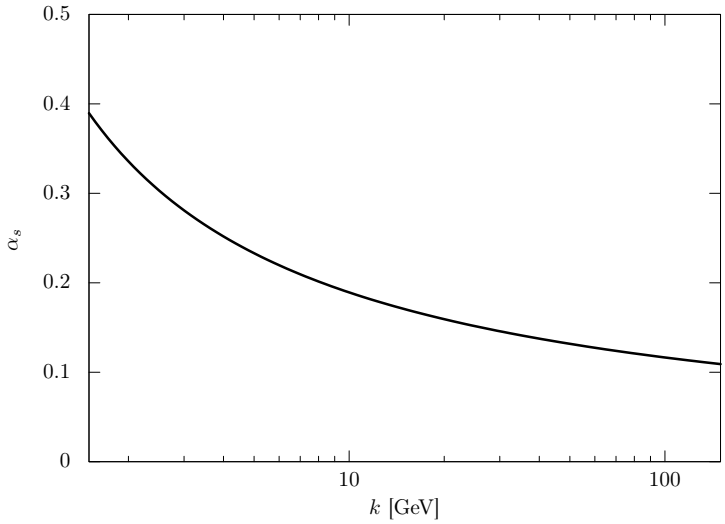

Figure 2.4: The running QCD coupling α_s[6].

α_s becomes too large for perturbation theory to work because a Taylor series in α_s would give an infinite number of non-negligible contributions. Therefore the exact behaviour of the β-function at lower energies is still unknown.

7 Chiral symmetry breaking

Let us remove the gauge field from Eq. (2.18) for a bit, and focus on a possible symmetry of the free massive Dirac equation. It becomes a bit more transparent if we rewrite the Lagrangian to be dependent upon the left- and right handed components of the fermion fields separately. In the standard representation of the spinors, the Dirac spinors (lower case ψ) are made up of left- and right handed Weyl spinors (upper case Ψ) in the following manner

$$\psi = \frac{1}{\sqrt{2}} \begin{pmatrix} \Psi_R + \Psi_L \\ \Psi_R - \Psi_L \end{pmatrix}, \tag{2.23}$$

and they can be projected out by applying the left- and right handed projection operators

$$\hat{R}\psi = \frac{1+\gamma^5}{2}\psi = \frac{1}{\sqrt{2}} \begin{pmatrix} \Psi_R \\ \Psi_R \end{pmatrix} \equiv \psi_R, \tag{2.24}$$

$$\hat{L}\psi = \frac{1-\gamma^5}{2}\psi = \frac{1}{\sqrt{2}} \begin{pmatrix} \Psi_L \\ -\Psi_L \end{pmatrix} \equiv \psi_L. \tag{2.25}$$

It might be worth mentioning that in the massless limit, Ψ_R and Ψ_L are helicity eigenstates of the Dirac equation. Anyway, expressed in terms of ψ_R and ψ_L, the Dirac Lagrangian reads

$$\mathcal{L}_{\text{Dirac}} = i\bar{\psi}_R \partial\!\!\!/ \psi_R + i\bar{\psi}_L \partial\!\!\!/ \psi_L - m\bar{\psi}_R\psi_L - m\bar{\psi}_L\psi_R. \tag{2.26}$$

We already know that the Dirac Lagrangian has a standard $U(1)$ symmetry, but we see from the representation above that by setting the mass terms to zero (often called the *chiral limit*), the left- and right-handed fields decouple, and a second $U(1)$ symmetry appears as we can now transform these two fields independently,

$$\psi_R \to e^{i\alpha_R}\psi_R, \qquad \psi_L \to e^{i\alpha_L}\psi_L. \tag{2.27}$$

In terms of the full Dirac spinor, choosing $\alpha_V \equiv \alpha_R = \alpha_L$ results in the standard $U(1)$ transform

$$\psi \to e^{i\alpha_V}\psi, \tag{2.28}$$

while a separate choice $\alpha_A \equiv \alpha_R = -\alpha_L$ results in the *chiral* transformation

$$\psi \to e^{i\alpha_A\gamma^5}\psi, \tag{2.29}$$

and its corresponding Noether current is the axial current

$$j^\mu_A = \bar{\psi}\gamma^\mu\gamma^5\psi. \tag{2.30}$$

It is therefore common to refer to the $U(1)_R \times U(1)_L$ symmetry as $U(1)_V \times U(1)_A$, where V stands for vector and A for axial.

Another set of symmetries can be identified if we extend the Lagrangian to include more quark flavours. It then reads

$$\begin{aligned}\mathcal{L}_{\text{Dirac}} &= i\bar{\psi}_i(\partial\!\!\!/ - m_i)\psi_i, \\ &= i\bar{\psi}_{Ri}\partial\!\!\!/\psi_{Ri} + i\bar{\psi}_{Li}\partial\!\!\!/\psi_{Li} - m_i\bar{\psi}_{Ri}\psi_{Li} - m_i\bar{\psi}_{Li}\psi_{Ri}.\end{aligned} \tag{2.31}$$

From the first of these, we see that by setting all quark masses identical, an $SU(n_f)$ symmetry emerges, as we can rotate ψ_i in flavour-space. This is commonly referred to as isospin symmetry, and is almost an exact symmetry when $n_f = 2$ as the u- and d quarks have almost identical masses ($m_u = 1.7 - 3.3$ MeV, $m_d = 4.1 - 5.8$ MeV [25]). Setting all masses to zero, produces a second axial $SU(n_f)$ symmetry as ψ_L and ψ_R can be rotated independently, similar to the axial $U(1)$ just introduced. All in all, we have $SU(n_f)_V \times SU(n_f)_A \times U(1)_V \times U(1)_A$ symmetry in the chiral limit. Actually, even in the chiral limit, $U(1)_A$ is broken by a peculiar process in QFT known as the *axial vector anomaly*, or the Adler-Bell-Jackiw anomaly after its discoverers [31, 32]. Ten years later, Kazuo Fujikawa showed that the anomaly was a result of the fermionic integration measure $\mathcal{D}\bar{\psi}\mathcal{D}\psi$ not being invariant under the axial $U(1)$ transformation [3] [33, 34].

As for the $SU(n_f)_A$ symmetry, it is said to be softly broken in the $n_f = 2$ sector, owing to the small masses of both u and d. In Sec. 1.5 we saw how a continuously broken symmetry resulted in massless Goldstone bosons. The $SU(2)_A$ symmetry is obviously not an exact symmetry at all, it is explicitly broken by the u and d masses, which is fundamentally different from spontaneous symmetry breaking. But as the u and d masses are very small, the symmetry is softly broken, and we expect there to be three pseudo-Goldstone bosons with small masses matching the axial $SU(2)$

[3] More accurately, we come to a point in the calculation where we have to choose between vector and axial $U(1)$ symmetry, but as breaking the vector symmetry implies that flavour charge is no longer conserved, that choice would be unphysical

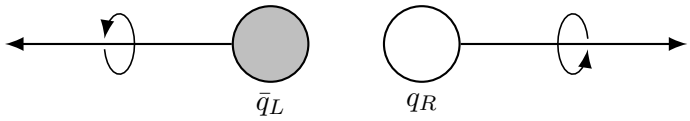

Figure 2.5: The chiral condensate.

symmetry. Searching particle data tables, we see that the three pions are perfect candidates as they are pseudoscalar spin-less bosons with relatively small masses ($m \sim 140$ MeV).

We have just argued that mass terms on the form $\bar{\psi}\psi$ are responsible for chiral symmetry breaking. A natural candidate for a measure of how "bad", if at all, the chiral symmetry is broken, is the chiral condensate $\langle\bar{\psi}\psi\rangle$. This condensate is directly related to the pions, as they are the lowest energy configuration of this type, and should therefore be the dominating contribution. When analysing the deconfinement transition in the next chapters, we will use $\langle\bar{\psi}\psi\rangle$ as an order parameter to identify when we have reached the deconfined phase. A rough picture of the chiral condensate is shown in Fig. 2.5.

8 The linear sigma model

The linear sigma model (LSM), is one of many models aiming at an effective description of QCD at low energies where where quarks and gluons for the most part only appear confined within hadrons. The model was proposed by Gell-Mann and Lévy in 1960 [35], and it is based on the chiral condensate introduced in the last chapter. At low energies, the quarks and anti-quarks in QCD should have formed bound states of spinless mesons, and an effective Lagrangian describing the dynamics of the mesons can replace the QCD Lagrangian. With no quark degrees of freedom, the two-flavour, isospin symmetric ($m_d = m_u$), LSM Lagrangian is

$$\mathcal{L}_{LSM} = \frac{1}{2}\partial_\mu\phi_\alpha\partial^\mu\phi_\alpha - \frac{1}{2}m^2\phi_\alpha\phi_\alpha - \frac{1}{4}\lambda\big(\phi_\alpha\phi_\alpha\big)^2 + h_\alpha\phi_\alpha. \tag{2.32}$$

The parameters m^2, λ and h_i have to be fixed by experimental measurements. Excluding the last term, this theory is $O(4)$ symmetric, which is isomorphic to the $SU(2)\times SU(2)$ symmetry of massless two-flavour QCD. The parameter h_α is introduced to break this symmetry explicitly, simulating how $SU(2)_A$ is explicitly broken by the quark masses. With $h = 0$, the $O(4)$ symmetry can be spontaneously broken, leaving us three massless Goldstone bosons taken to be the three pions. The fourth field is identified as the σ particle (referred to as $f_0(600)$ in the particle data group booklet [25]), which has a substantially higher mass compared to the pions with $m_\sigma = 400 - 1200$ MeV. In terms of the parameters above (still $h = 0$), $m_\sigma = -2m^2$ ($m^2 < 0$).

The model can also couple to quark degrees of freedom through Yukawa-coupling terms. This model is named the linear sigma model with quarks (abbreviated LSMq), or the quark-meson model. The two-flavour, isospin symmetric model reads:

$$\mathcal{L}_{LSMq} = i\bar{\psi}\big[\partial\!\!\!/ - g(\sigma + i\gamma^5\vec{\tau}\cdot\vec{\pi})\big]\psi + \mathcal{L}_{LSM}, \tag{2.33}$$

where we have chosen to spontaneously break the $O(4)$ symmetry of $\mathcal{L}_{LSM}$ in the ϕ_0 direction, and have renamed the fields $\phi_0 = \sigma$, $\phi_i = \pi_i$. The quark mass term has manifested itself into couplings

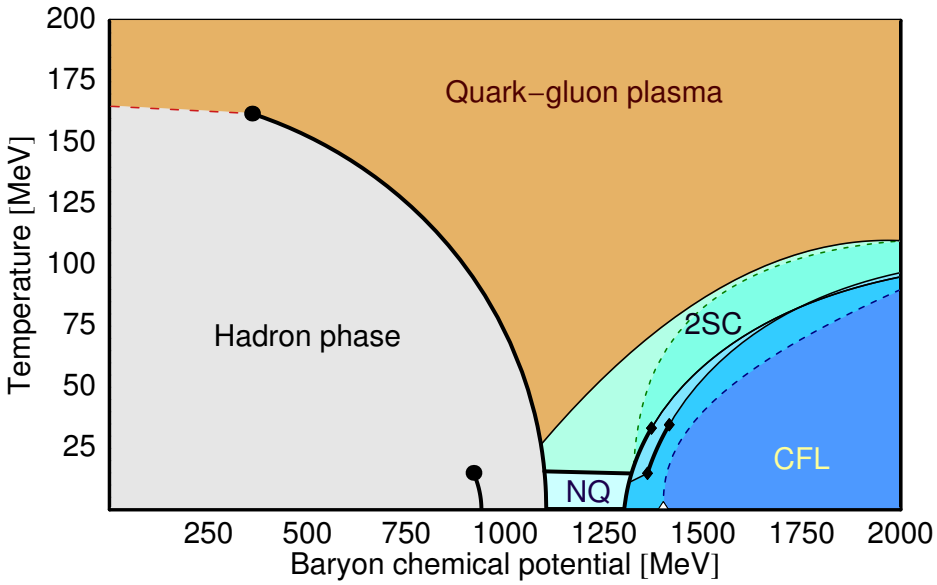

Figure 2.6: A T-μ_B phase diagram for QCD, taken from [36].

with mesons, which classically results in an effective mass term for the quarks,

$$m_f = g \langle \sigma \rangle . \tag{2.34}$$

9 QCD phase diagram

In the world we live in, at normal temperatures and not too high particle densities, QCD is in its confined phase, where quarks and gluons only appear in bound states such as the mesons and baryons. Due to the nature of the QCD coupling, one could argue that at extreme enough conditions we expect QCD to behave quite differently as the coupling weakens enough for quarks to free themselves from their bound states. Such conditions have been reached in heavy ion collision experiments at RHIC (Relativistic Heavy Ion Collider) and the LHC (Large Hadron Collider), and is speculated to exist in the core of compact stars (such as neutron starts), and to have existed in the very early universe. Our current understanding of this phase diagram is displayed in Fig. 2.6.

In this thesis we are mostly concerned with the *deconfinement transition*, in which quarks and gluons break free from their confined states, and move around as individual particles rather than being bound within the borders of the mesons and baryons. This can happen in one of two ways. Either, at very high temperatures, there is enough thermal energy to weaken the strong force sufficiently, so the quarks can break lose. In this case they will move around in a "soup" of interacting quarks and gluons. This is known as the quark-gluon plasma, which experiments have been able to create for a fraction of a second during heavy ion collisions at the great colliders. Alternatively, the hadrons can be packed so close together that their borders start to overlap making a description of separate hadrons nonsensical, and we once again have a deconfined state. This is known as the (normal) quark matter (NQ) phase, and is speculated to exist at the core of very dense stars, such as neutron stars.

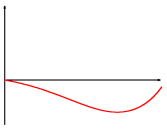

At zero temperature and zero chemical potential we have vacuum, and it is here calculations with QFT are carried out, predicting the result of results of e.g. proton-proton collision experiments. Moving towards higher chemical potential, i.e. higher particle density, the first phase transition one encounters is the familiar gas-liquid phase transition. It happens at roughly $\mu_B \approx 924$ MeV [1], and above this limit the hadrons condense into "drops". At higher density, we encounter the NQ phase described above.

At higher particle densities still, one argues by Cooper's theorem that we should have a superconducting state involving quarks. It can be rigorously shown for asymptotically high densities, but one expects from calculations with various models to reach this phase also for intermediate values. Colour superconductivity is a bit more complicated than normal superconductivity as there are more quantum numbers present which need to form anti-symmetric states, and therefore there are multiple superconducting phases. The first of these one encounters is the 2-flavour colour superconducting (2SC) phase where the up and down quarks form Cooper pairs. To satisfy the anti-symmetry condition, these need to have different colour values, for example up-green with down-blue. Next up is the superconducting state in which we have sufficient energy to include the strange quark. This phase is known as the colour-flavour-locked (CFL) phase in which all three quarks form pairs using all colours. These states are invariant under rotation in flavour and colour-space, but they have to be simultaneously transformed to satisfy the anti-symmetry requirement, hence the name CF *locked*

CHAPTER 3

Mean-field approximation

Our first approach at identifying the deconfinement phase transition is utilising the mean-field approximation [37, 38]. It uses the linear sigma model with quarks to describe QCD at low energies, and it assumes no bosonic quantum fluctuations. In the language of perturbation theory, it is a "one-loop" approximation. We will in this chapter visit both a two- and three-flavour quark meson model evaluated at both $h = 0$ (the chiral limit) and $h > 0$ (the *physical point*).

10 Two-flavour quark-meson model

The Lagrangian of the two-flavour linear sigma model with quark degrees of freedom is

$$\mathcal{L}_{2fl} = \bar{q}\big[i\partial\!\!\!/ - g(\sigma + i\gamma^5\vec{\tau}\cdot\vec{\pi})\big]q + \frac{1}{2}\partial_\mu\sigma\partial^\mu\sigma + \frac{1}{2}\partial_\mu\vec{\pi}\partial^\mu\vec{\pi} - U(\sigma,\vec{\pi}) + h\sigma, \tag{3.1}$$

where U is an $O(4)$ symmetric potential of the vector $\big[\sigma,\vec{\pi}\big]$, and $h\sigma$ is a term for explicitly breaking this symmetry down to $O(3)$, simulating how chiral symmetry is broken by the quark masses. We choose the classical potential to be

$$U(\sigma,\vec{\pi}) = \frac{1}{2}m^2\big(\sigma^2+\vec{\pi}^2\big) + \frac{\lambda}{4}\big(\sigma^2+\vec{\pi}^2\big)^2, \tag{3.2}$$

as it is the simplest $O(4)$ symmetric potential with bosonic couplings.

10.1 Thermodynamic potential

The first step is to add a quark chemical potential to the above Lagrangian. To do this, we need to find an expression for the quark number density, which can be obtained by applying Noether's theorem to the $U(1)$ symmetry of the quarks. On infinitesimal form, this transformation is

$$q \longrightarrow (1+i\theta)q \quad \Longrightarrow \quad \delta q = iq, \tag{3.3}$$

$$\bar{q} \longrightarrow (1-i\theta)\bar{q} \quad \Longrightarrow \quad \delta\bar{q} = -i\bar{q}, \tag{3.4}$$

which gives the following Noether current

$$j^\mu = \frac{\partial\mathcal{L}_{2fl}}{\partial\partial_\mu\psi}\delta\psi + \frac{\partial\mathcal{L}_{2fl}}{\partial\partial_\mu\bar{\psi}}\delta\bar{\psi} = \bar{\psi}\gamma^\mu\psi. \tag{3.5}$$

Its zeroth component is a conserved charge density which is identified as the quark number density. The Lagrangian with a quark chemical potential is therefore

$$\mathcal{L}_{2fl} \longrightarrow \mathcal{L}_{2fl} + \mu\bar{q}\gamma^0 q. \tag{3.6}$$

Next we want to find an analytic expression for the thermodynamic potential defined in Eq. (1.74) using the mean-field approximation. Removing all bosonic quantum fluctuation, we simply substitute σ and $\vec{\pi}$ by their space-time independent expectation values, meaning that up to a normalisation constant, the partition function is

$$\mathcal{Z} = e^{-\beta V U(\langle\sigma\rangle,\langle\vec{\pi}\rangle)} \int \mathcal{D}\bar{q}\mathcal{D}q \exp\Big\{ - \int_x \bar{q}\big[\gamma^0\partial_\tau - \vec{\gamma}\cdot\nabla + g(\langle\sigma\rangle + i\gamma^5\vec{\tau}\cdot\langle\vec{\pi}\rangle) - \mu\gamma^0\big]q \Big\}, \tag{3.7}$$

and in turn, using the calculation in Appendix B6, the thermodynamic potential is

$$\Omega(T,\mu) = U\big(\langle\sigma\rangle,\langle\vec{\pi}\rangle\big) + \Omega_{q\bar{q}}, \tag{3.8}$$

where the quark anti-quark contribution is

$$\Omega_{q\bar{q}} = -2N_f N_c \int \frac{\mathrm{d}\mathbf{p}}{(2\pi)^3} \Big\{ \omega + T\log\Big[1 + e^{-(\omega+\mu)\beta}\Big] + T\log\Big[1 + e^{-(\omega-\mu)\beta}\Big] \Big\}. \tag{3.9}$$

We have defined $\omega^2 = \mathbf{p}^2 + m_q^2$ and $m_q^2 = g^2\big(\langle\sigma\rangle^2 + \langle\vec{\pi}\rangle^2\big)$. Note that a factor N_c has been added to compensate for the extra colour degrees of freedom of the quarks. The first term is identified as a contribution from the vacuum energy, and is therefore discarded. We find the expectation value of the fields σ and $\vec{\pi}$ by the minimum of the thermodynamic potential

$$\frac{\partial\Omega}{\partial\sigma} = 0, \tag{3.10}$$

$$\frac{\partial\Omega}{\partial\vec{\pi}} = 0. \tag{3.11}$$

As the scalar fields σ and $\vec{\pi}$ correspond to the chiral quark condensates, we find the chiral phase transition at the point in T-μ space where their expectation values are zero. $\langle\vec{\pi}\rangle = 0$ is always a solution of the above equations with the given potential, and therefore the value of $\langle\sigma\rangle$ determines the phase transition.

10.2 Characterising phase transitions

One defines a phase transition by either the point where an order parameter has become zero, or where it jumps discontinuously. If it jumps discontinuously it is said to be a first-order phase transition, while if it goes continuously to zero it is higher order. The definition of the higher order phase transitions follows the same logic. A second-order phase transition goes to zero with a discontinuous first derivative, while a third order has a discontinuous second derivative, and so on. Examples of a first and second-order phase transition is shown in Figs. 3.1a and 3.1b. On top of the various orders of phase transitions, there is also an additional possibility, which is not a proper phase transition, but is often associated with them. If the order parameter goes towards zero but does never quite reaches it, we have a crossover. In those circumstances there are multiple ways to define the crossover point. We will define it as the inflection point, or the point with the most rapid change. Another alternative is to use the point at which the order parameter's value is half of that of the vacuum.

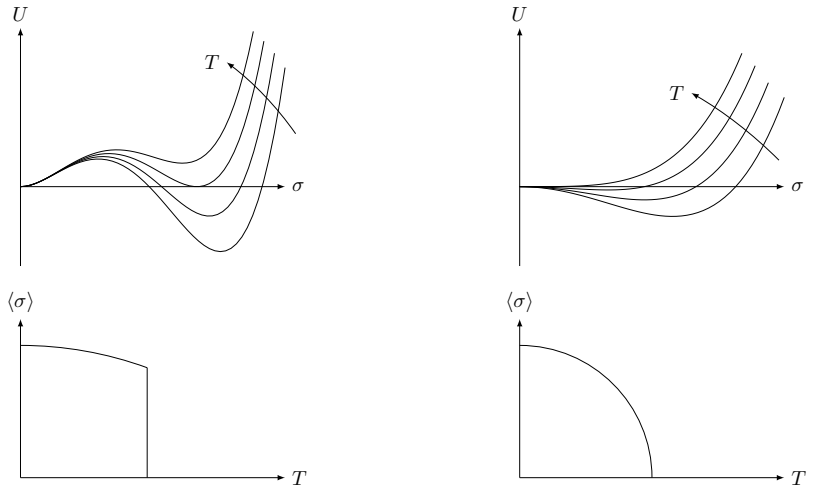

(a) First-order phase transition. (b) Second-order phase transition.

Figure 3.1: Examples of 1st and 2nd order phase transitions.

10.3 Matching parameters

The Lagrangian in Eq. (3.1) has four still undetermined parameters, m, λ, h and g, and therefore we need four experimental measurements to match the parameters with. The comparison is done in the vacuum, zero temperature and chemical potential, where we have no thermodynamic fluctuations. The four experimental values we will use are the constituent quark mass m_q (one-third of the proton mass), the pion decay constant f_π, the pion mass m_π, and the sigma mass m_σ. Their values are

$$\begin{aligned} m_q &\quad 312.8 \text{ MeV}, \\ f_\pi &\quad 93 \text{ MeV}, \\ m_\pi &\quad 138 \text{ MeV}, \\ m_\sigma &\quad 450 \text{ MeV}. \end{aligned}$$

The partial conservation of axial current (PCAC) relations gives us $\langle\sigma\rangle = f_\pi$, and from this we can immediately see from the definitions in Eq. (3.9) that $g = m_d/f_\pi = 3.36$. The meson masses are given as the curvature of Ω at the minimum:

$$zam_\pi^2 = \left.\frac{\partial^2\Omega}{\partial\vec{\pi}^2}\right|_{\langle\sigma\rangle,\langle\vec{\pi}\rangle} = m^2 + \lambda f_\pi^2, \tag{3.12}$$

$$m_\sigma^2 = \left.\frac{\partial^2\Omega}{\partial\sigma^2}\right|_{\langle\sigma\rangle,\langle\vec{\pi}\rangle} = m^2 + 3\lambda f_\pi^2 = m_\pi^2 + 2\lambda f_\pi^2. \tag{3.13}$$

Inverted, they determine m and λ:

$$m^2 = \frac{\left(3m_\pi^2 - m_\sigma^2\right)}{2} = -(269.6\,\text{MeV})^2, \tag{3.14}$$

$$\lambda = \frac{m_\sigma^2 - m_\pi^2}{2f_\pi^2} = 10.6. \tag{3.15}$$

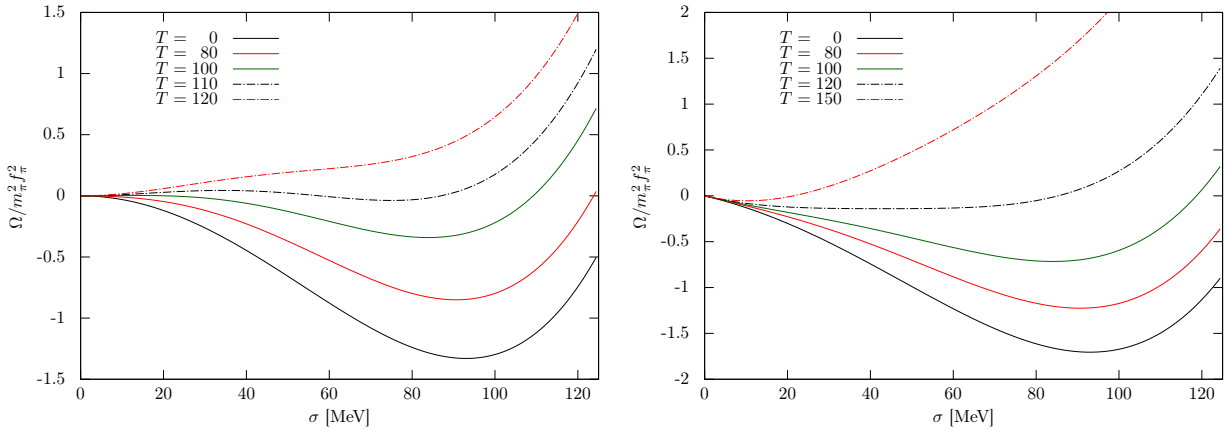

(a) $h = 0$ (b) $h = f_\pi m_\pi^2$

Figure 3.2: Thermodynamic potential at $\mu = 0$ for various T in the mean-field approximation. The left plot is in the chiral limit while the right plot is at the physical point, see main text for more details.

Finally, using Eq. (3.10), we find h to be

$$h = m_\pi^2 f_\pi = (121.0\,\text{MeV})^3. \tag{3.16}$$

In the chiral limit ($h = 0$) we only need to match three parameters as $m_\pi = 0$. They are $m^2 = -m_\sigma^2/2$ and $\lambda = m_\sigma^2/2f_\pi^2$, while g is the same.

10.4 Results

The plots in Fig. 3.2 show the thermodynamic potentials at zero chemical potential for various temperatures (both $h = 0$ and $h \neq 0$). In the left plot, one sees that the potential develops two minima as T increases, and at $T \approx 111$ MeV, the minimum jumps discontinuously to zero, marking a first-order phase transition. In the plot on the right we see how the minima continuously shifts to the left towards zero, but never quite reaches it. This can be seen directly from the equation determining the minimum

$$\left(m^2 + \lambda\sigma^2\right)\sigma + 2N_f N_c \sigma g^2 \int \frac{\mathrm{d}\mathbf{p}}{(2\pi)^3}\frac{1}{\omega}\left[n_q(T,\mu) + n_{\bar{q}}(T,\mu)\right] = h \tag{3.17}$$

where $n_q(T.\mu) = \left(e^{(\omega-\mu)/T} + 1\right)^{-1}$ is the quark distribution function and $n_{\bar{q}}(T,\mu) = n_q(T,-\mu)$ is the anti-quark distribution function. One can sees that as long as $h \neq 0$, $\sigma = 0$ will never be a possible solution, no matter the value of T and μ. The position of the minima as a function of temperature for zero chemical potential has been plotted in Fig. 3.3. In this plot it is clear that the system undergoes a first-order transition in the chiral limit, while it is a crossover at the physical point, as argued above. The inflection point of the crossover-curve is at $T \approx 120$ MeV.

The resulting phase diagrams are plotted in Fig. 3.4. At chemical potentials higher than 105 MeV, the thermodynamic potential develops a second minimum at the physical point. As T is increased for these values of μ, the minimum jumps discontinuously to the second minimum, and

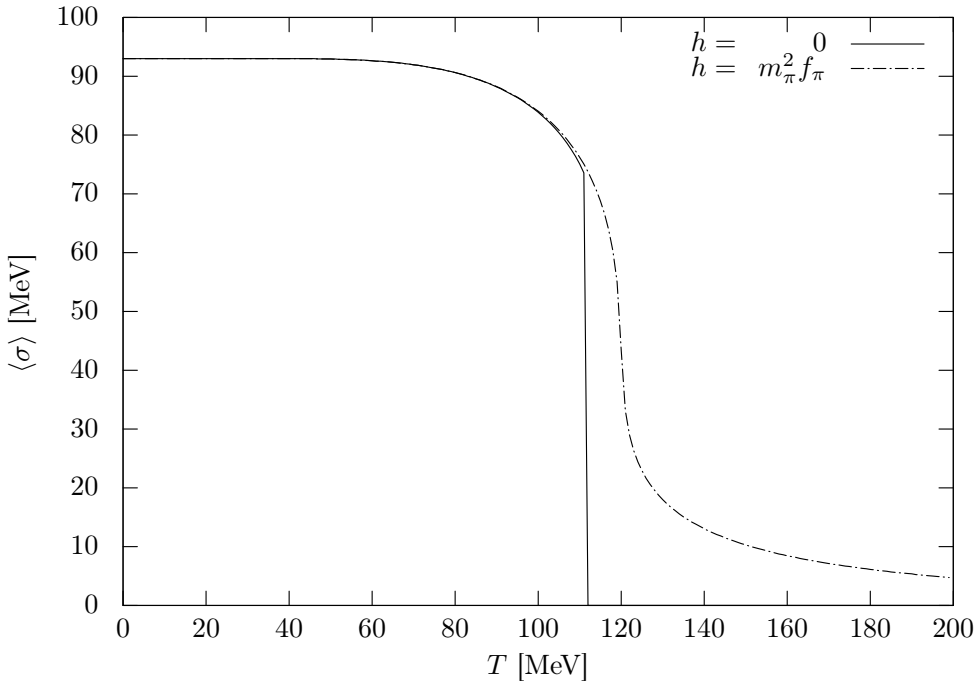

Figure 3.3: Plots of the minimum of the thermodynamic potential with varying T at $\mu = 0$. The plot shows a first-order phase transition at $T = 111$ MeV in the chiral limit, while we have a crossover at the physical point, its inflection point at $T = 120$ MeV.

we have a first-order transition instead of a crossover. The point $(T, \mu) \approx (109, 105)$ MeV therefore marks what is known as the critical endpoint, at which the phase transition should be second-order (discontinuous first derivative). The existence and position of this point is still debated among physicists, see e.g. Ref. [39] for an analysis and Ref. [40] for a lattice QCD perspective.

In Fig. 3.5 the phase diagram has been plotted for various values of m_σ, and one can see a strong correlation between the phase diagram and the value of the sigma mass. In addition to raising the whole phase diagram, an increased sigma mass also pushes back the critical endpoint (CEP), and at high enough m_σ, it should disappear completely. As most lattice simulations [40, 41, 42] places the (pseudo)critical temperature with zero chemical potential in the range 150-170 MeV, the results from these plots suggests that the sigma mass should be somewhere between 600 and 800 MeV. The results will be discussed further in Sec. 14 when all approximations have been presented.

An important clarification has to be made regarding the phase diagram in the chiral limit. When we calculated the quark contribution to the thermodynamic potential given in Eq. (3.9), we threw away the quark vacuum energy contribution. If we had renormalised the vacuum contribution using e.g. the cut-off regularisation scheme which was introduced in Sec. 1.6, we would have found a second-order phase transition in the chiral limit instead of a first-order, as shown by Skokov *et al* in Ref. [43]. It was later shown by Andersen, Khan and Kyllingstad in Ref. [44] that the phase-transition would be second-order in the whole T-μ plane, not going through a critical endpoint. The argument presented by Skokov *et al* is the following: Close to the critical temperature, the

quark mass, which is proportional to the order parameter σ, should be small compared with the temperature, meaning that we can expand the quark contribution to the thermodynamic potential in powers of m_q/T

$$\Omega_{q\bar{q}} = N_c N_f T^4 \Bigg\{ -\frac{7\pi^2}{180} + \frac{1}{12}\frac{m_q^2}{T^2} + \frac{1}{8\pi^2}\frac{m_q^4}{T^4}\left[\log\left(\frac{m_q}{\pi T}\right) + \gamma_E - \frac{3}{4}\right]\Bigg\} + \mathcal{O}\left(\frac{m_q^6}{T^6}\right). \tag{3.18}$$

Added to the mesonic potential, and using the expression for m_q, we get the full potential

$$\Omega = \frac{1}{2}\left(m^2 + g^2\frac{N_f N_c}{6T^2}\right)\sigma^2 + \frac{1}{4}\left(\lambda + g^4\frac{N_f N_c}{4\pi^2}\left[\log\left(\frac{g\sigma}{\pi T}\right) + \gamma_E - \frac{3}{4}\right]\right)\sigma^4 + \Omega_0. \tag{3.19}$$

With a potential on this form, it is the sign of the quartic term which determines the order of the phase transition. If the quartic term is positive we have a second-order phase transition, while it is first-order if it is negative. The λ term therefore compete with the logarithm term to determine the order of the transition, but as the temperature is high and the order parameter is small close to the phase transition, the logarithmic term can become very large, and negative, leaving us a first-order phase transition. To see how this is countered by the vacuum fluctuation of the quarks we regularise the term with a UV cut-off Λ, and expand the result in powers of m_q/Λ

$$\begin{aligned}\Omega_{q\bar{q}}^{vac} &= -\frac{N_f N_c}{\pi^2}\int_0^\Lambda p^2 \mathrm{d}p\,\sqrt{p^2 + m_q^2}, \\ &= -\frac{N_f N_c}{4\pi^2}\Lambda^4\left\{1 + \frac{m_q^2}{\Lambda^2} + \frac{1}{8}\frac{m_q^2}{\Lambda^4}\left[1 + 4\ln\left(\frac{m_q}{2\Lambda}\right)\right]\right\} + \mathcal{O}\left(\frac{m_q^6}{\Lambda^6}\right).\end{aligned} \tag{3.20}$$

The first two terms that are $\mathcal{O}(\Lambda^4)$ and $\mathcal{O}(\Lambda^2)$ and needs to be renormalised, but we see that the logarithmic term exactly matches that of Eq. (3.18), cancelling the σ-dependence of the logarithm leaving us

$$\Omega = \frac{1}{2}\left(m^2 + g^2\frac{N_f N_c}{6T^2}\right)\sigma^2 + \frac{1}{4}\left(\lambda + g^4\frac{N_f N_c}{4\pi^2}\left[\log\left(\frac{2\Lambda}{\pi T}\right) + C\right]\right)\sigma^4 + \Omega_0. \tag{3.21}$$

where C is an unimportant constant. From this we see that as long as we choose a cut-off scale Λ large enough, the quartic term will be positive and we have a second-order phase transition.

11 Three-flavour quark-meson model

The simple model introduced in the previous section can be extended by adding the strange quark to the mix. At temperatures up to 150 - 200 MeV, it is certainly possible for the strange quark ($m_s = 101^{+29}_{-21}$ MeV[25]) to contribute to the results. We will in this analysis follow the work of Schaefer and Wagner [45].

11.1 Thermodynamic potential

Similar to the arguments presented when we wrote down the two-flavour Lagrangian, we require the three-flavour Lagrangian to be symmetric under the $U(3)_L \times U(3)_R$ symmetry group in the chiral

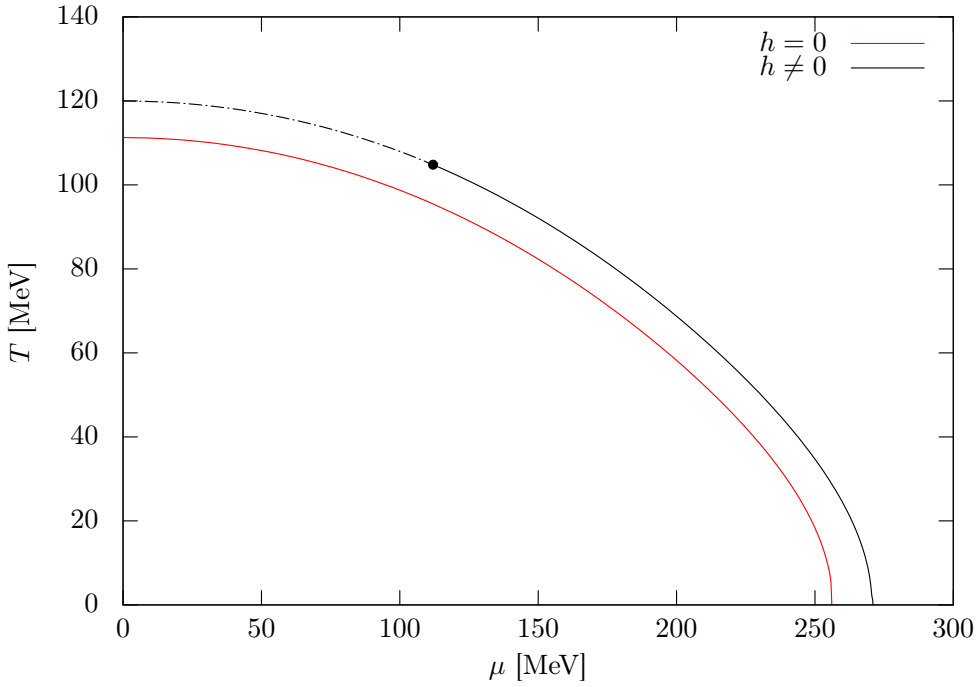

Figure 3.4: The phase diagrams for chiral symmetry breaking with $m_\sigma = 450$ MeV. First-order transition drawn as a solid line, while a crossover is drawn with dashed lines. The critical endpoint is marked by a dot •.

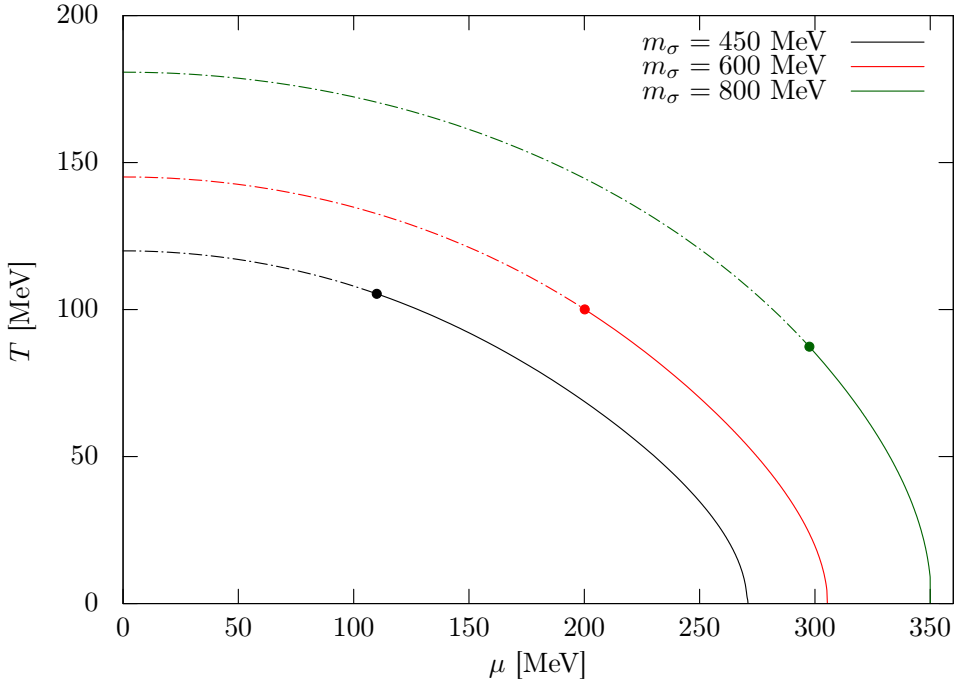

Figure 3.5: Phase diagrams for varying m_σ at the physical point $h = m_\pi^2 f_\pi$.

limit, and then introduce an extra term to explicitly break this symmetry. Looking back at how we constructed the QCD Lagrangian, the Lagrangian of the quark-meson model is

$$\mathcal{L}_{3fl} = \bar{q}\big(i\partial\!\!\!/ - gT_i(\sigma_i + i\gamma^5\pi_i)\big)q + \mathrm{tr}\big[\partial_\mu\phi^\dagger\partial^\mu\phi\big] - U_S(\phi) - U_B(\phi). \tag{3.22}$$

The matrices T_i are the nine generators of $U(3)$ (which are the eight generators of $SU(3)$ plus the identity), and $\phi = T_i(\sigma_i + i\pi_i)$. The potentials U_S and U_B are the symmetric and symmetry breaking potentials respectively, and are

$$U_S(\phi) = m^2\mathrm{tr}\big[\phi^\dagger\phi\big] + \lambda_1\Big(\mathrm{tr}\big[\phi^\dagger\phi\big]\Big)^2 + \lambda_2\mathrm{tr}\Big[\big(\phi^\dagger\phi\big)^2\Big], \tag{3.23}$$

$$U_B(\phi) = -c\big(\det[\phi] + \det[\phi^\dagger]\big) - \mathrm{tr}\big[h_iT_i(\phi + \phi^\dagger)\big]. \tag{3.24}$$

The chiral anomaly in QCD, which was introduced in Sec. 7, and was shown by 't Hooft in 1976 to be an effect of instanton configurations in the vacuum [46], is accounted for by the parameter c. The parameters h_i are introduced to break the $SU(3)_A$ chiral symmetry, In Ref. [47] it is shown that only diagonal matrices h_iT_i give symmetry breaking leading to the PCAC's, meaning that only h_0, h_3 and h_8 can be different from zero (we have chosen $T_0 = \frac{1}{\sqrt{6}}I$, and T_i to be the Gell-Mann matrices). We will also choose h_3 to be zero to conserve isospin symmetry between u and d, meaning that we only break one component of flavour symmetry. This is often referred to as the $2+1$ flavour quark-meson model. Evaluated in the mean-field approximation we get finite expectation values for σ_0 and σ_8 only. The quark contribution is thus

$$\mathcal{L}_{q\bar{q}} = \bar{q}_f\big(i\partial\!\!\!/ - m_f\big)q_f, \quad f \in \{u, d, s\}, \tag{3.25}$$

where m_f are the effective quark masses, $m_{u,d} = \frac{1}{\sqrt{6}}\big(\sigma_0 + \frac{1}{\sqrt{2}}\sigma_8\big)$ and $m_s = \frac{1}{\sqrt{6}}\big(\sigma_0 + \sqrt{2}\sigma_8\big)$. One can see that in this basis, σ_0 and σ_8 are superpositions of a strange and a non-strange condensate. It is more convenient to separate them, therefore a change of basis is made:

$$\begin{pmatrix}\sigma_{ud}\\ \sigma_s\end{pmatrix} = \frac{1}{\sqrt{3}}\begin{pmatrix}\sqrt{2} & 1\\ 1 & -\sqrt{2}\end{pmatrix}\begin{pmatrix}\sigma_0\\ \sigma_8\end{pmatrix}, \tag{3.26}$$

resulting in new effective quark masses $m_{u,d} = g\sigma_{ud}/2$ and $m_s = g\sigma_s/\sqrt{2}$. Similarly, we transform h_0 and h_8 to h_{ud} and h_s. Once again, the quarks in the mean-field approximation has gained effective masses by their interactions with the mesons, and the thermodynamic potential can be calculated analytically

$$\Omega = U_S + U_B + \Omega_{q\bar{q}}(T, \mu_i) \tag{3.27}$$

where the quark contribution is given by

$$\Omega_{q\bar{q}} = -2N_C\sum_{f=\{u,d,s\}}\int\frac{\mathrm{d}\mathbf{p}}{(2\pi)^2}\bigg\{T\log\Big[1 + e^{-(\omega_f+\mu_f)\beta}\Big] + T\log\Big[1 + e^{-(\omega_f-\mu_f)\beta}\Big]\bigg\}, \tag{3.28}$$

with $\omega = \sqrt{\mathbf{p}^2 + m_f^2}$. We will also here discard the vacuum energy of the fermions, even though we argued in the previous section that this term can have an effect on the order of the phase transition. To the best of the author's knowledge, this contribution has not yet been analysed in the three-flavour model, and is therefore a possible avenue for future research.

11.2 Matching parameters

Analogous to the parameter matching we did in Sec. 10.3, we have seven parameters to match in our current Lagrangian, g, h_{ud}, h_s, m, λ_1, λ_2, and c. The parameters h_{ud} and h_s can still be determined by the PCAC relations which relates the condensates at zero temperature and chemical potential to the pion and kaon decay constants [47, 48]

$$\langle \sigma_{ud} \rangle = f_\pi, \quad \langle \sigma_s \rangle = \frac{1}{\sqrt{2}}(2f_K - f_\pi). \tag{3.29}$$

We can use the pion and sigma masses to determine m^2 and λ_1, while λ_2 is set by the kaon mass. Lastly the anomaly parameter c is fixed by the average η-particle mass, $\frac{1}{2}(m_\eta^2 + m_{\eta'}^2)$. To be able to evaluate the particle masses, we need to transform the condensates to their meson basis. The $U(3)_V \times U(3)_A$ symmetry the Lagrangian was constructed from results in $9 + 9 = 18$ mesons. The nine belonging to $U(3)_V$, σ_i, make up the zero spin scalar nonet ($J^P = 0^+$), while the nine from $U(3)_A$, π_i, compose the zero spin pseudo scalar nonet ($J^P = 0^-$, depicted in Fig. 2.1). The σ and π matrices can therefore be written as [48]

$$\sigma = T_i \sigma_i = \frac{1}{\sqrt{2}} \begin{pmatrix} \frac{1}{\sqrt{2}}\sigma_{ud} + \frac{1}{\sqrt{2}}a_0 & a_0^- & K_0^{*-} \\ a_0^+ & \frac{1}{\sqrt{2}}\sigma_{ud} - \frac{1}{\sqrt{2}}a_0 & \bar{K}_0^* \\ K_0^{*+} & K_0^* & \sigma_s \end{pmatrix}, \tag{3.30}$$

$$\pi = T_i \pi_i = \frac{1}{\sqrt{2}} \begin{pmatrix} \frac{1}{\sqrt{2}}\pi_{ud} + \frac{1}{\sqrt{2}}\pi^0 & \pi^- & K^- \\ \pi^+ & \frac{1}{\sqrt{2}}\pi_{ud} - \frac{1}{\sqrt{2}}\pi^0 & \bar{K}^0 \\ K^+ & K^0 & \pi_s \end{pmatrix}, \tag{3.31}$$

where σ_{ud} and σ_s are mixtures of the σ particle and $f_0(1370)$ particle [1], while π_{ud} and π_s are mixtures of the η and η' particles. This results in the following parameters for sigma masses of 450, 600 and 800 MeV

m_σ [MeV]	m^2 [(MeV)^2]	λ_1	λ_2	c [MeV]	h_{ud} [(MeV)^3]	h_s [(MeV)^3]
450	$(467.53)^2$	-4.40	46.49	4807.25	$(120.73)^3$	$(336.41)^3$
600	$(342.50)^2$	1.40	46.49	4807.25	$(120.73)^3$	$(336.41)^3$
800	$-(306.29)^2$	13.49	46.49	4807.25	$(120.73)^3$	$(336.41)^3$

while g is still determined by the proton mass, $g = 2m_p/3f_\pi \approx 6.5$.

11.3 Results

We have plotted the two condensates, σ_{ud} and σ_s in Fig. 3.6 as a function of T at $\mu = 0$, and added lines showing the inflection points of the two curves. The nonstrange σ_{ud} condensate quickly

[1] $f_0(980)$ would also be a viable candidate, having the correct spin and parity, but the theory predicts a mass $m(\sigma_s) \approx 1200$ MeV, which is closer to 1370 MeV.

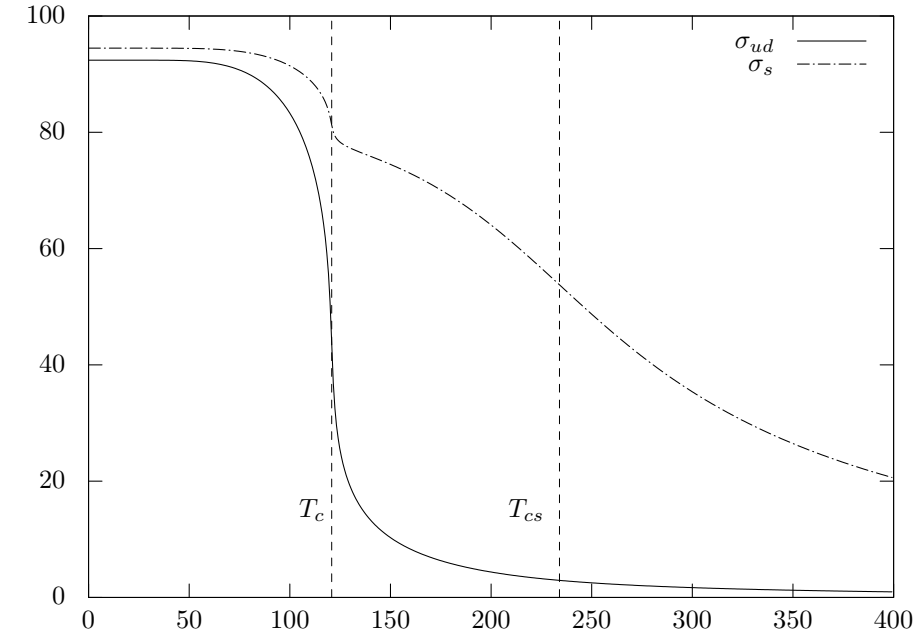

Figure 3.6: The two condensates in three-flavour LSMq at zero quark chemical potential for various temperatures. We have chosen $m_\sigma = 450$ MeV. One can see that the nonstrange condensate has a sharp corssover at $T = 120.8$ MeV, while the strange condensate has a much smoother crossover at higher $T \approx 234$ MeV.

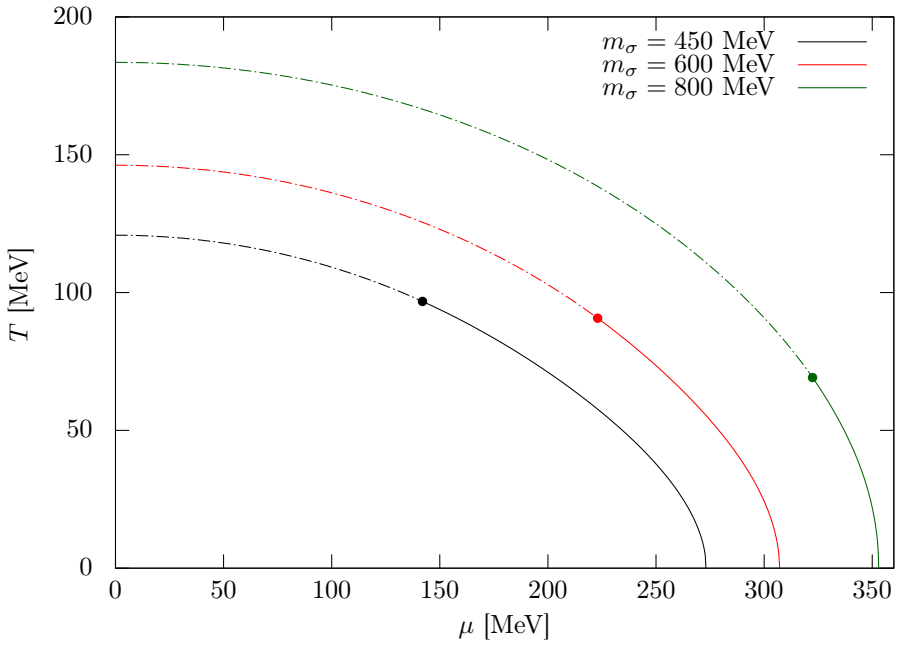

Figure 3.7: Phase diagrams for $m_\sigma = 450$, 600 and 800 MeV. Crossover transitions are drawn with dashed lines and first-order transition with solid lines. The CEP marked by •.

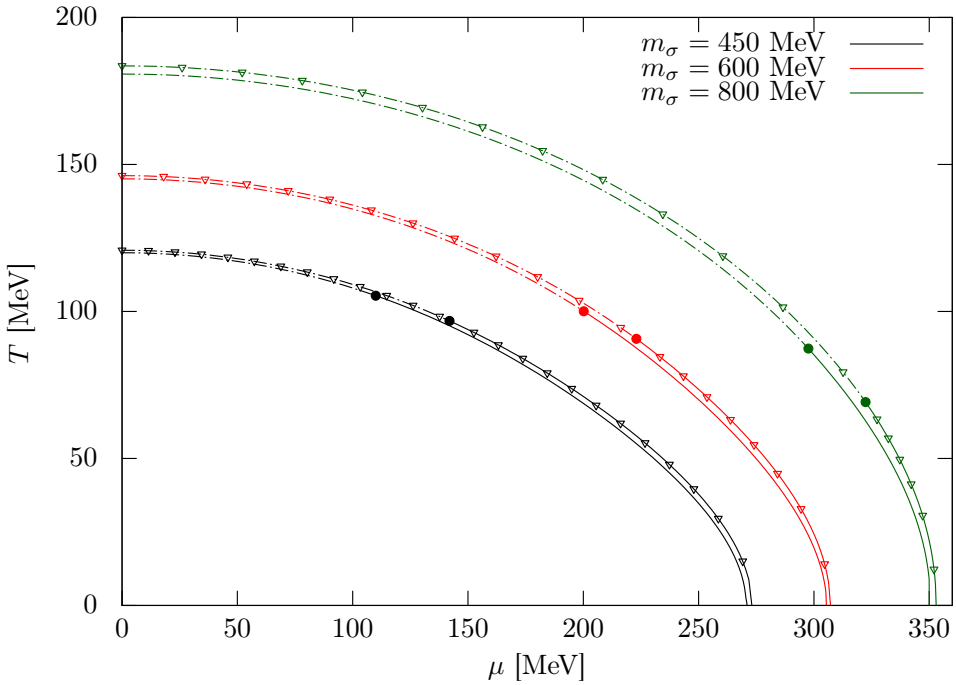

Figure 3.8: Phase diagrams for $m_\sigma = 450$, 600 and 800 MeV with both the two- and three-flavour LSMq models. Two-flavour results are plotted with plain lines while the three flavour results are marked by —▽—.

reaches its pseudocritical temperature T_c at 120.8 MeV, close to the two-flavour value (119.7 MeV). The strange σ_s condensate however reaches its pseudocritical temperature at a higher temperature of $T_{cs} = 234$ MeV. Its transition is also much smoother than that of σ_{ud}.

We once again plot phase diagrams for various sigma masses in Fig. 3.7. The critical temperature of the nonstrange condensate has been used to identify the phase transition for a given quark chemical potential, effectively marking the restoration of the $SU(2) \times SU(2)$ sub-symmetry of u and d, with the full $SU(3) \times SU(3)$ following at higher temperatures and/or particle densities. We have chosen the quark chemical potential to be independent of quark flavour, only considering identical chemical potentials $\mu_u = \mu_d = \mu_s \equiv \mu$. A comparison between the two- and three-flavour phase diagrams are made in Fig. 3.8. It is clear that the addition of the strange quark has a small effect on the overall result, but that it becomes more prominent at higher energy scales, meaning higher sigma mass as it is correlated to the temperature and density scale of the phase transition. This comes as no surprise, as higher energy scales are needed to produce the strange quark than the much lighter up and down quarks which dominates QCD at energies below 200 MeV.

In Appendix C7 the temperature dependence of the effective meson masses is displayed and discussed. The phase transition is just as pronounced in these plots as it is in Fig. 3.6, as the meson masses become degenerate when chiral symmetry is restored. The plots also show differences between the pseudocritical temperatures for the nonstrange and strange condensates, as for example the f_0 mass coincides with the other masses after the latter phase transition.

CHAPTER 4

Functional renormalisation group methods

Having produced phase diagrams with the slightly crude mean-field approximation in the last chapter, we now move on to a more advanced method, the functional renormalisation group. With this method we can find a nonperturbative expression for the thermodynamic potential in form of RG differential equations, as described in Sec. 3. This RG equation, being just as hard to solve as finding the exact thermodynamic potential, will have to be approximated, which we will do using the local potential approximation. This approach has become very popular since the introduction of the effective average action by Wetterich [49, 50, 51], and the application of it can be divided into two subgroups. One approach is to expand the potential in a Taylor series and truncate it after a few terms

$$U_k(\rho) = \sum_{n=1}^{N} t_n(k)\rho^n. \tag{4.1}$$

One can then insert this expression into the local potential approximated RGE and obtain coupled differential equations for the parameters t_n. Examples of this approach can be found in e.g. Refs. [52, 53]. An alternative approach, which is the one we will use here, is to discretise the fields, and treat the potential at the discrete values of the fields as separate variables, which again results in as many coupled differential equations as there are discrete values of the field, see for example Refs. [54, 55, 56].

12 The RG equation

Once again we will use the linear sigma model with two quark flavours to represent our system, its Lagrangian with an added quark chemical potential is given by

$$\mathcal{L}_E = \bar{q}\Big[\gamma^0\partial_\tau - i\vec{\gamma}\cdot\nabla + g\big(\sigma + i\gamma^5\vec{\tau}\cdot\vec{\pi}\big) - \mu\gamma^0\Big]q + \frac{1}{2}\big(\nabla_4\phi\big)^2 + U(\phi) - h\sigma. \tag{4.2}$$

where $\phi = \big[\sigma, \vec{\pi}\big]$. Also here, $U(\phi)$, is an $O(4)$ symmetric potential and an additional term, $h\sigma$, is added to the Lagrangian to explicitly break this symmetry. With the local potential approximation this Lagrangian gives the effective action

$$\Gamma_k[\phi, q, \bar{q}] = \int_0^\beta \mathrm{d}\tau \int \mathrm{d}\mathbf{x} \left\{\bar{q}\big[\gamma^0(\partial_\tau - \mu) - i\vec{\gamma}\cdot\nabla + g(\sigma + i\gamma^5\vec{\tau}\cdot\vec{\pi})\big]q + \frac{1}{2}\big(\nabla_4\phi\big)^2 + U_k(\phi) - h\sigma\right\}. \tag{4.3}$$

We assume that the quark-meson coupling g is already renormalised (is independent of k), and we see from Eq. (1.130) that h also must be k independent as $h\sigma$ is linear in sigma, and the right hand side of the RGE is only dependent on second derivatives in the fields. The full RG equation with

both boson and quark contributions is simply the sum of the right hand sides of Eqs. (1.130) and (1.135) [57], and can be written in diagrammic form as

$$\partial_k \Gamma_k \;=\; \frac{1}{2}\mathrm{tr}$$ 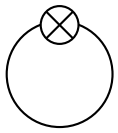 $$-$$ 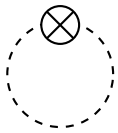 , (4.4)

where the trace is over the components of ϕ. There is also a trace implied in the fermionic term, but that trace is over spinor, flavour and colour indices. Writing out the diagrams, the RGE is

$$\partial_k \Gamma_k\big[\phi,\psi,\bar{\psi}\big] = \frac{1}{2}\mathrm{tr}\int_q \partial_k R_k(q)\bigg(\frac{\delta^2\Gamma_k}{\delta\phi_i(p)\delta\phi_j(p')} + \delta_{ij}\delta(p+p')R_k(p)\bigg)^{-1}_{q,-q} - \mathrm{tr}\int_q \partial_k P_k(q)\bigg(\frac{\delta^2\Gamma_k}{\delta\psi(q)\bar{\psi}(q)} + P_k(q)\bigg)^{-1}. \tag{4.5}$$

Using the effective action from Eq. (4.3), we want an RG equation for the potential U_k as it is the only k dependent term in Γ_k. Therefore similar to what we did in Sec. 3.4 we evaluate the RGE with space-time independent (uniform) fields. In this case, the double derivatives can be easily worked out:

$$\frac{\partial^2\Gamma_k}{\partial\phi_i(p)\partial\phi_j(p')} = \delta(p+p')\Big[p^2\delta_{ij} + \frac{\partial^2 U}{\partial\phi_i\partial\phi_j}\Big], \tag{4.6}$$

$$\frac{\partial^2\Gamma_k}{\partial\psi(p)\partial\bar{\psi}(p)} = \delta(0)\big[i\gamma^0(\nu_n+i\mu) + \vec{\gamma}\cdot\mathbf{p} + g(\sigma + i\gamma^5\vec{\tau}\cdot\vec{\pi})\big]. \tag{4.7}$$

We have Fourier transformed Eq. (4.3), and have denoted the zeroth component of the momentum four-vector as ω_n for bosons and ν_n for fermions, same as the notation introduced in Sec. 2.2. Next we have to choose the bosonic and fermionic cut-off functions $R_k(q)$ and $P_k(q)$, which have to satisfy the conditions stated in Eqs. (1.113) to (1.115). An approximate way to achieve the second of these conditions is by substituting infinity by the order of the renormalisation scale, which should be chosen to be much higher than every other energy scale present. With this slight relaxation, the second condition becomes

$$R_{k=\Lambda}(q) \sim \Lambda^2, \tag{4.8}$$

$$P_{k=\Lambda}(q) \sim \Lambda, \tag{4.9}$$

It is also important to note that P_k must have the same Lorentz structure as a momentum term, i.e. $P_k(q) \sim \gamma_\mu q^\mu$. If it was similar to a mass term ($P_k(q) \sim \sqrt{q^2}$) or an axial current term ($P_k(q) \sim \gamma^5\gamma_\mu q^\mu$), it would explicitly break chiral symmetry. A thorough discussion can be found in [57]. We will choose the same cut-off functions as e.g. [55, 58],

$$R_k(q) = (k^2 - \mathbf{q}^2)\,\theta(k^2-\mathbf{q}^2), \tag{4.10}$$

$$P_k(q) = \left(\sqrt{\frac{(\nu_n+i\mu)^2+k^2}{(\nu_n+i\mu)^2+\mathbf{q}^2}} - 1\right)\big[i\gamma^0(\nu_n+i\mu) + \vec{\gamma}\cdot\mathbf{q}\big]\,\theta(k^2-\mathbf{q}^2), \tag{4.11}$$

where the function $\theta(x)$ is the Heaviside step function.

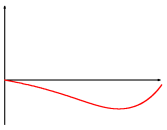

12.1 Bosonic contribution

We will first evaluate the bosonic contribution to the RG equation using the cut-off function defined in Eq. (4.10). Its contribution to the differential equation of U_k is

$$\partial_k U_k(\phi)_B = T\sum_{n=-\infty}^{\infty}\int\frac{\mathrm{d}\mathbf{q}}{(2\pi)^3}k\,\theta(k^2-\mathbf{q}^2)\mathrm{tr}\left[\frac{\partial_k U^2}{\partial\phi_i\partial\phi_j}+\delta_{ij}\big(q^2+(k^2-\mathbf{q}^2)\,\theta(k^2-\mathbf{q}^2)\right]^{-1} \tag{4.12}$$

The potential U is $O(4)$ symmetric, and can therefore be expressed as a function of $\rho=\frac{1}{2}(\sigma^2+\vec{\pi}^2)$. In this basis, the second derivative of U is $\frac{\partial^2 U}{\partial\phi_i\partial\phi_j}=\delta_{ij}U'(\rho)+\phi_i\phi_j U''(\rho)$, where $U'(\rho)$ denotes derivative with respect to ρ. We have assumed that U will retain its symmetry as it is renormalised, and we can therefore pick out a single direction in ϕ space on which U depends, and set the rest to zero. As we have explicitly broken the $O(4)$ symmetry in the direction of σ, we will choose this as the primary direction, and set $\vec{\pi}=0$, and $\rho=\frac{1}{2}\sigma^2$. With this the matrix in Eq. (4.12) is diagonal

$$\begin{pmatrix} U'+2\rho U''+q^2+R_k & 0 & 0 & 0\\ 0 & U'+q^2+R_k & 0 & 0\\ 0 & 0 & U'+q^2+R_k & 0\\ 0 & 0 & 0 & U'+q^2+R_k\end{pmatrix}, \tag{4.13}$$

which simplifies the expression considerably:

$$\partial_k U_k(\phi)_B=\frac{T}{2\pi^2}\sum_{n=-\infty}^{\infty}\int_0^\infty q^2\mathrm{d}q\,k\,\theta(k^2-\mathbf{q}^2)\left[\frac{1}{\omega_n^2+\mathbf{q}^2+R_k(q)+U'+2\rho U''}\right.$$
$$\left.+\frac{3}{\omega_n^2+\mathbf{q}^2+R_k(q)+U'}\right]. \tag{4.14}$$

The first Heaviside function ensures that the integrand is zero for all values of q higher than k. We can therefore substitute the upper limit of the integral with k instead of infinity. As q now is ensured to be less than k, all step-functions are evaluated to be one, in which case $\mathbf{q}^2+R_k(q)=\mathbf{q}^2+(k^2-\mathbf{q}^2)\theta(k^2-\mathbf{q}^2)=k^2$, and we are left with

$$\partial_k U_k(\phi)_B=\frac{T}{2\pi^2}\sum_{n=-\infty}^{\infty}\int_0^k p^2\mathrm{d}p\,k\left[\frac{1}{\omega_n^2+k^2+U'+2\rho U''}+\frac{3}{\omega_n^2+k^2+U'}\right]. \tag{4.15}$$

The only momentum dependence remaining is that from the integral measure, and the integral is therefore easily carried out

$$\partial_k U_k(\phi)_B=\frac{Tk^4}{6\pi^2}\sum_{n=-\infty}^{\infty}\left[\frac{1}{\omega_n^2+k^2+U'+2\rho U''}+\frac{3}{\omega_n^2+k^2+U'}\right]. \tag{4.16}$$

The Matsubara sums are both on the form calculated in Appendix B5, and are given by Eq. (B.17):

$$\partial_k U_k(\phi)_B=\frac{k^4}{12\pi^2}\left\{\frac{1}{\omega_\sigma}\big[1+2n_B(\omega_\sigma)\big]+\frac{3}{\omega_\pi}\big[1+2n_B(\omega_\pi)\big]\right\}, \tag{4.17}$$

where $n_B(\omega) = \left(e^{\omega}/T - 1\right)^{-1}$ is the Bose-Einstein distribution, and the sigma and pion dispersion relations are

$$\omega_\sigma^2 = k^2 + U' + 2\rho U'', \tag{4.18}$$

$$\omega_\pi^2 = k^2 + U'. \tag{4.19}$$

12.2 Fermionic contribution

Just as in the previous calculation, the step function in the numerator ensures that $\mathbf{q} \leq k$, and we can therefore replace the step function in the denominator by 1. This implies that we have to evaluate an object on the form

$$\mathrm{tr}\frac{\left[i\gamma^0(\nu_n + i\mu) + \vec{\gamma}\cdot\mathbf{q}\right]\partial_k A_k}{\left[i\gamma^0(\nu_n + i\mu) + \vec{\gamma}\cdot\mathbf{q}\right]A_k + g\sigma}, \tag{4.20}$$

where A_k is the square root term in P_k, and we have set $\vec{\pi} = 0$. To evaluate this we can expand it in a power series:

$$\frac{1}{g\sigma + \left[i\gamma^0(\nu_n + i\mu) + \vec{\gamma}\cdot\mathbf{q}\right]A_k} = \frac{1}{g\sigma}\sum_{n=0}^{\infty}\left(\frac{-A_k}{g\sigma}\right)^n\left[i\gamma^0(\nu_n + i\mu) + \vec{\gamma}\cdot\mathbf{q}\right]^n. \tag{4.21}$$

Utilising that all the γ matrices are traceless and follow the anti-commutation relation $\left\{\gamma^\mu, \gamma^\nu\right\} = \eta^{\mu\nu}$, we can trace the expression order by order

$$\begin{aligned}
n = 0: &\quad i\gamma^0(\nu_n + i\mu) + \vec{\gamma}\cdot\mathbf{q} &&\quad \mathrm{tr} \to 0,\\
n = 1: &\quad -(\nu_n + i\mu)^2 - \mathbf{q}^2 &&\quad \mathrm{tr} \to -4N_cN_f\left[(\nu_n + i\mu)^2 + \mathbf{q}^2\right],\\
n = 2: &\quad \left(i\gamma^0(\nu_n + i\mu) + \vec{\gamma}\cdot\mathbf{q}\right)^3 &&\quad \mathrm{tr} \to 0,\\
&\quad \vdots
\end{aligned} \tag{4.22}$$

which again can be recognised as a different power series. The expression in Eq. (4.20) is therefore

$$\begin{aligned}
4N_cN_f(\partial_k A_k)\frac{A_k}{(g\sigma)^2}\left[(\nu_n + i\mu)^2 + \mathbf{q}^2\right]\sum_{n=0}^{\infty}\left(\frac{-A_k^2}{(g\sigma)^2}\right)^n&\left[(\nu_n + i\mu)^2 + \mathbf{q}^2\right]^n\\
&= A_k(\partial_k A_k)\frac{4N_cN_f\left[(\nu_n + i\mu)^2 + \mathbf{q}^2\right]}{(g\sigma)^2 + A_k^2\left[(\nu_n + i\mu)^2 + \mathbf{q}^2\right]}.
\end{aligned} \tag{4.23}$$

Inserting the expression for A_k, the fermion contribution is greatly simplified, and we are left with

$$\partial_k U_{kF} = -T\frac{2N_cN_f}{\pi^2}\sum_{n=-\infty}^{\infty}\int_0^k q^2\mathrm{d}q\,\frac{k}{(\nu_n + i\mu)^2 + k^2 + (g\sigma)^2}. \tag{4.24}$$

Once again the only q dependence left is that of the integration measure, and the integral is readily calculated, leaving the sum. The sum is also on the form presented in Appendix B5, and utilising Eq. (B.21) we end up with the final result

$$\partial_k U_{kF} = -\frac{N_cN_f}{3\pi^2}\frac{k^4}{\omega_q}\left[1 - n_F(\omega_q, \mu) - n_{\bar{F}}(\omega_q, \mu)\right], \tag{4.25}$$

where the quark energy is

$$\omega_q^2 = k^2 + (g\sigma)^2, \tag{4.26}$$

and $n_F(\omega_q, \mu)$ is the fermion distribution function introduced in the last Chapter.

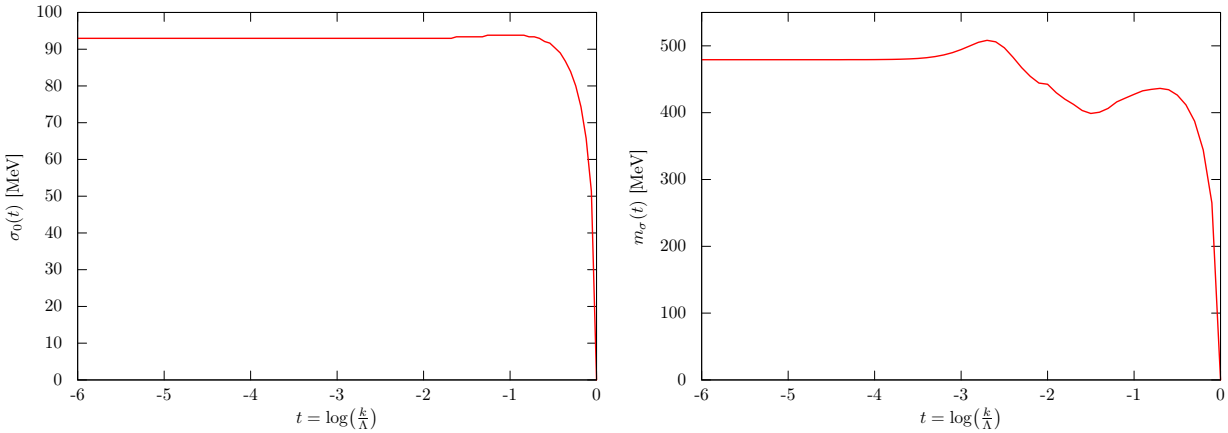

(a) Minimum of U_k.

(b) Curvature of U_k at the minimum.

Figure 4.1: Plots showing the convergence of the parameter conditions as a function of RG time.

12.3 Full RG equation

Combining the meson and quark contribution we obtain the full RG equation for U_k

$$\partial_k U_k(\rho) = \frac{k^4}{12\pi^2}\left\{\frac{1}{\omega_\sigma}\Big[1+2n_B(\omega_\sigma)\Big] + \frac{3}{\omega_\pi}\Big[1+2n_B(\omega_\pi)\Big]\right\} - \frac{N_c N_f}{3\pi^2}\frac{k^4}{\omega_q}\Big[1-n_F(\omega_q,\mu)-n_{\bar{F}}(\omega_q,\mu)\Big]. \tag{4.27}$$

By setting the meson fluctuations to zero, we recover the expression given by the mean-field approximation. This approach will therefore hopefully give more accurate results for the thermodynamic potential and in extension the phase transition, as it includes both quantum- and thermal fluctuations of the meson fields in addition to the quark fluctuations.

The RG equation is a two dimensional partial differential equation in the sense that it has partial derivatives with respect to k on the left hand side and with respect to ρ on the right hand side. As mentioned in the introduction to this chapter, two possible approaches one can take to solve this is either to parametrise U_k and find one ordinary differential equation (ODE) for each parameter, or to discretise $\rho \longrightarrow \rho_i$ and find an ODE for each $U_i(k) = U_k(\rho_i)$. In this work the latter has been chosen, and the details behind discretisation and how the partial derivatives in ρ are evaluated are given in chapter 5.

13 Initial conditions and parameters

Before we can solve Eq. (4.27), we need to provide a continuous set of initial conditions for the potential U_k. These should be given at $k = \Lambda$, where all quantum fluctuations are suppressed and we regain the classical potential. For the initial condition we will use the same potential we used in Sec. 10 when utilising the mean-field approximation,

$$U_\Lambda(\rho) = m^2\rho + 4\lambda\rho^2. \tag{4.28}$$

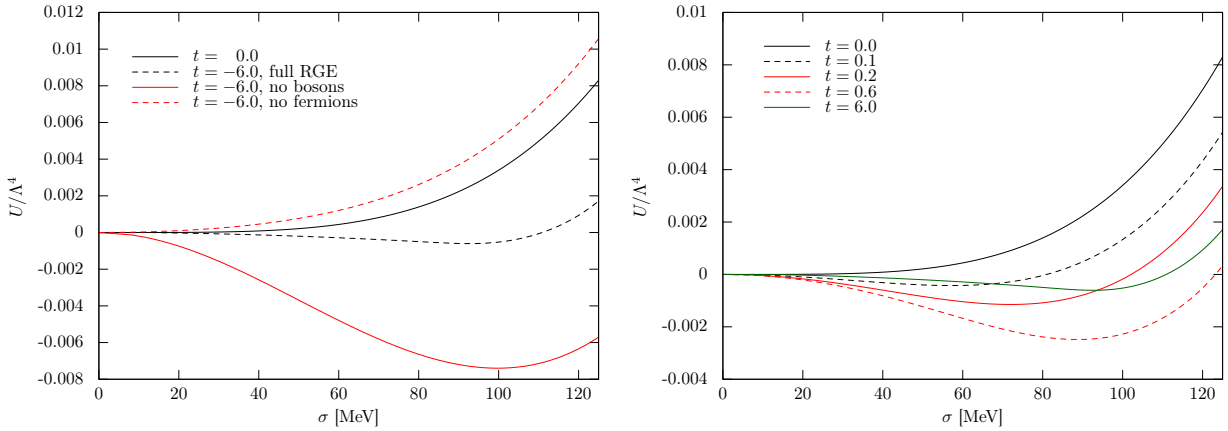

(a) Different contributions to the renormalisation of $U_k(\sigma)$.

(b) The potential $U_k(\sigma)$ at various RG times t.

Figure 4.2: Plots displaying various aspects of the renormalisation of U_k at $h = 0$.

With this choice, the Lagrangian has four free parameters, which we will match to f_π, m_π, m_σ, and the proton mass m_p. We will map out the phase diagram both with and without explicit symmetry breaking by the $h\sigma$ term, and therefore need to determine m^2 and λ for both these cases. The parameters h and g are set to $g = m_q/3f_\pi$ and $h = 0$ or $h = m_\pi^2 f_\pi$, while m^2 and λ are set by the two conditions

$$\left.\frac{\partial\Omega}{\partial\sigma}\right|_{\sigma=f_\pi} = \left.\frac{\partial U_{k=0}}{\partial\sigma}\right|_{\sigma=f_\pi} - h = 0, \tag{4.29}$$

$$\left.\frac{\partial^2\Omega}{\partial\sigma^2}\right|_{\sigma=f_\pi} = \left.\frac{\partial^2 U_{k=0}}{\partial\sigma^2}\right|_{\sigma=f_\pi} = m_\sigma^2, \tag{4.30}$$

both at zero temperature and zero chemical potential. When integrating the full RG equation numerically, it is convenient to change integration variable from k to the dimensionless variable $t = \log\left(\frac{k}{\Lambda}\right)$, which we will call RG time. In Fig. 4.1 we can see how the minimum, which should be equal to f_π at $t = -\infty$, and the square root of the curvature of U at the minimum, which should be m_σ at $t = -\infty$, evolve as t moves from zero towards minus infinity. While the minimum quickly stabilises at around $t \approx -2$, the curvature continues to vary, but settles close to $t \approx -3.5$. We will assume that the contribution from $t < -6$ ($k < 2.5\,10^{-3}\Lambda$) is negligible, and therefore truncate the numerical integration at $t = -6$.

On top of the four parameters of the Lagrangian, the initial condition for U presented in Eg. (4.28) has an additional parameter, Λ. Analytically, all physical quantities (such as m_σ, f_π and T_c) are independent of the cut-off scale Λ as long as it is larger than the highest energy scale of the system. Unfortunately the numerical results are not, but the dependence on Λ is weak. We have chosen a cut-off scale $\Lambda = 500$ MeV, which is larger than our choice for m_σ, just as Schaefer and Wambach did in [54]. As we will analyse further in Chapter 5, the value of the sigma mass is somewhat problematic to determine in this model. While the minimum is very resilient to change, the curvature at the minimum does not only depend on the five parameters, but also on the numerical method used to solve the ODEs, which is unfortunate. The sigma mass will therefore be set by an interval approximately 350 - 500 MeV instead of by a specific value. With this is place, the

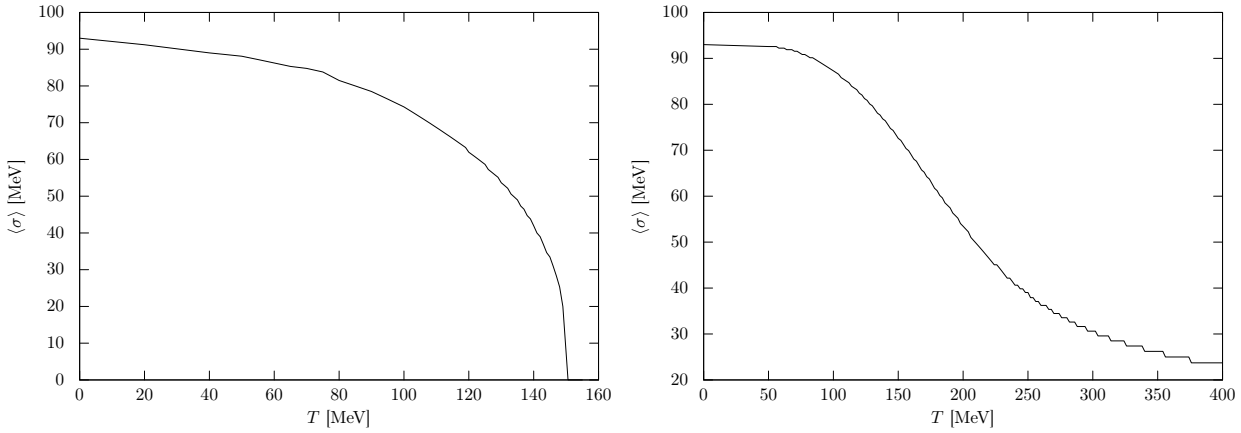

(a) $h = 0$ (b) $h = m_\pi^2 f_\pi$

Figure 4.3: Minimum of the potential U_0 as a function of T with $\mu = 0$. The left plot is taken in the chiral limit, and it shows second-order phase transition as the minimum goes continuously to zero. The right plot is at the physical point and it shows a crossover where the minimum approaches zero as T increases.

values chosen for m^2 and λ are

	$h = 0$	$h = m_\pi^2 f_\pi$
m^2 [(MeV)^2]	0	$(98.1)^2$
λ	2.125	2.45

14 Results

From the full RG equation given in Eq. (4.27) it can immediately be seen that the renormalisation is a competition between the meson and quark contributions. The meson contribution, having a positive sign, drives the potential to higher values, weakening its symmetry breaking and pushes the minimum towards zero, while the quark contribution has the opposite effect. This is even clearer in Fig. 4.2a, where the renormalised potential has been plotted with either the quark- or the meson contribution turned off. The unrenormalised and fully renormalised potential has also been plotted as a reference. Combined with the plots in Fig. 4.2b which show the potential at different renormalisation times t, we can conclude that the quark contribution is dominant in the high k region, while the mesons contribute more towards the end. Because the meson contribution is dependent on the derivatives of U, we see that as the potential starts to decline, we get a feedback reaction where the meson contribution takes over as a result of the quark contribution pushing the potential down. At around $t = -0.6$ or $k \approx 0.5\Lambda$ we see that the feedback has reached its limits and the potential is driven towards higher values again. These complex interplays between the two contributions are the reason why the fully renormalised potential is not simply the average between the pure meson and pure quark renormalised potentials.

In Fig. 4.3 the minimum of the renormalised potential U_0 as a function of temperature has been plotted. In the chiral limit (the left plot) we have a second-order phase transition at zero quark

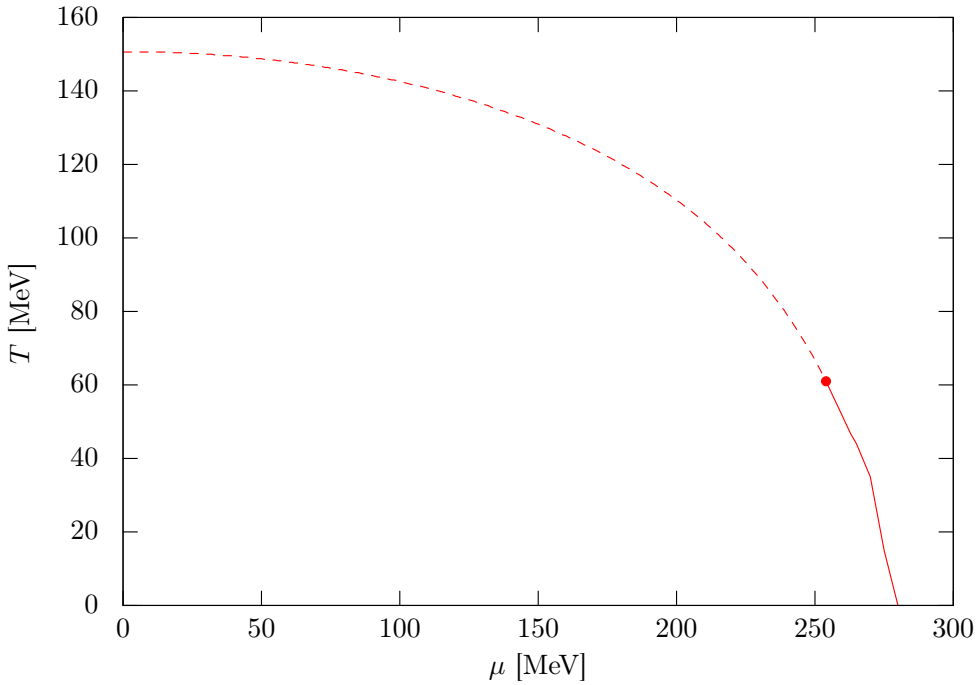

Figure 4.4: Phase diagram in the chiral limits. The second-order phase transition is plotted with a dashed line, while the first-order phase transition is plotted with a solid line. The critical endpoint is marked by a dot •.

chemical potential. At higher chemical potentials, this transition eventually turns into a first-order transition, and we therefore also in the chiral limit find a critical endpoint. This was not seen in either of the two mean-field approximations (although not explicitly shown for the three-flavour model), telling us that the inclusion of both the thermal and quantum fluctuations of the mesons add to the phase diagram. The resulting phase diagram is plotted in Fig. 4.4, and one can see the critical endpoint at $(T, \mu) \approx (253, 62)$ MeV. The plot to the right in Fig. 4.3 shows a crossover transition at the physical point. Because we lack precise knowledge of the position of the minimum, due to the discretisation of σ, the inflection point cannot be found with numerical derivatives like we did previously. The data points were therefore fitted to a similar curve, from which we could calculate the inflection point. The phase diagram at the physical point has been plotted in Fig. 4.5. The standard deviation of the fitting parameters, resulting in a standard deviation for the critical temperature, has been added as error bars. After $\mu \approx 260$ MeV, the fitting function is no longer good, and the transitions have therefore been taken as an educated guesses based on the shape of the $\sigma_0(T)$ plots, the error bars given accordingly. The fitting procedure and the resulting errors are discussed in more detail in Sec. 17.4. One should also notice the lack of a critical endpoint in the phase diagram at the physical point. It should be stressed that this is not because none exists, but is simply a consequence of the numerics, as they are less accurate at small, but nonzero, temperatures. It was therefore difficult both to find the transition temperature, and also the order of the transition. The critical endpoint has therefore been omitted.

The plots in Fig. 4.6 shows a comparison between phase diagrams produced using the LPA

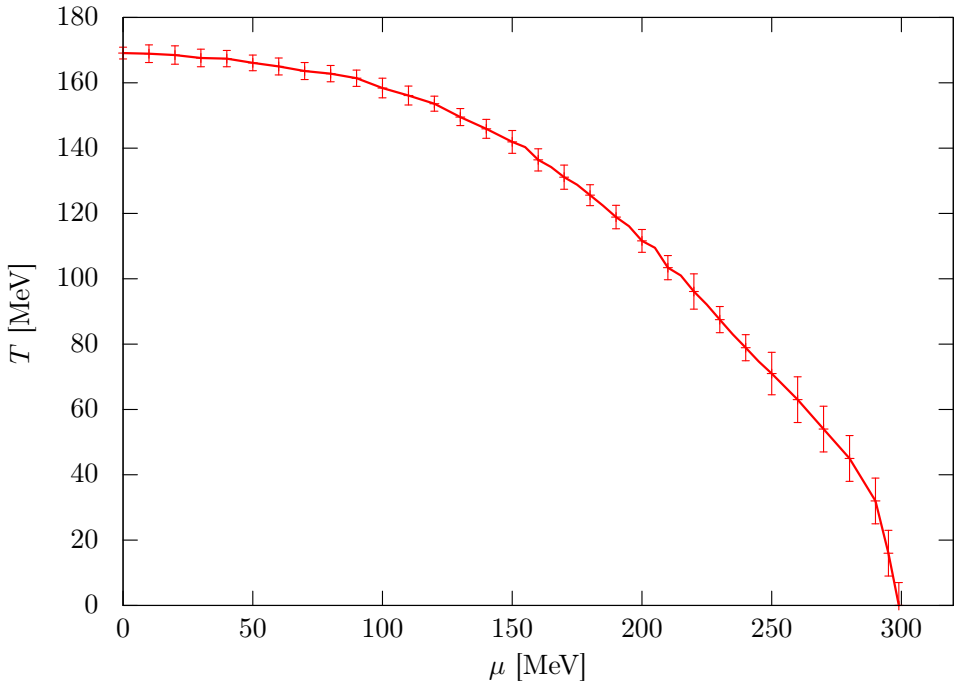

Figure 4.5: Phase diagram at the physical point. The error bars indicate the error of the parameter fit which had to be carried out to identify the crossover transition, see the full text and Sec. 17 for more details.

and the mean-field approximation. In both the chiral limit and the physical point we see that the inclusion of meson fluctuations has pushed the critical temperature at zero chemical potential to a higher value, despite the lower value for the sigma mass. On the other hand, in the region of high μ and low T the phase diagrams calculated with the LPA drops quicker than that of the mean-field approximation. The two curves even cross before they hit the μ axis. The explanation for this behaviour can be found in the RG equation, Eq. (4.27). At zero temperature the fermionic contribution to the potential is:

$$\partial_k U_{kF}(T=0) = -\frac{N_f N_c}{3\pi^2}\frac{k^4}{\omega_q}\big[1-\theta(\mu-\omega_q)\big], \tag{4.31}$$

where once again θ is the Heaviside step function. Therefore, for all values of k and σ such that $\omega_q < \mu$, the quark contribution is zero, and as a result, at high μ and low T the meson contribution is dominating. Earlier we argued that the meson contribution weakens the symmetry breaking, driving the minimum towards zero, which is why we should expect the phase diagram to drop quicker at high μ if this contribution is included.

15 Thermodynamic quantities

In Sec. 2.1 we introduced the thermodynamic potential Ω and the various thermodynamic quantities which could be calculated based on it. In this section we will use the LSMq with the local potential

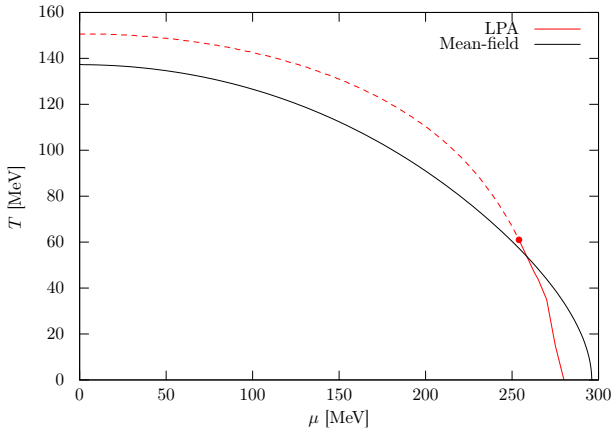

(a) In the chiral limit. First-order transition marked with solid line, second-order with dashed line.

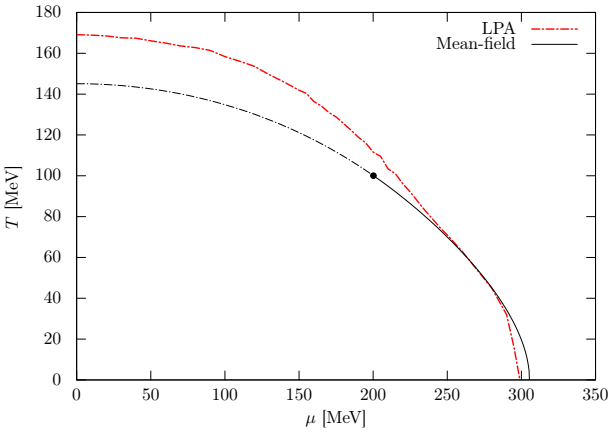

(b) At the physical point. First-order transition plotted with solid line, crossover with dashed line.

Figure 4.6: Comparison between phase diagrams resulting from the LPA ($m_\sigma \approx 450$ MeV) and the mean-field approximation ($m_\sigma = 600$ MeV).

approximation to calculate these quantities and compare them to that of a free gas of massless quarks and gluons.

15.1 Additional contributions to the high temperature region

If we had used Eqs. (1.75) to (1.78) to calculate the thermodynamic quantities using the results for Ω obtained after having integrated down from the ultraviolet cut-off scale Λ, we would find the results lacking in the high temperature regions when compared to e.g. mean-field calculations or lattice results. The reason for this is that we are missing the temperature dependence of the modes with energies higher than Λ, and these need to be reincluded in to obtain correct results for the thermodynamic quantities. We write the corrected Ω as

$$\Omega = \Omega_0 + \Omega_\Lambda, \tag{4.32}$$

where Ω_0 is the contribution from $k = \Lambda$ to $k = 0$, the one calculated in the previous section, and Ω_Λ is the contribution from $k = \infty$ to $k = \Lambda$. Due to the asymptotic freedom of the quarks and gluons we assume that the meson condensates have melted, and that we are left with free quarks and gluons for energies above Λ. Therefore, for $k > \Lambda$, the RG equations are

$$\partial_k U_k = \frac{k^3}{12\pi^2}\left\{ N_g\big[1 + 2n_B(k)\big] - 4d_F\big[1 - n_F(k) - n_{\bar{F}}(k)\big]\right\}, \tag{4.33}$$

where $N_g = 2(N_c^2 - 1)$ is the degrees of freedom for the gluons and $d_F = N_f N_c$ is the degrees of freedom for the quarks. We have excluded the quark mass from the dispersion relation of the quarks as it is negligible compared to values of k larger than Λ. The addition from the high temperature limit to the thermodynamic potential is therefore

$$\Omega_\Lambda = \frac{1}{12\pi^2}\int_\infty^\Lambda k^3 \mathrm{d}k \left\{ N_g\big[1 + 2n_B(k)\big] - 4d_F\big[1 - n_F(k) - n_{\bar{F}}(k)\big]\right\}. \tag{4.34}$$

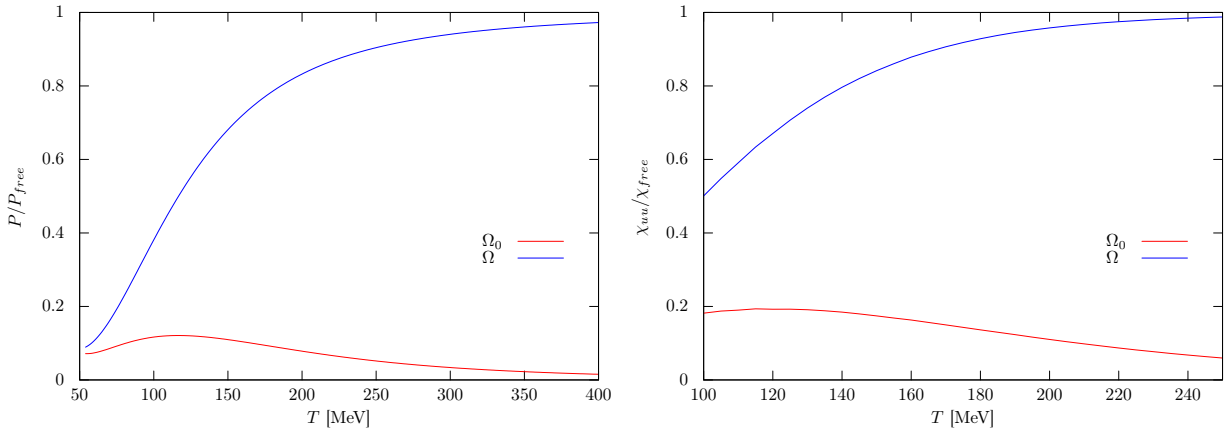

(a) Pressure as a function of temperature at the physical point normalised to that of a free gas of quarks and gluons P_{free}.

(b) The u quark number susceptibility as a function of temperature at zero quark chemical potentials.

Figure 4.7: The pressure and quark number susceptibility at the physical point using the LPA both with and without corrections from the high energy modes. The lower curve is without corrections while the upper one is with.

The two divergent terms are also this time not dependent on either T nor μ, and they therefore only contribute to an unobservable shift of the potential. The thermodynamic potential can be renormalised simply by subtracting the potential of the vacuum from the final result.

15.2 Results

All the results of this section will be normalised to those of a free gas of massless quarks and gluons, and will be given at zero quark chemical potential. The thermodynamic potential of a free gas of massless quarks and gluons is given by

$$\Omega_{free} = -\Big(N_g + \frac{7}{2}d_F\Big)\frac{\pi^2}{90}T^4 - \frac{d_F}{6}T^2\mu^2 - \frac{d_F}{12\pi^2}\mu^4. \tag{4.35}$$

The pressure with and without the high temperature correction has been plotted in Fig. 4.7a normalised with the pressure of an ideal gas. The plot clearly demonstrates that the high energy modes becomes more important as one cranks up the temperature, but there is a problem. Already at $T = 50$ MeV, around 20% of the pressure comes from the high energy modes, and as T rises above 250 MeV, the contribution from the modes with energy less than Λ becomes negligible. The same behaviour can be seen from the quark number susceptibility

$$\chi_{ij} = \frac{\partial^2 P}{\partial\mu_i\partial\mu_j} \tag{4.36}$$

which has been plotted in Fig. 4.7b.

The problem arises from the choice we made for Λ. While 500 MeV was sufficient to obtain information about the critical region and find the chiral transition for a sigma mass approximately

450 MeV, it is too low to acquire information on the thermodynamics of the system at high temperatures. Unfortunately, choosing a higher cut-off scale requires a lot of time both tuning parameters and calculating the quantities themselves. We therefore did not have enough time to finish these calculations, and it will therefore be a natural continuation of this work. This will be discussed further in the last chapter.

CHAPTER 5

Numerical methods

In this chapter we will analyse the underlying numerics of the results presented in this thesis. We will focus on numerical methods, numerical instability and minor details one has to pay attention to. There will be both pseudocode and C++ code included to describe the numerical methods and ideas.

16 The mean-field approximation

First, a short summary of the numerics at the base of the mean-field results will be given. The GNU Scientific Library (GSL) [59], a C library for numerical computation, has been used extensively. Most notably it includes a C implementation of QUADPACK [60], a FORTRAN77 library for numerical integration of one-dimensional functions, which was used to evaluate the integrals in Eqs. (3.9,3.28). We also used two of the library's many root finding algorithms. The Brent algorithm was utilised to find the roots of the two-flavour model, and the Hybrid algorithm with a multi-dimensional finite difference scheme to calculate the Jacobian was used for root-finding with the three flavour model, see [59, p. 383] for more detail.

16.1 Crossover transitions

Finding the phase transitions for small chemical potentials is quite straight forward. For both the two- and three flavour case, the root of the derivative of the thermodynamic potential was found rather than the minimum, as an analytic expression for this derivative could be easily calculated. We only had a crossover at the physical point, whose inflection point was found by numerical derivatives in T. When scanning for this inflection point, steps of around 10^{-2} MeV were taken in T, being more than sufficient to get accurate enough results to take numerical derivatives, which we will see is not the case with results from the renormalisation group methods.

16.2 First-order phase transitions

Finding the first-order phase transition when $h = 0$ is trivial as we know that the minimum jumps to zero at the phase transition. Therefore one only has to check if the thermodynamic potential at the local minimum is less than the value at zero for every iteration. When this no longer is the case, we have found the critical temperature.

At the physical point it is a little bit trickier as the new minimum to which we jump discontinuously also has to be found. Therefore, knowing both the shape of the potential and the nature of the root finding method in use is essential. When using numerical root-finding functions, one has to

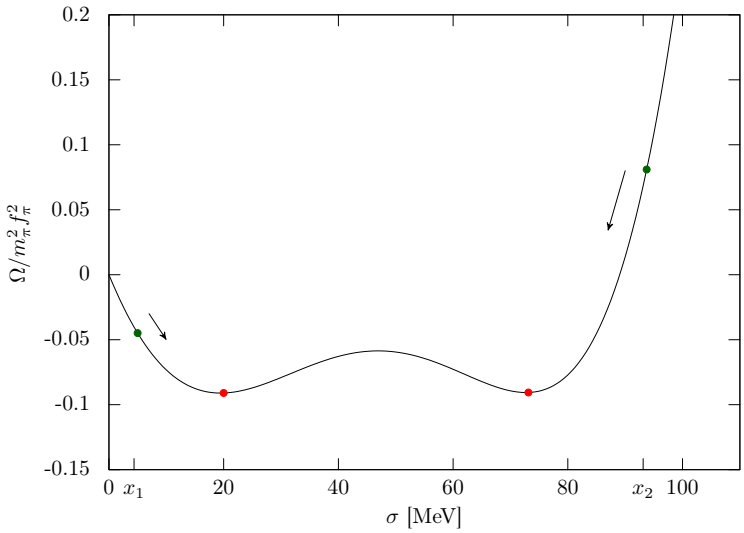

Figure 5.1: A plot showing multiple root finding with multiple guesses. Potential taken from two-flavour linear sigma model with $m_\sigma = 600$ MeV at $(T, \mu) = (70, 250)$ MeV at the physical point.

specify an initial guess where the root might be. If the function has multiple roots, the numerical method usually finds a root close to where the guess said it would be. When looking for a first-order transition we therefore have to make two guesses to where the minima are. From Fig. 5.1 we can see that in our case, a good idea is to let one guess be close to the original minimum (f_π), and the other guess be around zero. Below is a pseudocode snippet describing how the phase transitions were found and identified:

```
mins[5] stores 5 minima, needed for numerical double derivative
findMinimum() takes two input, temperature and a guess, returns minimum
for i = 0 to 5 do {find the first 5 minima}
   mins[i] = findMinimum(T,f_π)
   T = T + dT
end for
while T < T_max do
   min1 = findMinimum(T, mins[4])
   min2 = findMinimum(T, 0)
   if min1 ≠ min2 then
      if Ω(min2) < Ω(min1) then
         return T {T_c found, first-order transition}
      end if
   end if
   for i = 1 to 5 do {throw away one minimum to make room for min1}
      mins[i − 1] = mins[i]
   end for
   mins[4] = min1
   ddx = doubleDerivative(mins) {calculate numerical double derivative}
   if ddx > 0 then
      return (T − 2dT) {inflection point, second-order transition}
   end if
```

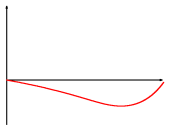

$T = T + \mathrm{d}T$
end while

17 Renormalisation group approach

We solved the RG equation, which is a partial differential equation in k and ρ numerically by discretising $U_k(\rho) \longrightarrow U_k(\rho_i)$, where ρ_i are the discrete values of ρ and i runs from 1 to n. This way we are left with an n-dimensional ODE instead, which we proceeded to solve using Runge-Kutta algorithms of varying order. We tested the results for $n = 100$, 200, 500 and 1000. While the three first choices had no affect on our final result, the third choice gave worse results than the others. This is to be expected as we do not have the precision in k to account for the precision in ρ. A good analysis of errors in numerical solutions to PDEs can be found in [61, p. 1036]. Most of the results are therefore calculated with $n = 200$. Actually, for most of the results $n = 256$ was used. The reason for this is that the code used to solve the ODEs was paralellised using a messenger passing interface (MPI) library for C++, and as processors have a tendency to come with the number of processing cores equal to a power of two, $256 = 2^8$ was used for portability.

17.1 Runge-Kutta method

Probably the most used method for numerical solutions to ODEs is the Runge-Kutta method. To illustrate it, we will use an ODE on the form

$$\frac{\mathrm{d}y(t)}{\mathrm{d}t} = f(y, t). \tag{5.1}$$

Let us descretise it in time, $t \longrightarrow t_i = t_0 + ih$ and $y(t) \longrightarrow y_i = y(t_i)$. The lowest order Runge-Kutta method (normally called the Euler method) is obtained by substituting the derivative in Eq. (5.1) with a first-order forward difference formula:

$$y_{i+1} = y_i + hf(y_i, t_i) \tag{5.2}$$

With this formula, we can give an initial value for y, $y_0 = y(t_0)$, and evolve it in time towards the final result $y_f = y(t_f)$, but there is a problem. Not only is is the algorithm only correct to first-order in h, meaning that we need very small step-sizes, it is also quite unstable. We can obtain a better result by also taking into account the derivative at the mid-point, known as the midpoint method (or second-order Runge-Kutta). This needs to be done in two steps:

$$\begin{aligned} k_1 &= hf(t_i, y_i), \\ y_{i+1} &= y_i + hf\big(t_i + \tfrac{1}{2}h, y_i + \tfrac{1}{2}k_1\big), \end{aligned} \tag{5.3}$$

and this method is correct to order h^2. So by taking into account derivatives at more and more points in between t_i and t_{i+1} we can increase the accuracy of the method. An n-th order Runge-Kutta

method is therefore on the form

$$\begin{aligned} k_1 &= hf(t_i, y_i), \\ k_2 &= hf(t_i + c_2 h, y_i + a_{21} k_1), \\ &\vdots \\ k_m &= hf(t_i + c_m h, y_i + \sum_{j=1}^{m-1} a_{mj} k_j), \\ y_{i+1} &= y_i + \sum_{j=1}^{m} d_j k_j, \end{aligned} \tag{5.4}$$

where generally $m \geq n$. The algorithm is fully defined by the parameters c_i and d_i and the lower triangular matrix a_{ij}. The classical fourth order Runge-Kutta is defined by the following set of parameters:

$$c_i = \begin{pmatrix} 0 \\ \frac{1}{2} \\ \frac{1}{2} \\ 1 \end{pmatrix}, \quad a_{ij} = \begin{pmatrix} 0 & 0 & 0 & 0 \\ \frac{1}{2} & 0 & 0 & 0 \\ 0 & \frac{1}{2} & 0 & 0 \\ 0 & 0 & 1 & 0 \end{pmatrix}, \quad d_i = \begin{pmatrix} \frac{1}{6} \\ \frac{1}{3} \\ \frac{1}{3} \\ \frac{1}{6} \end{pmatrix}. \tag{5.5}$$

17.2 Stepsize control

While there is nothing wrong with using a fourth order (or higher) Runge-Kutta with a constant stepsize h, we can save a lot of computer time by varying h depending on whether f is smooth or not at the current t_i. To do this we need an estimate of the error relating to the current stepsize. The simplest approach to this is through step doubling. We could first calculate y_{n+1} with one step of size h, and then again calculate y^*_{n+1} using two steps at half the stepsize, $h/2$. The difference $\delta = y^*_{n+1} - y_{n+1}$ gives an estimate for the error associated with the stepsize h. This technique could unfortunately require as many as $3n-1$ evaluations of f, which would be costly, but better methods have been developed.

One such method is the 4,5-Dormand-Prince (Dopr45) algorithm [62], where two sets of parameters, their only difference being the values of d_i, give one result correct to $\mathcal{O}(h^4)$ and another correct to order $\mathcal{O}(h^5)$. The difference between these two values for y_{i+1} gives the error estimate needed to decide whether the current value of h is sufficient. These two sets both require six function evaluations, which is substantially better than the step doubling technique which would require 11 evaluations for the fourth-order Runge-Kutta.

In this work, we have a set of n coupled ODEs, let us denote them by $y(t_i, \rho_j) = y_{i,j}$. Let $y_{i+1,j}$ and $y^*_{i+1,j}$ be two different methods for calculating the next step, correct to different orders in h. For example y is calculated with the fourth-order expression of the Dopr45 algorithm, while $y*$ is calculated with the fifth-order expression. The total error is then

$$err = \sqrt{\frac{1}{n} \sum_{j=1}^{n} \left(\frac{y_{i+1,j} - y^*_{i+1,j}}{scale_j} \right)^2}, \tag{5.6}$$

where the $scale_i$ is an error bound which we set to be

$$scale_j = atol + rtol \, \mathrm{MAX}\big(|y_{i+1,j}|, |y^*_{i+1,j}|\big). \tag{5.7}$$

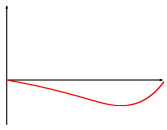

Hence, *atol* denotes the absolute error tolerance while *rtol* is the relative error tolerance. Therefore if *err* is greater than one, we reject the step and reduce h by a factor depending on *err*, while if $err \leq 1$ we accept the step and increase h accordingly.

Both Dopr45 and Dopr853 (8,9-Dormand-Prince algorithm with a fifth- and a third order error estimate and 12 function evaluations [63]), as well as the classical fourth-order Runge-Kutta as listed in Eq. (5.5) have been implemented and used to solve the RG equation. Whenever fourth-order Runge-Kutta was utilised, a stepsize of $h = -10^{-6}$ was used. We checked that neither halving nor doubling this value had any effect on the final result. With both Dopr45 and Dopr853, we mostly used an absolute error tolerance of either 10^{-12} or 10^{-13} depending on whether we calculate U_t with a high or low T. This choice was made on the basis that the potential U possesses no additional structure on scales less than these values.

17.3 Handling complex numbers

Due to the truncation of the integral over k (or t), the potential U_k obtains an imaginary part during the numerical integration. Therefore, instead of having n ODEs we end up with twice as many as we need to account for the running of the imaginary part as well. This is as straightforward to account for as one would think except for the square roots in Eq. (4.27), where one has to be a bit careful when evaluating. The square root has two different solutions, separated by a complex phase π, and the physical result should trace a continuous line in the complex plane. Meaning that if one plots U_k in the complex plane as a function of ρ, this line has to be continuous. This was achieved by comparing the real and imaginary parts of the complex square roots at point ρ_i with its values at the previous point, ρ_{i-1}. This is most easily explained with C++ code for the complex square root function, and pseudocode for the continuity check. First comes the complex square root function, which has a branch cut at the negative real axis. The resulting real part will therefore always be positive:

```
//Input: real and imaginary part of the number which will be used, and
//containers to store the result in
void complexSqrt(const double re, const double im, double &sqrtRe, double &sqrtIm↩
    → )
{
    double w;
    double aRe = fabs(re);
    double aIm = fabs(im);

    if(re==0 and im==0){
        sqrtRe = 0; sqrtIm = 0;
        return;
    }else if( aRe >= aIm){
        w = sqrt(0.5*aRe + 0.5*aRe*sqrt(1. + aIm*aIm/(aRe*aRe)));
    }else{
        w = sqrt(0.5*aRe + 0.5*aIm*sqrt(1. + aRe*aRe/(aIm*aIm)));
    }

    if(re >= 0){
        sqrtRe = w; sqrtIm = 0.5*im/w;
    }else if(im >= 0){
        sqrtRe = 0.5*aIm/w; sqrtIm = w;
```

```
    }else{
        sqrtRe = 0.5*aIm/w; sqrtIm = -w;
    }
}
```

Next is a piece of pseudocode explaining how we make sure the resulting contributions are continuous as we increase ρ.

f^i_{Re} and f^i_{Im} are the values we will take the root of
the result stored in $\sqrt{f^i}_{Re}$ and $\sqrt{f^i}_{Im}$
for $i = 0$ to n **do**
  complexSqrt(f^i_{Re}, f^i_{Im}, $\sqrt{f^i}_{Re}$, $\sqrt{f^i}_{Im}$)
  if $i \neq 0$ **and** $|\sqrt{f^i}_{Re}| > |\sqrt{f^i}_{Im}|$ **then**
    $sign = \text{SIGN}(\sqrt{f^{i-1}}_{Re})$
  else if $i \neq 0$ **then**
    $sign = \text{SIGN}(\sqrt{f^{i-1}}_{Im}) \cdot \text{SIGN}(\sqrt{f^i}_{Im})$
  end if
  $\sqrt{f^i}_{Re} = sign \cdot \sqrt{f^i}_{Re}$
  $\sqrt{f^i}_{Im} = sign \cdot \sqrt{f^i}_{Im}$
  do additional calculations
end for

Another alternative would be to convert from Cartesian to polar coordinates, and then at each iteration check if the complex phase is continuous.

17.4 Phase transition at the physical point

As presented in the previous chapter, the phase transition for small chemical potentials at the physical point ($h = f_\pi m_\pi^2$) is a crossover, the same as we had in both mean-field field approximation. We will also here define the transition to be at the inflection point of either the σ_0-T curve or the σ_0-μ curve, but contrary to the mean-field approximation, we have discretised σ, and therefore do not have the precision necessary to find this point consistently using numerical derivatives. Instead we fitted the data from the calculations to similar looking curves whose inflection point is known. We have, similar to Andersen and Tranberg in Ref. [64] chosen to fit the plots to the function

$$\sigma_0(T) = a + \frac{b^n}{T^n + c^n}. \tag{5.8}$$

The parameter n was varied by hand rather than fitted. For small μ, $n = 4$ was found to provide good fits, while a lower value were used for higher μ. At each step, multiple values for n were tested, and when it had been determined, the critical temperature is given by the parameter c as

$$T_c = \sqrt[n]{\frac{n-1}{n+1}}c. \tag{5.9}$$

where e.g. $n = 4$ was found to give excellent agreement for small μ. After c has been decided from the fit, the critical temperature is given as $T_c = (3/5)^{0.25}c$. An example fit with $\mu = 0$ is shown in Fig. 5.2, which shows excellent agreement. The fits were calculated using the Levenberg-Marquardt algorithm, using an implementation provided by GSL.

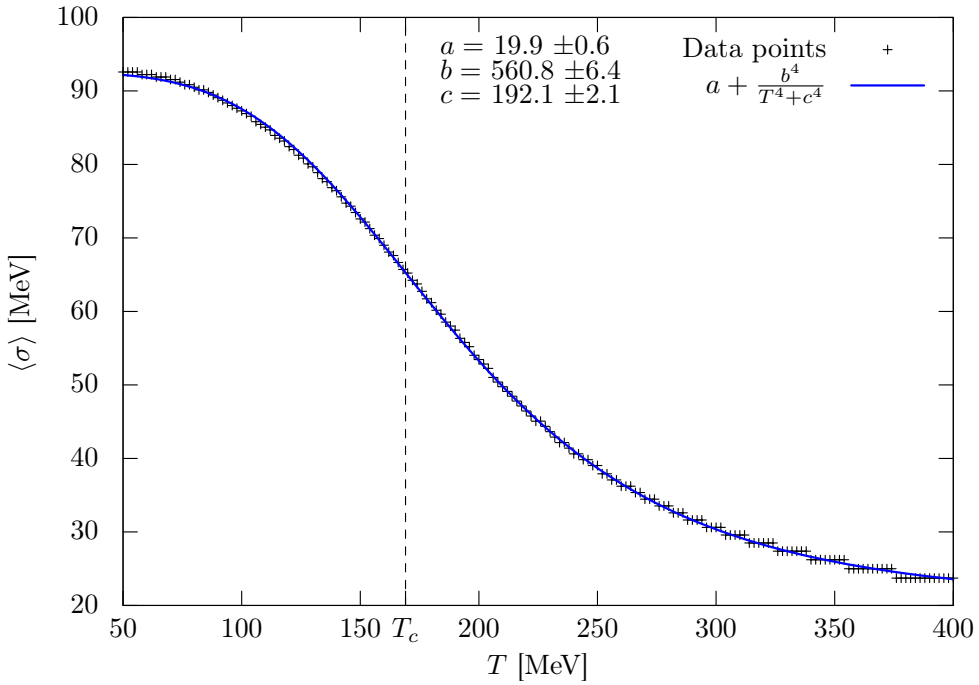

Figure 5.2: A fit of the σ_0-T curve at $\mu = 0$ using Eq. (5.8).

17.5 Numerical instability

While the position of the minimum has been found the be very resilient to change in the numerical methods used, the potential itself seems to be more unstable, which is why it was argued that the sigma mass was hard to fix exactly. Numerical unstable differential equations are often referred to as *stiff* equations, and are often related to possible divergences. In our equations, we have terms like $\frac{1}{\omega_\sigma}$ and $\frac{1}{\omega_\pi}$ which can be singular for an unfortunate set of initial conditions. While an algorithm utilising constant stepsize might blissfully skip past these problematic points (and they often do) with only minor numerical inaccuracies to show, the adaptive stepsize algorithms have an unfortunate tendency to hone in on these configurations, decreasing the stepsize until it is below the precision of the computer, and then fail. It is hard to say which approach produces the most correct results, and they should both be used with a bit of caution. Stepsize control certainly seem like the safest option as it would rather stop than letting inaccuracies propagate through, it does however not always produce any results. In addition, stepsize control algorithms can also obtain new instabilities resulting from having too many function evaluations (which themselves carry faults). Ideally one would use an algorithm to solve the differential equation more suited for solving stiff equations such as the implicit methods, but they require the Jacobian of the right hand side ($\frac{\partial^2 f}{\partial\rho_i\partial\rho_j}$, where ρ_i are the discrete values for ρ), which is both difficult and costly to calculate.

CHAPTER 6

Conclusion and outlook

In this thesis we have studied the chiral transition in QCD at high temperatures, resulting in a quark-gluon plasma, or high quark densities, resulting in quark matter. We used the linear sigma model with quarks to model QCD at low energies where the quarks are confined to hadrons. First we applied the mean-field approximation to one-loop, which neglects all quantum and thermal fluctuations of the mesons. We saw that even with this simple approximation, many of the critical phenomena in QCD were found. In the chiral limit we found a first-order phase transition for all values of T and μ, while at the physical point the melting of the condensate is a crossover transition for low quark chemical potentials, which turns into a first-order transition as we increase μ. Similar behaviour was found when we extended the two-flavour LSMq to include the strange quark. We saw that the addition of the strange quark had little effect on the phase diagram, only pushing the transitions to slightly higher temperatures and the critical endpoint to higher chemical potentials. The effect of the strange quark became more prominent for higher sigma masses, but even at $m_\sigma = 800$ MeV the phase diagram was only pushed up ~ 3 MeV, its shape unchanged.

In Chapter 4 we replaced the perturbative method used in the previous chapter with a renormalisation group method, and the mean-field approximation with the nonperturbative local potential approximation. With this we were able to include the thermal and quantum fluctuations that were missing from the first approach. We saw that with the mesonic contribution, the transition was pushed up to higher temperatures at zero quark chemical potential, while the transition curve dropped much faster as we increased μ. This was to be expected as the mesonic contribution, which is dominant in the region of high μ and low T, weakens the symmetry breaking, driving the condensate towards zero. Finally we tried to calculate the thermodynamic quantities associated with the thermodynamic potential to see how these compared to that of a free gas of quarks and gluons. We saw that the choice we had made for Λ was too small to find the proper behaviour at high temperatures.

18 Outlook

Reading Chapter 4 one notices that there is still much left to do. The numerical work was more demanding than anticipated, and therefore a great amount of time was spent simply obtaining correct renormalised potentials which were needed for all subsequent calculations. First the high chemical potential region of the phase diagram at the physical point, displayed in Fig. 4.5, needs to be calculated again at higher precision. In this region the fit proposed in Eq. (5.8) is not very good, and a better fitting function must be found.

As we were unable to determine the high temperature behaviour of the LSMq due to our choice of Λ being too small. We should therefore calculate the thermodynamic quantities again at a higher renormalisation scale. Of particular interest is the quark number susceptibilities defined in Eq. (4.36), as these have, to the authors knowledge, not yet been calculated using the nonperturbative approximation presented in this work. It would be interesting to see how these results would compare to other approximations such as the mean-field approximation and hard thermal loop perturbation theory, see e.g. the work of Andersen *et al.* for a $N_f = 3$ study [65]. The results should also be compared with recent lattice results, e.g. Ref. [66] for $N_f = 2$ and Refs. [67, 68] for $N_f = 2 + 1$.

It should be noted that the computation time needed to calculate the renormalised potential at higher renormalisation time does not follow a simple scaling relation. The reason is that we need to take the integral over $t = \log(k/\Lambda)$ to lower values than -6 to reach the same value in k, but this also needs to be done with smaller stepsizes.

18.1 Polyakov loop

In this work we have identified chiral symmetry restoration with deconfinement by the argument that when the chiral condensate has melted, the quarks no longer favour bound states, such as the mesons. While this is more of a suggestive argument than anything else, lattice calculations have found the chiral- and deconfinement transitions to take place at the same (pseudo)critical temperature [69]. The deconfinement transition actually has a different order parameter associated with it, found by Polyakov [70], which is

$$L(\mathbf{x}) = \frac{1}{N_c}\mathrm{tr}\,\mathcal{P}\exp\left[i\int_0^\beta \mathrm{d}\tau\, A_4(\mathbf{x},\tau)\right], \tag{6.1}$$

where $\mathcal{P}$ is the path-ordering operator and the trace is taken over the indices of the resulting matrix (remember that $A_4 = A_4^i T^i$ is the QCD gauge-field, which is a three-by-three matrix in the fundamental representation). The object $L(\mathbf{x})$ is commonly referred to as the Polyakov loop. The deconfinement transition can therefore be analysed by including the effect the gluons have on the system. Without any further approximations this would only yield the QCD Lagrangian, which is what the low energy models are trying to avoid. We therefore only couple the quarks of the LSMq to a constant background A_0, meaning that we use space-time independent gauge-fields A^i. We see from Eq. (2.18) that the coupling between the gluonic background field and the quarks are like that of an imaginary chemical potential. The fact that we can include the background field as an imaginary chemical potential was shown by Fukushima in Ref. [71]. This model is named the Polyakov extended quark-meson model (PQM), and using the local potential approximation the RG equation for the potential is readily calculated, see e.g. Ref. [58]:

$$\partial_k U_k = \partial_k U_{kB} - \frac{N_f N_c}{3\pi^2}\frac{k^4}{\omega_q}\Big[1 - N(\ell,\ell^*,T,\mu) - \tilde{N}(\ell,\ell^*,T,\mu)\Big], \tag{6.2}$$

where $\partial_k U_{kB}$ is the bosonic contribution given in Eq. (4.17), $\ell = \langle L\rangle$ and $\ell^* = \langle L^\dagger\rangle$ are the space-averaged Polyakov loops and the functions N and $\tilde{N}$ are given by

$$N(\ell,\ell^*,T,\mu) = \frac{1 + 2\ell^* e^{\beta(\omega_q-\mu)} + \ell e^{2\beta(\omega_q-\mu)}}{1 + 3\ell e^{2\beta(\omega_q-\mu)} + 3\ell^* e^{\beta(\omega_q-\mu)} + e^{3\beta(E_q-\mu)}}, \tag{6.3}$$

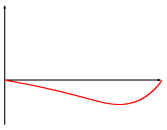

and $\tilde{N}(\mu) = N(-\mu)$. One can verify that they reduce to the fermion distribution functions for $\ell = \ell^* = 0$. One also has to add an effective gluon potential to the final thermodynamic potential, but it is customary to assume that this is independent of the renormalisation parameter k:

$$\Omega \longrightarrow \Omega_{k=0} + \mathcal{U}(\ell, \ell^*). \tag{6.4}$$

We have replaced the Polyakov loop with its expectation values, which can be found by the equations:

$$\frac{\partial \Omega}{\partial \ell} = 0, \tag{6.5}$$

$$\frac{\partial \Omega}{\partial \ell^*} = 0. \tag{6.6}$$

In addition to having an effect on the chiral transition, the PQM model can be used to identify the deconfinement transition, which happens at the point where the Polyakov loop vanishes.

18.2 Three-flavour LSMq model with FRG methods

Working on this thesis, a fair amount of work has been spent trying to find and solve an RG equation for the three-flavour LSMq, which we solved using the mean-field approximation in Sec. 11. When we solved the two-flavour LSMq using the RG equation, we wanted the potential U_k to retain its $O(4)$ symmetry throughout renormalisation, and we therefore introduced the variable $\rho = \sigma^2 + \vec{\pi}^2$ to make sure of this. With the three-flavour model, we want the meson potential to retain its $U(3) \times U(3)$ symmetry, for which two variables must be chosen (just as we had two condensates when we solved it with the mean-field approximation). Two such variables can be

$$\rho = \mathrm{tr}\Big[\phi^\dagger \phi\Big], \tag{6.7}$$

$$\tau = \frac{3}{2}\mathrm{tr}\Big[\big(\phi^\dagger \phi\big)^2\Big] - \frac{1}{2}\rho^2, \tag{6.8}$$

where the meson matrix ϕ was defined in Sec. 11. Finding RG equations for the meson potential is just as straight forward as it was for the two-flavour model, but a problem arises when one tries to solve them numerically. The two variables that were introduced to preserve the symmetry of U are not independent, and therefore if we choose a value for one of them we restrict the value the other can take. Not only does this make finite differencing schemes problematic, it also means that we have multiple expressions for $\sigma_0(\rho, \tau)$ and $\sigma_8(\rho, \tau)$ resulting in Eqs. (6.7) and (6.8). Unfortunately, due to time restrictions, less time than one would deem sufficient was spent trying to solve this problem, and a second attempt at solving it is definitely a viable continuation of the work presented in this thesis.

Finally, in Sec. 11.1, when using the linear-sigma model, we neglected the contribution to the thermodynamic potential from the fermion vacuum energy. It could be very interesting to study how this addition would impact the phase diagram as it has not yet, to the best of the author's knowledge, been studied in the case of three-quark LSM.

APPENDIX A

Definitions and algebras

1 Field theory representation

I have used the standard representation of both quantum mechanics and quantum field theory. This representation is described below:

1.1 Quantum mechanics

Let $|0\rangle$ describe the ground state of our system and let $\hat{q}_i$ and $\hat{p}_i$ be the coordinate- and momentum operators. The index i runs over all spatial coordinates. Eigenstates of these operators are perpendicular and follow these rules:

$$\hat{q}_i |q_j\rangle = \delta_{ij} q_i |q_j\rangle , \tag{A.1}$$

$$\hat{p}_i |p_j\rangle = \delta_{ij} p_i |p_j\rangle \tag{A.2}$$

The commutation relations between the operators are

$$\left[\hat{q}_i, \hat{q}_j\right] = 0 \tag{A.3}$$

$$\left[\hat{p}_i, \hat{p}_j\right] = 0 \tag{A.4}$$

$$\left[\hat{q}_i, \hat{p}_j\right] = i\delta_{ij} \tag{A.5}$$

The normalisation of the eigenstates are chosen so that

$$\langle q|p\rangle = e^{ixp} \tag{A.6}$$

1.2 Field theory

In field theory let $|\Omega\rangle$ be the vacuum state, and let $\hat{\phi}(x)$ be the field-operator, and $\hat{\pi}(x)$ its canonical momentum operator. Similarly to quantum mechanics, the eigenstates and operators are defined to follow

$$\hat{\phi}(x) |\phi\rangle = \phi(x) |\phi\rangle , \tag{A.7}$$

$$\hat{\pi}(x) |\pi\rangle = \pi(x) |\pi\rangle , \tag{A.8}$$

$$\langle\phi|\pi\rangle = \exp\left\{ i \int \mathrm{d}^d x \, \pi(x)\phi(x) \right\}, \tag{A.9}$$

$$\left[\hat{\phi}(x), \hat{\phi}(y)\right] = 0, \tag{A.10}$$

$$\left[\hat{\phi}(x), \hat{\phi}(y)\right] = 0, \tag{A.11}$$

$$\left[\hat{\phi}(x), \hat{\pi}(y)\right] = \delta^d(x-y). \tag{A.12}$$

2 $SU(3)$ algebra

Using a linear representation of $SU(3)$, every member $u \in SU(3)$ can be written in exponential form using the generators T_R^i:

$$D_R(u) = e^{i\alpha_u^i T_R^i}. \tag{A.13}$$

The algebra of $SU(3)$ is also contained within the generators, and can be expressed through the structure constants f^{ijk}:

$$\left[T_R^i, T_R^j\right] = i f^{ijk} T_R^k. \tag{A.14}$$

The structure constants are independent on the representation R, and are completely antisymmetric ($f^{ijk} = -f^{jik} = -f^{ikj} = -f^{kji}$). Therefore, only a few structure constants are needed, from which the rest is easily calculated. For $SU(3)$ these are given as:

$$f^{123} = 1, \quad f^{147} = f^{246} = f^{257} = f^{345} = f^{516} = f^{637} = \frac{1}{2}, \quad f^{258} = f^{678} = \frac{\sqrt{3}}{2} \tag{A.15}$$

The representation in which $\mathrm{tr}[T_F^i T_F^j] = \frac{1}{2}\delta^{ij}$ are called the fundamental representation. A common choice is $T_F^i = \frac{1}{2}\lambda^i$, where λ^i are the Gell-Mann matrices depicted in Tab. A.1.

$$\lambda^1 = \begin{pmatrix} 0 & 1 & 0 \\ 1 & 0 & 0 \\ 0 & 0 & 0 \end{pmatrix} \qquad \lambda^2 = \begin{pmatrix} 0 & -i & 0 \\ i & 0 & 0 \\ 0 & 0 & 0 \end{pmatrix} \qquad \lambda^3 = \begin{pmatrix} 1 & 0 & 0 \\ 0 & -1 & 0 \\ 0 & 0 & 0 \end{pmatrix}$$

$$\lambda^4 = \begin{pmatrix} 0 & 0 & 1 \\ 0 & 0 & 0 \\ 1 & 0 & 0 \end{pmatrix} \qquad \lambda^5 = \begin{pmatrix} 0 & 0 & -i \\ 0 & 0 & 0 \\ i & 0 & 0 \end{pmatrix} \qquad \lambda^6 = \begin{pmatrix} 0 & 0 & 0 \\ 0 & 0 & 1 \\ 0 & 1 & 0 \end{pmatrix}$$

$$\lambda^7 = \begin{pmatrix} 0 & 0 & 0 \\ 0 & 0 & -i \\ 0 & i & 0 \end{pmatrix} \qquad \lambda^8 = \frac{1}{\sqrt{3}} \begin{pmatrix} 1 & 0 & 0 \\ 0 & 1 & 0 \\ 0 & 0 & -2 \end{pmatrix}$$

Table A.1: Gell-Mann matrices

APPENDIX B

Useful mathematical formulas and derivations

3 Gaussian integrals

The standard one dimensional Gaussian integral is often needed calculating quantities in QFT and TFT, with and without a linear term, it is

$$G_1(a,0) = \int_{-\infty}^{\infty} \mathrm{d}x\, e^{-ax^2} = \sqrt{\frac{\pi}{a}}, \tag{B.1}$$

$$G_1(a,b) = \int_{-\infty}^{\infty} \mathrm{d}x\, e^{-ax^2+bx} = \sqrt{\frac{\pi}{a}} e^{\frac{b^2}{4a}}. \tag{B.2}$$

The n-dimensional Gaussian integrals are also needed and is gives as

$$G_n(A_{ij},0) = \int \mathrm{d}^n x_i\, e^{-x_i A_{ij} x_j} = \sqrt{\frac{\pi}{\det(A_{ij})}} \tag{B.3}$$

$$G_n(A_{ij},b_i) = \int \mathrm{d}^n x_i\, e^{-x_i A_{ij} x_j + b_i x_i} = \sqrt{\frac{\pi}{\det(A_{ij})}} e^{\frac{1}{4} b_i A^{-1}_{ij} b_j} \tag{B.4}$$

4 Grassmann algebra

Fermions, being particles following the Fermi-Dirac distribution, need to be described by fields with somewhat different algebraic properties from normal variables. The proper algebra is called Grassmann algebra, and it has said properties. The defining property of these numbers is that they are anti-commuting similar to the fermions themselves. Let η and θ be two Grassmann variables, then they should follow this set of rules

$$\eta\theta = -\theta\eta, \tag{B.5}$$

$$\theta^2 = 0, \tag{B.6}$$

$$(\eta\theta)^* = \theta^*\eta^*. \tag{B.7}$$

The second property is used to argue that any function of a Grassmann variable can be expanded to a linear function in that variable. The argument being that all other terms in the Taylor series is zero. The normalisation of integrals over Grassmann variables is a little ambiguous, but the following definition is widely used,

$$\int \mathrm{d}\theta\, (A + B\theta) = B, \tag{B.8}$$

$$\int \mathrm{d}\theta \int \mathrm{d}\eta\, \eta\theta = 1. \tag{B.9}$$

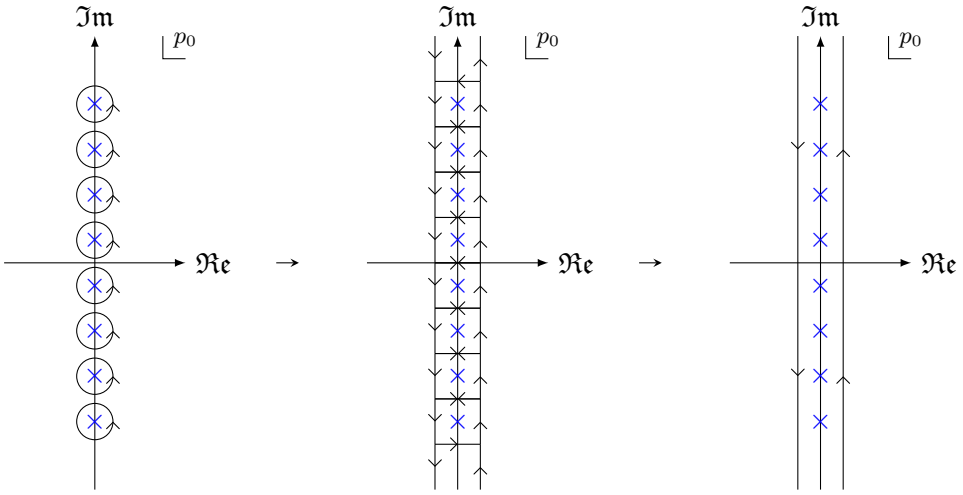

Figure B.1: Contours circling the residues of $g(p_0)$.

Also here, a version of the Gaussian integrals are frequently encountered, therefore the one-dimensional and n-dimensional results are given

$$\int \mathrm{d}\theta^* \mathrm{d}\theta \, e^{-\theta^* b \theta} = b \tag{B.10}$$

$$\left(\prod_i \mathrm{d}\theta_i^* \mathrm{d}\theta_i \right) e^{-\theta_i^* B_{ij} \theta_j} = \det(B) \tag{B.11}$$

5 Matsubara sums

Throughout the thesis, the Matsubara sums appear multiple times, and we will therefore introduce the contour trick for both bosons and fermions to evaluate them. The Matsubara sums are sums on the form

$$\sum_{n=-\infty}^{\infty} f(\omega_n), \qquad \begin{cases} \omega_n = 2\pi n T & \text{for bosons,} \\ \omega_n = (2n+1)\pi T & \text{for fermions.} \end{cases} \tag{B.12}$$

The contour trick is names so because it involves rewriting the sum as a contour integral over the variable $p_0 = i\omega_n$,

$$\sum_{n=-\infty}^{\infty} f(p_0 = i\omega_n) = \frac{1}{2\pi i} \oint_{\mathcal{C}} \mathrm{d}p_0 \, f(p_0) g(p_0) \tag{B.13}$$

$g(p_0)$ is some function with poles along the imaginary axis for values $p_0 = i\omega_n$ and is normalised so we regain the left hand side. $\mathcal{C}$ is a contour circling all these poles, example shown in Fig. B.1.

A convenient choice for $g(p_0)$ is

$$g(p_0) = \begin{cases} \frac{1}{2}\beta \coth\left(\frac{1}{2}\beta p_0\right), & \text{for bosons,} \\ \frac{1}{2}\beta \tanh\left(\frac{1}{2}\beta p_0\right), & \text{for fermions,} \end{cases} \tag{B.14}$$

which will be used here.

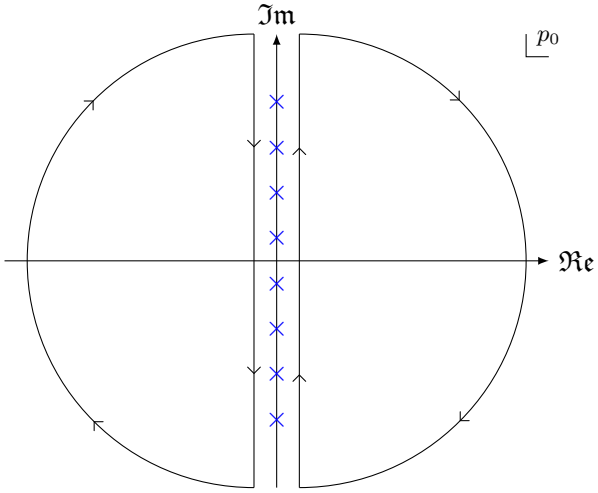

Figure B.2: The new contour circling $f(p_0)$'s residues.

The next step is to locate the poles of $f(p_0)$, and if these are not on the imaginary axis, we add two new paths to the integral, and close it outside, picking up the poles of $f(p_0)$ instead. The new contour is shown in the Fig. B.2. One should check that the contribution from the semicircles in fact vanishes as its radius goes to infinity. For the example below this is easy.

The sum below is one of the most frequently encountered, therefore we will quickly calculate it,

$$F \equiv T \sum_{n=-\infty}^{\infty} \frac{1}{\omega_n^2 + \Delta^2}. \tag{B.15}$$

This is rewritten using the contour trick to

$$F = \frac{T}{2\pi i} \oint_{\mathcal{C}} \frac{\mathrm{d}p_0}{\Delta^2 - p_0^2} \frac{1}{2} \beta \coth\Big(\tfrac{1}{2}\beta p_0\Big). \tag{B.16}$$

The function $f(p_0)$ has simple poles at $p_0 = \pm\Delta$, which are picked out by the new contour of Fig. B.2. Using the residue theorem, this can be calculated to be

$$F = \frac{1}{2\Delta} \coth\big(\tfrac{1}{2}\beta\Delta\big) = \frac{1}{2\Delta}\Big[1 + 2n_B(\Delta)\Big]. \tag{B.17}$$

Where $n_B(\Delta) = (e^{\beta\Delta} - 1)^{-1}$ is the standard Bose-Einstein distribution. The fermionic counterpart uses tanh instead of coth and is just as easily evaluated

$$F = \frac{1}{2\Delta} \tanh\big(\tfrac{1}{2}\beta\Delta\big) = \frac{1}{2\Delta}\Big[1 - 2n_F(\Delta)\Big], \tag{B.18}$$

and this time $n_F(\Delta) = (e^{\beta\Delta} + 1)^{-1}$ is the Fermi-Dirac distribution. We will also encounter the sum in Eq. (B.15) with a chemical potential included for fermions, meaning

$$F \equiv T \sum_{n=-\infty}^{\infty} \frac{1}{(\nu_n + i\mu)^2 + \Delta^2}, \tag{B.19}$$

where we have chosen to call the Fourier components ν_n instead of ω_n to emphasise the use of fermions. In this case we can redefine p_0 and $g(p_0)$ to

$$p_0 = i(\nu_n + i\mu), \quad g(p_0) = \tfrac{1}{2}\tanh\big(\tfrac{1}{2}(p_0+\mu)\beta\big), \tag{B.20}$$

in which case we can use the same contour as in the previous calculations. This results in

$$\begin{aligned} F &= \frac{1}{4\Delta}\Big[\tanh\big(\tfrac{1}{2}(\Delta-\mu)\beta\big) + \tanh\big(\tfrac{1}{2}(\Delta+\mu)\beta\big)\Big], \\ &= \frac{1}{2\Delta}\Big[1 - n_F(\Delta,\mu) - n_{\bar{F}}(\Delta,\mu)\Big], \end{aligned} \tag{B.21}$$

where $n_F(\Delta,\mu) = \big(e^{(\Delta-\mu)\beta}+1\big)^{-1}$ is the fermion distribution function and $n_{\bar{F}}(\Delta,\mu) = n_F(\Delta,-\mu)$ is the anti fermion distribution function.

6 Fermion partition function

Similar to the calculation done in Seq. 2.2, we will here derive the partition function for two massless fermionic fields coupled to one scalar meson field and three pseudo-scalar mesons fields, chemical potential included. The result will be used in Chapter 3 when we find the chiral phase transition in a mean-field approximation. The (TFT) Lagrangian ($\mathcal{L}_E$) is given by

$$\mathcal{L} = \bar{\psi}\big[\gamma^0\partial_\tau - i\vec{\gamma}\cdot\nabla + g(\sigma + i\gamma^5\vec{\tau}\cdot\vec{\pi}) - \mu\gamma^0\big]\psi, \tag{B.22}$$

and its resulting partition function is

$$\mathcal{Z} = \int \mathcal{D}\psi\mathcal{D}\bar{\psi}\exp\Big\{-\int_0^\beta \mathrm{d}\tau\int_{\mathbf{x}}\bar{\psi}(\gamma^0\partial_\tau - i\vec{\gamma}\cdot\nabla + g(\sigma+i\gamma^5\vec{\tau}\cdot\vec{\pi}) - \mu\gamma^0)\psi\Big\}. \tag{B.23}$$

Again we Fourier transform the fields ψ and $\bar{\psi}$

$$\psi(x) = \frac{1}{\sqrt{V}}\sum_n\sum_{\mathbf{p}} e^{i(\omega_n\tau+\mathbf{p}\cdot\mathbf{x})}\psi(p), \tag{B.24}$$

$$\bar{\psi}(x) = \frac{1}{\sqrt{V}}\sum_n\sum_{\mathbf{p}} e^{-i(\omega_n\tau+\mathbf{p}\cdot\mathbf{x})}\bar{\psi}(p), \tag{B.25}$$

the normalisation $1/\sqrt{V}$ chosen so the Fourier components are dimensionless numbers. Inserting this into Eq. (B.23) and calculating the space-time integral, we are left with

$$\mathcal{Z} = \int\Big(\prod_{n,\mathbf{p}}\mathrm{d}\psi_{n,\mathbf{p}}\mathrm{d}\bar{\psi}_{n,\mathbf{p}}\Big)\exp\Big\{-\beta\sum_{n,\mathrm{p}}\bar{\psi}_{n,\mathbf{p}}(i\gamma^0\omega_n + \vec{\gamma}\cdot\mathbf{p} + g(\sigma+i\gamma^5\vec{\tau}\cdot\vec{\pi}) - \mu\gamma^0)\psi_{n,\mathrm{p}}\Big\}. \tag{B.26}$$

Using the Gaussian Grassmann integral given in Eq. (B.11), we get

$$\mathcal{Z} = \det\Big[\beta\big(i\gamma^0(\omega_n+i\mu) + \vec{\gamma}\cdot\mathbf{p} + g\sigma + ig\gamma^5\vec{\tau}\cdot\vec{\pi}\big)\Big]. \tag{B.27}$$

We can take the logarithm of both sides to find Helmholtz' free energy, and use the trace-log identity

$$\mathcal{F} = -T\sum_{n,\mathbf{p}}\mathrm{tr}\log\Big[\beta\big(i\gamma^0(\omega_n+i\mu) + \vec{\gamma}\cdot\mathbf{p} + g\sigma + ig\gamma^5\vec{\tau}\cdot\vec{\pi}\big)\Big]. \tag{B.28}$$

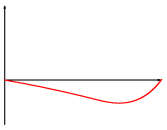

The trace is over both Dirac and flavour indices. It can be evaluated by first expanding the logarithm around $g\sigma$ and utilising that all the γ matrices are traceless. This results in

$$\mathcal{F} = -2TN_f \sum_{n,\mathbf{p}} \log\Big[\beta^2\big((\omega_n + i\mu)^2 + \mathbf{p}^2 + g^2(\sigma^2 + \vec{\pi}^2)\big)\Big], \tag{B.29}$$

which can be rewritten to

$$\mathcal{F} = -TN_f \sum_{n,\mathbf{p}} \log\Big[\beta^2\big(\omega_n^2 + (\omega + \mu)^2\big)\Big] + \log\Big[\beta^2\big(\omega_n^2 + (\omega - \mu)^2\big)\Big], \tag{B.30}$$

where $\omega^2 = \mathbf{p}^2 + m^2$ and $m^2 = g^2(\sigma^2 + \vec{\pi}^2)$. The Matsubara sums of the logarithms can each be evaluated in a similar way to how we did it for bosons, by rewriting the logarithms as integrals, and using the contour tick introduced in the previous section. Rewriting the logarithms

$$\log\Big[\beta^2(\omega_n^2 + (\omega + \mu)^2)\Big] = \int_1^{\beta^2(\omega+\mu)^2} \frac{\mathrm{d}a^2}{\beta^2\omega_n^2 + a^2} + \text{constant}, \tag{B.31}$$

and using the result from Eq. (B.18)

$$\sum_n \frac{1}{\beta^2\omega_n^2 + a^2} = \frac{1}{2a}\big[1 - 2n_F(a/\beta)\big], \tag{B.32}$$

we end up with an integral on the form

$$\int_1^{\beta(\omega\pm\mu)} \mathrm{d}a \left[1 - \frac{2}{e^a + 1}\right] = \beta(\omega \pm \mu) + 2\log\big[1 + e^{-\beta(\omega\pm\mu)}\big] + \text{constant}. \tag{B.33}$$

Throwing away all constant terms, we finally get an expression for Helmholtz' free energy of a free gas of fermions,

$$\mathcal{F} = -2N_f V \int \frac{\mathrm{d}\mathbf{p}}{(2\pi)^3} \Big\{\omega + T\log\Big[1 + e^{-(\omega+\mu)\beta}\Big] + T\log\Big[1 + e^{-(\omega-\mu)\beta}\Big]\Big\}. \tag{B.34}$$

The first term in the integral is identified as the vacuum energy, and is commonly discarded.

APPENDIX C

Additional Results

In this appendix additional results which were not included in the main chapters are presented and discussed.

7 Mean-field meson masses

The meson masses in the LSMq model is defined as the curvature of thermodynamic potential at the minimum

$$m_\phi^2 = \left.\frac{\partial^2\Omega}{\partial\phi^2}\right|_{\phi_0}. \tag{C.1}$$

In the case of multiple fields ϕ_i, a mass matrix M can be constructed

$$M_{ij} = \left.\frac{\partial^2\Omega}{\partial\phi_i\partial\phi_j}\right|_{\phi_0}, \tag{C.2}$$

whose eigenvalues define the meson masses.

7.1 Two-flavour LSMq

In the two-flavour mean-field approximation, the mass matrix M is diagonal, and the sigma and pion masses are simply given as

$$m_\sigma^2 = m^2 + 3\lambda\sigma^2 + \frac{6g^2}{\pi^2}\int_0^\infty \frac{p^2\mathrm{d}p}{\omega^2}\left\{\frac{p^2}{\omega}\big(n_q + n_{\bar{q}}\big) + (g\sigma)^2\big(m_q + m_{\bar{q}}\big)\right\}, \tag{C.3}$$

$$m_\pi^2 = m^2 + \ \lambda\sigma^2 + \frac{6g^2}{\pi^2}\int_0^\infty \frac{p^2\mathrm{d}p}{\omega}\big(n_q + n_{\bar{q}}\big) \tag{C.4}$$

where we have defined

$$m_q = \frac{\partial n_q}{\partial\omega} = -\frac{1}{2T}\frac{1}{1+\cosh\big[(\omega-\mu)/T\big]}, \quad m_{\bar{q}}(T,\mu) = m_q(T,-\mu). \tag{C.5}$$

These equations has to be evaluated at the minimum, given by the solution of Eqs. (3.10,3.11). In Fig. C.1 the pion and sigma masses has been plotted at zero chemical potential for increasing temperature. It shows the position of the critical temperature (T_c), and beyond this point the sigma and pion masses converge to the same curve. This mass degeneration is effectively a restoration of chiral symmetry as their mass can only be equal if the condensates are equal as well.

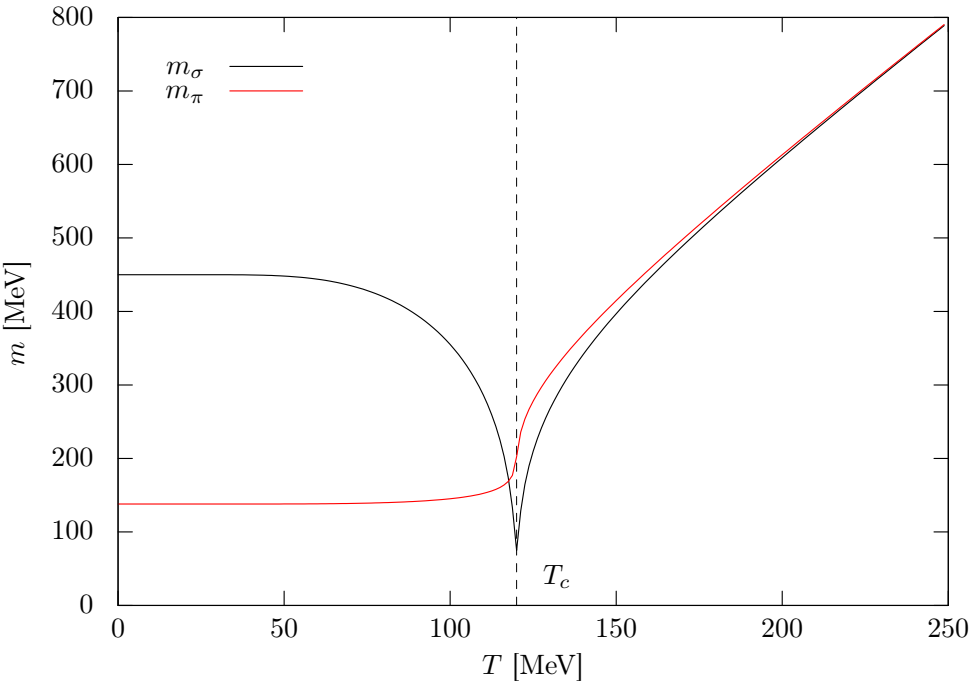

Figure C.1: Two-flavour meson masses at zero quark chemical potential, we have chosen $m_\sigma = 450$ MeV in vacuum.

7.2 Three-flavour LSMq

The procedure for calculating the meson masses in the tree flavour model is in principle the same as in the two-flavour model, but as the mass matrix M is not diagonal, it is slightly more difficult. Fortunately, it is block diagonal with only two 2×2 matrices mixing the mesons. One corresponding to the mixing of the σ and the $f_0(1370)$ particles, and the other to the mixing of the η and η' particles. One should also note that when evaluating the quark contribution, the quark basis must be re diagonalised for every mass calculation. Analytic expressions for the double derivatives of the potentials, as well as a more detailed approach to the mass calculations can be found in Ref. [45].

The resulting meson masses has been plotted in Figs. C.2 and C.3. We see that the meson pairs plotted in Fig. C.2 both degenerate at $T \approx T_c$ just like we saw in Fig. C.1, while the masses in Fig. C.3 degenerates a bit slower (even though a clear change is seen at T_c). The f_0 mass is the slowest to align with the other masses, happening in line with the phase transition for the strange condensate rather than that of the u-d condensate. The inflection point of the strange condensate, as shown in Fig. 3.6 is therefore also added, and it is interesting to see that this pseudocritical temperature coincides with the intersection between the f_0 mass and the other three meson masses.

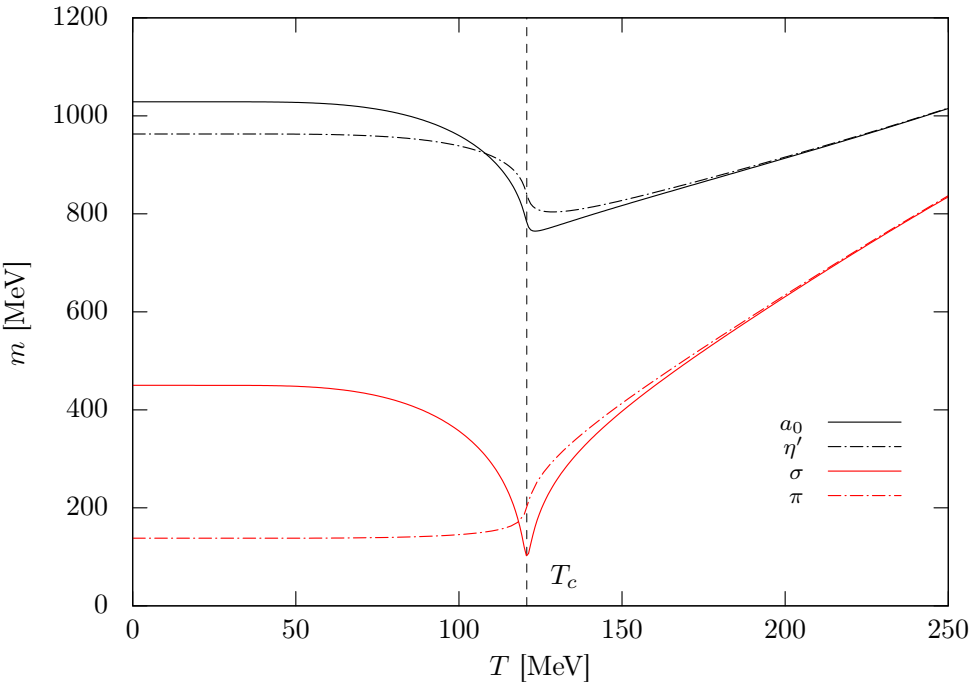

Figure C.2: Masses for the a_0, η', σ and π mesons at zero quark chemical potential.

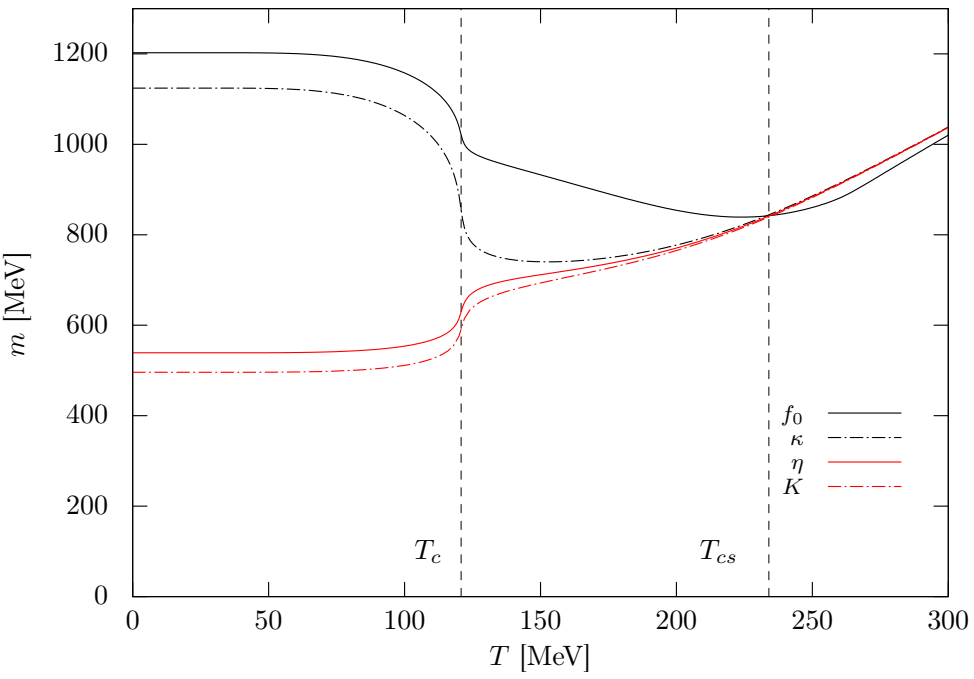

Figure C.3: Masses for the f_0, κ, η and K particles at zero quark chemical potential.

APPENDIX D

Computer code

The full code used to solve the RG equations will not be given as that would probably take more than a hundred pages. Instead the code used to calculate the right hand side of the RG equation will be given as that should be sufficient to reproduce the results using the algorithms described in Chap. 5. It can also be easily modified, and then solved using e.g. the ODE solvers in numerical libraries such as GSL.

In the following code `Matrix` containers have been used to save intermediate values of U as they are renormalised. The data was ordered such that `y[0][i]` denotes the real part of U at $\rho = \rho_i$, and `y[1][i]` are the imaginary part. It is assumed that external parameters has been passed in a different manner, therefore the temperature (`temp`), chemical potential (`mu`), yukawa coupling constant (`gf`) and the ρ interval (`dRho`) are all assumed to be set by other means.

```
void rightHandSide(const Matrix &y, Matrix &dy, double t){

    //Constant factors
    const double pi            =  4.*atan(1.);
    const double bosonPref     =  1./(12.*pi*pi);
    const double fermionPref   = -2./(    pi*pi);

    //Temporary containers
    double sigmaContrib[2], pionContrib[2];
    double fermionContrib;

    double n1[2], z[2];
    double nF;
    double reEn, imEn, reSqEn, imSqEn;

  //Naming convention: S -> sigma
  //P -> pion, SP -> sigma previous
  //PP -> pion previous
    double reSqS, imSqS, reSqSP, imSqSP;
    double reSqP, imSqP, reSqPP, imSqPP;

    //Calculate the derivative and double derivative of y with finite
    //difference schemes, results saved in pre-declared Matrix
    //variables dU and ddU. dRho is the spacing in rho-space
    derivatives(y,dU,ddU,dRho);

    int n = y.sizeY(); //Returns the number of discrete rhos

    for(int i=0; i<n; i++){
```

```
double rho = i*dRho;

//Contribution from the sigma mesons
reEn = exp(2*t) + dU[0][i] + 2*rho*ddU[0][i];
imEn = dU[1][i] + 2*rho*ddU[1][i];

compelxSqrt(reEn,imEn,reSqS,imSqS);

if((i != 0) and (fabs(reSqSP) >= fabs(imSqSP))){
    //Function dsign takes in a double and returns its sign
    int pSig = dsign(reSqP);
    reSqS *= pSig;
    imSqS *= pSig;
}else if(i!=0){
    int sigIm = dsign(imSqS);
    int pSig = dsign(imSqSP);
    reSqS *= pSig*sigIm;
    imSqS *= pSig*sigIm;
}

reSqSP = reSqS; imSqSP = imSqS;

r = 1./(reSqS*reSqS + imSqS*imSqS);
if(temp > 0.){
    z[0] = reSqS/(temp);
    z[1] = imSqS/(temp);
    n1[0] = -sinh(z[0])/(cos(z[1]) - cosh(z[0]));
    n1[1] =   sin(z[1])/(cos(z[1]) - cosh(z[0]));
}else{
    n1[0] = 1.;
    n1[1] = 0.;
}

sigmaContrib[0] = r*( reSqS*n1[0] + imSqS*n1[1]);
sigmaContrib[1] = r*(-imSqS*n1[0] + reSqS*n1[1]);

//Contribution from the pion mesons
reEn = exp(2*t) + dU[0][i];
imEn = dU[1][n];

cmplxSqrt(reEn,imEn,reSqP,imSqP);

if((i != 0) and (fabs(reSqPP) >= fabs(imSqPP))){
    int pSign = dsign(reSqPP);
    reSqP *= pSign;
    imSqP *= pSign;
}else if(i!=0){
    int sigIm = dsign(imSqP);
    int pSign = dsign(imSqPP);
    reSqP *= pSign*sigIm;
    imSqP *= pSign*sigIm;
}

reSqPP = reSqP; imSqPP = imSqP;

r = 1./(reSqP*reSqP + imSqP*imSqP);
```

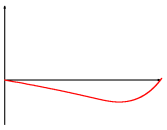

```
        if(temp > 0.){
            z[0] = reSqP/(temp);
            z[1] = imSqP/(temp);
            n1[0] = -sinh(z[0])/(cos(z[1]) - cosh(z[0]));
            n1[1] = sin(z[1])/(cos(z[1]) - cosh(z[0]));
        }else{
            n1[0] = 1.;
            n1[1] = 0.;
        }

        pionContrib[0] = r*( reSqP*n1[0] + imSqP*n1[1]);
        pionContrib[1] = r*(-imSqP*n1[0] + reSqP*n1[1]);

        //Contribution from the fermions
        r = sqrt(exp(2*t) + 2*gf*gf*rho);

        if(temp > 0.){
            nF = 0.5*(tanh( (r-mu) / (2*temp))+tanh( (r+mu) / (2*temp)));
        }else{
            nF = 1 - (double)(mu > r);
        }

        fermionContrib = nF/r;

        dy[0][i] = exp(5*t)*(bosonPref*(sigmaContrib[0] + 3*pionContrib[0]) + ↩
            → fermionPref*fermionContrib);
        dy[1][i] = exp(5*t)*(bosonPref*(sigmaContrib[1] + 3*pionContrib[1]));

    }

}
```

Bibliography

[1] D. H. Rischke, "The Quark gluon plasma in equilibrium," *Prog.Part.Nucl.Phys.*, vol. 52, p. 197, 2004.

[2] K. Rajagopal and F. Wilczek, "The Condensed matter physics of QCD," *eprint arXiv:hep-ph/0011333*, 2000.

[3] M. G. Alford, J. A. Bowers, and K. Rajagopal, "Color superconductivity in compact stars," *J.Phys.*, vol. G27, p. 541, 2001.

[4] H. Yukawa, "On the interaction of elementary particles," *Proc.Phys.Math.Soc.Jap.*, vol. 17, pp. 48–57, 1935.

[5] M. Maggiore, *A Modern Introduction to Quantum Field Theory*. Oxford University Press, 1st ed., 2005.

[6] M. E. Peskin and D. V. Schroeder, *An Introduction to Quantum Field Theory*. Westview Press, 1st ed., 1995.

[7] J. Goldstone, "Field Theories with Superconductor Solutions," *Nuovo Cim.*, vol. 19, p. 154, 1961.

[8] J. Goldstone, A. Salam, and S. Weinberg, "Broken Symmetries," *Phys.Rev.*, vol. 127, p. 965, 1962.

[9] G. 't Hooft and M. Veltman, "Regularization and Renormalization of Gauge Fields," *Nucl.Phys.*, vol. B44, p. 189, 1972.

[10] W. Pauli and F. Villars, "On the Invariant regularization in relativistic quantum theory," *Rev.Mod.Phys.*, vol. 21, p. 434, 1949.

[11] J. S. Schwinger, "On gauge invariance and vacuum polarization," *Phys.Rev.*, vol. 82, p. 664, 1951.

[12] J. I. Kapusta and C. Gale, *Finite-Temperature Field Theory Principles and Applications*. Cambridge University Press, 2nd ed., 2006.

[13] M. L. Bellac, *Thermal Field Theory*. Cambridge University press, 1st ed., 1996.

[14] J. O. Andersen, *Introduction to statistical mechanics*. Akademika forlag, 2012.

[15] C. G. Callan, "Broken scale invariance in scalar field theory," *Phys.Rev.*, vol. D2, p. 1541, 1970.

[16] K. Symanzik, "Small distance behavior in field theory and power counting," *Commun.Math.Phys.*, vol. 18, p. 227, 1970.

[17] K. Wilson and J. Kogut, "The renormalization group and the ϵ expansion," *Phys.Rept.*, vol. 12, p. 75, 1974.

[18] B. Delamotte, "An Introduction to the Nonperturbative Renormalization Group," *eprint arXiv:cond-mat/0702365*, Feb. 2007.

[19] D. F. Litim, "Optimization of the exact renormalization group," *Phys.Lett.*, vol. B486, p. 92, 2000.

[20] D. F. Litim, "Optimized renormalization group flows," *Phys.Rev.*, vol. D64, p. 105007, 2001.

[21] T. R. Morris, "The Exact renormalization group and approximate solutions," *Int.J.Mod.Phys.*, vol. A9, p. 2411, 1994.

[22] Y. Nambu, "QCD and the String Model," *Phys.Lett.*, vol. B80, p. 372, 1979.

[23] D. Gross and F. Wilczek, "Ultraviolet Behavior of Nonabelian Gauge Theories," *Phys.Rev.Lett.*, vol. 30, p. 1343, 1973.

[24] H. D. Politzer, "Asymptotic Freedom: An Approach to Strong Interactions," *Phys.Rept.*, vol. 14, p. 129, 1974.

[25] J. Beringer *et al.*, "Particle Data Group," *Phys.Rev.*, vol. D86, 2012.

[26] D. J. Griffiths, *Introduction to quantum mechanics*. Pearson, 2nd ed., 2005.

[27] B. Bransden and C. Joachain, *Quantum Mechanics*. Pearson, 2nd ed., 2000.

[28] M. Gell-Mann, "A Schematic Model of Baryons and Mesons," *Phys.Lett.*, vol. 8, p. 214, 1964.

[29] M. Gell-Mann and Y. Neemam, "The Eightfold way," 1964.

[30] C.-N. Yang and R. L. Mills, "Conservation of Isotopic Spin and Isotopic Gauge Invariance," *Phys.Rev.*, vol. 96, p. 191, 1954.

[31] S. L. Adler, "Axial-Vector Vertex in Spinor Electrodynamics," *Phys.Rev.*, vol. 177, p. 2426, 1969.

[32] J. Bell and R. Jackiw, "A PCAC puzzle: $\pi^0 \to \gamma\gamma$ in the σ-model," *Nuovo Cim.*, vol. A60, no. 1, p. 47, 1969.

[33] K. Fujikawa, "Path Integral Measure for Gauge Invariant Fermion Theories," *Phys.Rev.Lett.*, vol. 42, p. 1195, 1979.

[34] K. Fujikawa, "Path Integral for Gauge Theories with Fermions," *Phys.Rev.*, vol. D21, p. 2848, 1980.

[35] M. Gell-Mann and M. Lévy, "The axial vector current in beta decay," *Nuovo Cim.*, vol. 16, no. 4, p. 705, 1960.

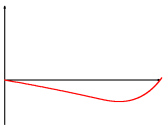

[36] S. Rüster, V. Werth, M. Buballa, I. Shovkovy, and D. Rischke, "Phase diagram of neutral quark matter: Self-consistent treatment of quark masses," *Phys.Rev.*, vol. D72, no. 3, p. 1, 2005.

[37] A. Masayuki and Y. Koichi, "Chiral restoration at finite density and temperature," *Nuclear Physics A*, vol. 504, no. 4, p. 668, 1989.

[38] A. Barducci, R. Casalbuoni, S. D. Curtis, R. Gatto, and G. Pettini, "Chiral-symmetry breaking in QCD at finite temperature and density," *Physics Letters B*, vol. 231, no. 4, p. 463, 1989.

[39] J. Berges and K. Rajagopal, "Color superconductivity and chiral symmetry restoration at nonzero baryon density and temperature," *Nucl.Phys.*, vol. B538, pp. 215–232, 1999.

[40] Z. Fodor and S. Katz, "Lattice QCD thermodynamics," *Acta Phys.Polon.*, vol. B42, p. 2791, 2011.

[41] G. Endrodi, Z. Fodor, S. Katz, and K. Szabo, "The QCD phase diagram at nonzero quark density," *JHEP*, vol. 1104, 2011.

[42] M. A. Stephanov, "QCD phase diagram and the critical point," *Prog.Theor.Phys.Suppl.*, vol. 153, p. 139, 2004.

[43] V. Skokov, B. Friman, E. Nakano, K. Redlich, and B.-J. Schaefer, "Vacuum fluctuations and the thermodynamics of chiral models," *Phys.Rev.*, vol. D82, p. 034029, 2010.

[44] J. O. Andersen, R. Khan, and L. T. Kyllingstad, "The chiral phase transition and the role of vacuum fluctuations," *eprint arXiv:hep-ph/1102.2779*, 2011.

[45] B.-J. Schaefer and M. Wagner, "The Three-flavor chiral phase structure in hot and dense QCD matter," *Phys.Rev.*, vol. D79, p. 014018, 2009.

[46] G. 't Hooft, "Symmetry Breaking Through Bell-Jackiw Anomalies," *Phys.Rev.Lett.*, vol. 37, p. 8, 1976.

[47] S. Gasiorowicz and D. A. Geffen, "Effective Lagrangians and Field Algebras with Chiral Symmetry," *Rev.Mod.Phys.*, vol. 41, p. 531, 1969.

[48] J. T. Lenaghan, D. H. Rischke, and J. Schaffner-Bielich, "Chiral symmetry restoration at nonzero temperature in the $SU(3)_r \times SU(3)_l$ linear sigma model," *Phys.Rev.*, vol. D62, p. 085008, 2000.

[49] C. Wetterich, "Average action and the renormalization group equations," *Nucl.Phys.*, vol. B352, p. 529, 1991.

[50] C. Wetterich, "Exact evolution equation for the effective potential," *Phys.Lett.*, vol. B301, p. 90, 1993.

[51] S. Bornholdt and C. Wetterich, "Average action for models with fermions," *Z.Phys.*, vol. C58, p. 585, 1993.

[52] D. Jungnickel and C. Wetterich, "Effective action for the chiral quark-meson model," *Phys.Rev.*, vol. D53, p. 5142, 1996.

[53] J.-P. Blaizot, A. Ipp, R. Mendez-Galain, and N. Wschebor, "Perturbation theory and non-perturbative renormalization flow in scalar field theory at finite temperature," *Nucl.Phys.*, vol. A784, p. 376, 2007.

[54] B.-J. Schaefer and J. Wambach, "The Phase diagram of the quark meson model," *Nucl.Phys.*, vol. A757, p. 479, 2005.

[55] J. O. Andersen and A. Tranberg, "The Chiral transition in a magnetic background: Finite density effects and the functional renormalization group," *JHEP*, vol. 1208, p. 002, 2012.

[56] K. Kamikado, T. Kunihiro, K. Morita, and A. Ohnishi, "Functional Renormalization Group Study of Phonon Mode Effects on Chiral Critical Point," *eprint arXiv:hep-ph/1210.8347*, 2012.

[57] J. Berges, N. Tetradis, and C. Wetterich, "Nonperturbative renormalization flow in quantum field theory and statistical physics," *Phys.Rept.*, vol. 363, p. 223, 2002.

[58] V. Skokov, B. Stokić, B. Friman, and K. Redlich, "Meson fluctuations and thermodynamics of the Polyakov loop extended quark-meson model," *Phys.Rev.*, vol. C82, p. 015206, 2010.

[59] M. Galassi *et al.*, "GNU Scientific Library Reference Manual." `http://www.gnu.org/software/gsl/`.

[60] R. Piessens, E. D. Doncker-Kapenga, and C. W. Überhuber, *QUADPACK: a subroutine package for automatic integration*. Springer, 1983.

[61] W. H. Press, S. A. Teukolsky, W. T. Vetterling, and B. P. Flannery, *Numerical Recipes*. Cambridge University Press, 3rd. ed., 2007.

[62] J. Dormand and P. Prince, "A family of embedded Runge-Kutta formulae," *J.Comput.Appl.Math*, vol. 6, no. 1, p. 19, 1980.

[63] E. Hairer, S. Nørsett, and G. Wanner, *Solving ordinary differential equations I. Nonstiff problems*. Springer Series in Computational Mathematics, 1987.

[64] J. O. Andersen and A. Tranberg, "Erratum: The Chiral transition in a magnetic background: Finite density effects and the functional renormalization group," 2013. to appear.

[65] J. O. Andersen, S. Mogliacci, N. Su, and A. Vuorinen, "Quark number susceptibilities from resummed perturbation theory," *Phys.Rev.*, vol. D87, p. 074003, 2013.

[66] R. V. Gavai, S. Gupta, and P. Majumdar, "Susceptibilities and screening masses in two flavor QCD," *Phys.Rev.*, vol. D65, p. 054506, 2002.

[67] A. Bazavov *et al.*, "Fluctuations and Correlations of net baryon number, electric charge, and strangeness: A comparison of lattice QCD results with the hadron resonance gas model," *Phys.Rev.*, vol. D86, p. 034509, 2012.

[68] S. Borsanyi, Z. Fodor, S. D. Katz, S. Krieg, C. Ratti, *et al.*, "Fluctuations of conserved charges at finite temperature from lattice QCD," *JHEP*, vol. 1201, p. 138, 2012.

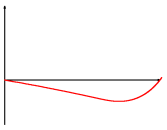

[69] M. Fukugita and A. Ukawa, "Deconfining and chiral transitions of finite temperature quantum chromodynamics in the presence of dynamical quark loops," *Phys.Rev.Lett.*, vol. 57, p. 503, 1986.

[70] A. M. Polyakov, "Thermal Properties of Gauge Fields and Quark Liberation," *Phys.Lett.*, vol. B72, p. 477, 1978.

[71] K. Fukushima, "Chiral effective model with the Polyakov loop," *Phys.Lett.*, vol. B591, p. 277, 2004.